



NTNU – Trondheim
Norwegian University of
Science and Technology

Parameter Sensitivity of Short-term Fatigue Damage of Spar-type Wind Turbine Tower

Inge Moy

Marine Technology

Submission date: June 2012

Supervisor: Torgeir Moan, IMT

Co-supervisor: Madjid Karimirad, IMT

Norwegian University of Science and Technology
Department of Marine Technology

M.Sc. THESIS IN MARINE TECHNOLOGY

SPRING 2012

FOR

STUD.TECHN. Inge Moy

Parameter Sensitivity of Short-term Fatigue Damage of Spar-type Wind Turbine Tower

Parameter sensitivitet av korttids utmattingskade av spar-type vindturbintårn

Background

There is a significant potential for offshore wind energy. Oil and gas industry has a good experience in using spar platforms in the exploitation of oil and gas. This concept has a potential as a support structure for offshore wind turbines. Hywind is an example of successful offshore wind turbine based on spar-type design for deep water. The good performance of the spar-type wind turbine motivates researchers to study the feasibility of using these turbines in moderate water depths. In this project, a spar-type wind turbine in moderate water depth supporting a 5-MW turbine system will be considered. The power performance and structural integrity of a spar-type floating wind turbine will be studied in this master thesis.

The purpose of this thesis is to design a feasible spar-type support structure for a 5-MW floating wind turbine in moderate water depth (i.e. 150 m). The final aim of the master-thesis is to carry out the dynamic response analyses of a floating wind turbine subjected to wave and wind loads concerning the fatigue limit states. Hence, the parameter sensitivity of short-term fatigue damage of spar-type wind turbine tower is considered.

Assignment

1. Literature study of floating wind turbines with an emphasis on the spar-type wind turbines, relevant load conditions and design criteria in design codes, as well as the software package Simo-Riflex for dynamic response analysis.
2. Design of a spar-type support structure as a base for a 5-MW wind turbine in moderate water depth. This includes:
 - a. Dimensioning the spar considering the design criteria
 - b. Design of the mooring system
 - c. Hydrostatic- and hydrodynamic-stability checks considering the required mass-distribution, displacement, shape of the spar and etc.
 - d. Coupled hydrodynamic analysis in the short-term perspective
3. Consider the wave and wind loads in the long-term perspective, and identifying load conditions based on the IEC-61400-3 and the other relevant standards.
4. Establish a model for dynamic response analysis and carry out the response analyses for selected load conditions. This includes the wave- and wind-induced dynamic motions and structural responses of the spar-type wind turbine as well as the mooring system.
5. The goal of the thesis is to study the parameter sensitivity of short-term fatigue damage of spar-type wind turbine tower.

6. Conclude and recommend future work towards structural-design of the wind turbine.

The work scope could be larger than anticipated. Subject to approval from the supervisors, topics may be deleted from the list above or reduced in extent.

In the thesis the candidate shall present his personal contribution to the resolution of problem within the scope of the thesis work.

Theories and conclusions should be based on mathematical derivations and/or logic reasoning identifying the various steps in the deduction.

The candidate should utilize the existing possibilities for obtaining relevant literature.

The thesis should be organized in a rational manner to give a clear exposition of results, assessments, and conclusions. The text should be brief and to the point, with a clear language. Telegraphic language should be avoided.

The thesis shall contain the following elements: A text defining the scope, preface, list of contents, summary, main body of thesis, conclusions with recommendations for further work, list of symbols and acronyms, reference and (optional) appendices. All figures, tables and equations shall be numerated.

The supervisor may require that the candidate, in an early stage of the work, present a written plan for the completion of the work. The plan should include a budget for the use of computer and laboratory resources that will be charged to the department. Overruns shall be reported to the supervisor.

The original contribution of the candidate and material taken from other sources shall be clearly defined. Work from other sources shall be properly referenced using an acknowledged referencing system.

The thesis shall be submitted in two copies as well as an electronic copy on a CD:

- Signed by the candidate
- The text defining the scope included
- In bound volume(s)
- Drawings and/or computer prints which cannot be bound should be organized in a separate folder.

Supervisors: Professor Torgeir Moan and Dr. Madjid Karimirad , NTNU

Torgeir Moan

Deadline: 10.06.12.

Preface

This master's thesis was conducted during my final semester of the five year Master of Science program in Marine Technology. The work has been carried out at the Department of Marine Technology at the Norwegian University of Science and Technology, under the supervision of Professor Torgeir Moan and Dr. Madjid Karimirad.

I wish to express my sincere thanks to both of my supervisors. They have engaged with great passion and knowledge and provided me with all the help I have needed. Professor Torgeir Moan has given me great motivation with his enthusiasm and Dr. Madjid Karimirad has given me all the necessary knowledge I have needed to write this thesis. In addition I would like to thank Zhen Gao, Marit I. Kvittem, Chenyu Luan and all the members of my office A1.007 for the help they have provided when needed.

I will also like to thank my parents for all the support they have given me through the studies. I will especially thank my girlfriend, Anette, for the massive support she has given me throughout the studies.

Trondheim, June 7, 2012

A handwritten signature in black ink, appearing to read 'Inge Moy', with a long horizontal line extending to the right from the end of the signature.

Inge Moy

Abstract

The World's energy demand is rapidly increasing and a good viable renewable energy source is wind power. The land-based knowledge and experience the onshore wind turbine industry possess is used to develop offshore wind turbines. With this knowledge together with the experience and knowledge of the marine industry we can design and produce a floating wind turbine. The main advantages of an offshore wind turbine are that the wind is stronger and less turbulent at sea, visual and noise annoyances can be avoided and there are large available areas at sea.

In this thesis coupled time domain analyses of a floating spar-type wind turbine are performed with the intention to study parameters affecting fatigue damage at base of the tower. The software applied is SIMO/Riflex with the extension TDHmill, which gives the wind thrust force and gyro moment on the wind turbine as point loads in the tower top.

Short term environment conditions are chosen from a joint distribution of simultaneous wind and waves which is based on measurements from a site in the North Sea in the period 1973 – 1999. In total 141 different environmental conditions are chosen for the sensitivity study. Mean value, standard deviation, skewness and kurtosis are calculated for axial stresses at the base of the tower. Fatigue damage is calculated from the Palmgren-Miner sum with a nominal stress SN-curve from the DNV fatigue standard. The axial stress-cycle distribution used in the Palmgren-Miner sum is found by rainflow counting.

Time domain simulations are carried out for the different sea states and fatigue damage is calculated for each case. The statistical properties and fatigue damage are averaged over seven samples with different random seed number to ensure acceptable statistical uncertainty. Accumulated standard deviation shows that 5 samples of each load case are sufficient to ensure acceptable statistical uncertainty.

Sensitivity study of different simulation length shows that 30 minute simulations give close to equal fatigue damage and standard deviation as 2.5 hour simulations. Sensitivity of fatigue to wave height and peak period is carried out to study the effect of varying parameters. This study suggests that the highest waves dominate the fatigue damage for the smallest peak periods. For some small wave heights the damage will be constant for a given peak period range. From this sensitivity study it is shown that if the deviation of fatigue damage between the different load cases is small, then the dominating load case of the accumulated long term fatigue damage will be dominated by the marginal probability of each load case.

Sammendrag

Verdens energietterspørsel er raskt økende og en god og levedyktig fornybar energikilde er vindkraft. Kunnskapen og erfaringen fra landbasert vindindustri kombinert med den marine kunnskapen offshoreindustrien besitter, gjør det det mulig og designe og produsere flytende vindturbiner. De største fordelene med offshore vindturbiner er at vinden er sterkere og mindre turbulent på sjøen og det er store områder tilgjengelig for utbygging av offshore vindparker.

I denne hovedoppgaven er det utført koblet dynamisk respons analyse i tidsdomene av en flytende vindturbin i moderat vanddyp med hensikt i og studere hvordan ulike parametre påvirker utmattingskaden ved foten av vindturbintårnet. Programvaren som er brukt i analysene er SIMO/Riflex med utvidelsen TDHmill som gir vindkraften og gyromomentet på vindturbinen som punktlast.

Kortsiktige lasttilfeller er valgt fra en kombinert vind og bølge fordeling som baserer seg på målinger fra Nordsjøen i perioden 1973-1999. I alt er det simulert 141 forskjellige lasttilfeller i denne avhandlingen. Statistiske verdier som gjennomsnittsverdi, standardavvik, skjevhet og kurtosis er kalkulert for aksialspenning i foten av tårnet. Utmattingskade er beregnet fra Palmgren-Miner summasjon med nominell spennings-SN-kurve fra utmattingsstandaren til DNV. Aksialspenningssyklusene som er brukt i Palmgren-Miner summen er funnet ved hjelp av regnstrømtellig.

Simuleringer i tidsdomene er utført for de forskjellige lasttilfellene hvor utmattingskade er kalkulert for hver av dem. For å sikre akseptabel statistisk usikkerhet av de statistiske verdiene og utmattingskaden er det utført syv simuleringer med tilfeldig fase for hvert lasttilfelle. Gjennomsnittet av de syv simuleringene er beregnet for hvert lasttilfelle. Akkumulert standardavvik viser at 5 simuleringer for hvert lasttilfelle er nok for å sikre akseptabel statistisk usikkerhet.

Sensitivitetsanalyse av simulerings-lengden viser at 30 minutt simuleringer gir nesten samme statistiske verdier og utmattingskade som en 2.5 times simulering. Sensitivitetsanalyse av utmattingskade er utført for varierende verdier av signifikant bølgehøyde og topp-perioden. Disse analysene antyder at de høyeste bølgehøydene dominerer utmattingskaden for de laveste topp-periodene. For noen små bølgehøyder vil utmattingskaden være konstant for gitte rekkevidder av topp-perioden. Fra denne analysen er det vist at hvis avviket i korttidsutmattingskaden er lite, vil langtidsutmattingskaden være dominert av den marginale sannsynligheten av hvert lasttilfelle.

Nomenclature

Abbreviation

CALM	Catenary Anchor Leg Mooring
CMS	Catenary Moored Spar
DICAS	Differentiated Compliance Anchoring System
DLL	Dynamic Linked Library
HMPE	High Modulus Polyethylene
MWL	Mean Water Level
NREL	National Renewable Energy Laboratory
OECD	Organization for Economic Co-operation and Development
RFC	Rainflow Counting
SALM	Single Anchor Leg Mooring
SFC	Stress Concentration Factor
SIMO	Simulation of Complex Marine Operations
TLS	Tension Leg Spar
TLP	Tension Leg Platform
WRC	Wire-Rope Construction

Roman symbols

a_x	Water particle acceleration in x-direction
A_{11}	Added mass in surge
A_{33}	Added mass in heave
A_{55}	Added mass in pitch
C	Potential damping matrix
C_D	Drag coefficient
C_M	Mass coefficient
D	Fatigue damage
D_{AW}	Water line diameter
D_{linear}	Linear viscous hydrodynamic damping matrix
$D_{quadratic}$	Quadratic viscous hydrodynamic damping matrix
E	Total energy
g	Acceleration of gravity
GM	Metacentric height

k	Wave number
K	Stiffness matrix
KG	Distance from MWL to centre of gravity
KB	Distance from MWL to centre of buoyancy
M	Mass matrix
$R(t)$	Retardation function
u	Velocity in x-direction
P_D	Dynamic pressure
x, \dot{x}, \ddot{x}	Displacement, velocity and acceleration vector
Z_G	Centre of gravity
Z_B	Centre of buoyancy

Greek symbols

ρ	Density
β	Wave direction
ε	Phase angle
π	3.14159265...
ω	Wave frequency
γ	Peakedness parameter
∇	Displacement
ζ	Wave elevation

Table of Contents

M.Sc. THESIS IN MARINE TECHNOLOGY	I
Preface.....	III
Abstract	IV
Sammendrag	V
Nomenclature.....	VI
1 Introduction.....	1
1.1 Background.....	1
1.2 Objectives and scope of the thesis.....	4
2 Theory.....	5
2.1 Equations of Motion.....	5
2.2 Linear Wave Potential Theory	6
2.3 Irregular Wave Theory.....	9
2.4 Wave loads	10
2.5 Wind Theory	11
2.6 Fatigue	13
3 Modelling and Programming.....	18
3.1 General	18
3.2 Floating Support Structure	18
3.3 Tower and Turbine System.....	21
3.4 Mooring system.....	23
3.4.1 Types of mooring system	23
3.4.2 Types of mooring lines	24
3.4.3 Design of mooring system	27
3.5 SIMO/RIFLEX.....	29
3.6 Free Decay Test	30

3.7	TDHmill	31
4	Environmental conditions	33
4.1	General	33
4.2	Joint Distribution of Simultaneous Wind and Waves.....	33
5	Load Cases	40
5.1	Load Cases for Sensitivity of Fatigue to Simulation Length.....	40
5.2	Load Cases for Sensitivity of Fatigue to Peak Period.....	42
5.3	Load Cases for Sensitivity of Fatigue to Wave Height	45
6	Analysis and Results	50
6.1	Fatigue	50
6.2	Sensitivity of Fatigue to Simulation Length	53
6.3	Sensitivity of Fatigue to Peak Period	60
6.4	Sensitivity of Fatigue to Wave Height	64
7	Conclusions and Further Work	69
8	References.....	71
APPENDIX A	Input files SIMO/RIFLEX.....	I
APPENDIX B	Python Scripts.....	X
APPENDIX C	Extract result files from outmod/s2xmod	XIV
APPENDIX D	Plot of joint probability distribution.....	XX
APPENDIX E	Matlab Scrips Used for post-processing.....	XXX

Table of Figures

Figure 1-1 Cumulative and annual offshore installations [2]	2
Figure 1-2 Different floating offshore wind turbine concepts [4]	3
Figure 2-1 Retardation function for spar type structure	6
Figure 2-2 Horizontal velocity distribution under a wave crest and wave trough [8]	7
Figure 2-3 Pressure variation under a wave crest and wave trough [8]	8
Figure 2-4 Motion of water particles in deep water (left) and shallow water depth (right) [8]	8
Figure 2-5 Dominating forces on marine structures [8]	11
Figure 2-6 Definition of the rainfall cycle [13]	14
Figure 2-7 Stress concepts for welded structure [14]	15
Figure 2-8 SN-curve in sea water with cathodic protection	17
Figure 3-1 Dimension of floating support structure	19
Figure 3-2 Model of floating support structure from HydroD	19
Figure 3-3 Model of Tower and Turbine from DeepC	22
Figure 3-4 Stud chain (left) and studless chain (right) [19]	25
Figure 3-5 Wire Rope Structure [19]	26
Figure 3-6 Six-strand wire rope construction [21]	27
Figure 3-7 Parallel rope construction [21]	27
Figure 3-8 Design of mooring system	28
Figure 3-9 Model of the catenary moored floating wind turbine	29
Figure 3-10 Thrust Coefficient as a function of relative wind speed	32
Figure 4-1 Marginal distribution of the mean wind speed	33
Figure 4-2 Conditional Distribution of Significant Wave Height for given wind speeds	34
Figure 4-3 Surface plot of the conditional distribution of peak period for given wind speed and wave height	36
Figure 4-4 Contour plot of the conditional distribution of peak period for given wind speed and wave height	37
Figure 4-5 Surface plot of the joint distribution of simultaneous wind and waves for selected wind speeds	38
Figure 4-6 Contour plot of the joint distribution of simultaneous wind and waves for selected wind speeds	39
Figure 5-1 Probability distribution of the load cases	41
Figure 5-2 Marginal probability of the different load cases in the peak period sensitivity analysis	42
Figure 5-3 Probability of occurrence of peak period for given wave height and wind speed	49
Figure 6-1 Shear force accumulated average standard deviation for LC6 and LC9	51

Figure 6-2 Bending moment accumulated average standard deviation for LC6 and LC9	51
Figure 6-3 Equivalent stress accumulated average standard deviation for LC6 and LC9	52
Figure 6-4 Axial stress accumulated average standard deviation for LC6 and LC9	52
Figure 6-5 Mean Value of Axial Stress of load case 1 - 6 for different simulation lengths	55
Figure 6-6 Standard Deviation of Axial Stress of LC1 –LC6 for different simulation lengths	55
Figure 6-7 Time series of equivalent stress for load case 6 with transients	56
Figure 6-8 Standard deviation of axial stress for 2.5 hours and 30 min simulation length	57
Figure 6-9 2.5 hour rainflow damage for 30 minute and 2.5 hour simulation lengths.....	58
Figure 6-10 Fatigue damage accumulated over one year for different simulation lengths	59
Figure 6-11 Mean Value of Axial Stress for Peak Period Sensitivity Analysis.....	62
Figure 6-12 Standard Deviation of axial Stress for Peak Period Sensitivity Analysis.....	62
Figure 6-13 30 minute rainflow damage for different peak periods with varying wave heights averaged over 7 samples.....	63
Figure 6-14 Fatigue damage accumulated over 1 year of peak period sensitivity.....	64
Figure 6-15 Mean Value of Axial stress for load cases in wave height sensitivity	66
Figure 6-16 Standard Deviation of Axial Stress for load cases in wave height sensitivity	66
Figure 6-17 30 minute rainflow damage for different wave heights with varying peak periods averaged over 7 samples.....	67
Figure 6-18 Fatigue damage accumulated over 1 year of wave height sensitivity	68

Table of Tables

Table 3-1 Properties of Floating Support Structure	20
Table 3-2 Tower and Wind Turbine Properties [18].....	21
Table 3-3 Minimum mechanical properties for chain cable materials [20]	25
Table 3-4 Properties of mooring system	28
Table 3-5 Natural periods and frequencies from decay tests	31
Table 5-1 Most Probable Load Cases for given wind speed.....	40
Table 5-2 Load Cases Wave Height Sensitivity Block 1.....	43
Table 5-3 Load Cases Wave Height Sensitivity Block 2.....	44
Table 5-4 Load Cases Wave Height Sensitivity Block 3.....	45
Table 5-5 Load Cases Peak Period Sensitivity Block 1	46
Table 5-6 Load Cases Peak Period Sensitivity Block 2	46
Table 5-7 Load Cases Peak Period Sensitivity Block 3	47
Table 5-8 Load Cases Peak Period Sensitivity Block 4	47

Table 5-9 Load Cases Peak Period Sensitivity Block 5	48
Table 5-10 Load Cases Peak Period Sensitivity Block 6	48
Table 5-11 Load Cases Peak Period Sensitivity Block 7	49
Table 6-1 Statistical properties of equivalent stress and axial stress averaged over 7 simulations with different random seed number.....	54
Table 6-2 Statistical properties of axial stress for 30 minute and 2.5 hours simulation length without start-up transients.....	57
Table 6-3 Statistical properties of axial stress averaged over seven samples with different random seed number.....	61
Table 6-4 Statistical properties of axial stress averaged over 7 samples with different random seed number.....	65

1 Introduction

1.1 Background

The world's demand for energy is rapidly increasing. The massive economic growth and industrialization of non-OECD countries like China, India and Brazil is pushing the energy demand to a new level. This energy demand is mostly covered by non-renewable resources like oil, gas, coal and nuclear power. The emission from burning fossil fuels is very harmful to the environment, and in a time with massive focus on global warming, the world screams for more environment-friendly energy resources. The radioactive waste nuclear power produces, the difficulties with storage and disposal of the waste and the catastrophic outcome of the tsunami that stroke Japan with great force in the spring of 2011 are reasons to avoid building nuclear power plants.

On the other hand renewable energy resources like solar power, geothermal, wave, tidal, hydroelectric and wind power are non-polluting, inexhaustible and indigenous. Among these wind power seems to be the most reliable and practical. For more than a decade land-based wind power has been the fastest growing energy source on a percentage basis. In the end of 2011 the world's total installed wind turbine capacity reached 239 GW, an increase of 42 GW, or 22 % from 2010. [1] The total capacity is enough to cover 3 % of the world's electricity demand. The strongest increase in wind power utilization is coming from the emerging markets, such as China, India, Brazil and Mexico. China alone has more than one fourth of the world's wind power capacity and installed over 40% of the world's new wind turbines in 2011.

In the end of 2011, 1.5 % of all installed wind turbine was offshore wind turbines, and almost all of them were installed in Europe. [2] The offshore wind installation trends for Europe are shown in figure 1-1. The total number of offshore turbines installed in Europe in 2011 was 1369, where 75% of the turbine substructure is monopile structure, 21% gravity based structure, 2% jacket, 2% tripile. Of all the offshore wind turbines there are only installed three wind turbines with floating support structure. For countries like China, Japan, United States and Norway much of the offshore wind resource potential is available in water deeper than 30 m. [3] To utilize these offshore wind resources the solution will be to develop and use floating wind turbines which can operate at water depth deeper than 50 m.

Some of the advantages of offshore wind turbines are:

- The wind is stronger and more stable and has less turbulence intensity and smaller shear at sea than on land.
- If the turbine is manufactured near the coast line the size of the wind turbine is not limited by logistical constraints of the road or rail way.
- If the wind turbines are installed in a sufficient distance from land, then the visual and noise annoyances can be avoided.
- The availability and area of open sea is much higher than area available at land to install wind turbines.

There are also some disadvantages in connection with installing offshore wind turbines:

- The capital investment is much higher for offshore wind turbines than for land-based wind turbine. The marine environmental conditions are much harsher and there are added complications of the support structure, installation and decommissioning.
- The operational and maintenance cost is much higher for offshore wind turbines than for land-based turbines due to the low accessibility and weather dependent operation conditions.
- Offshore wind turbine must handle both loading from wind and hydrodynamic loads from the ocean. This results in a more complex design.

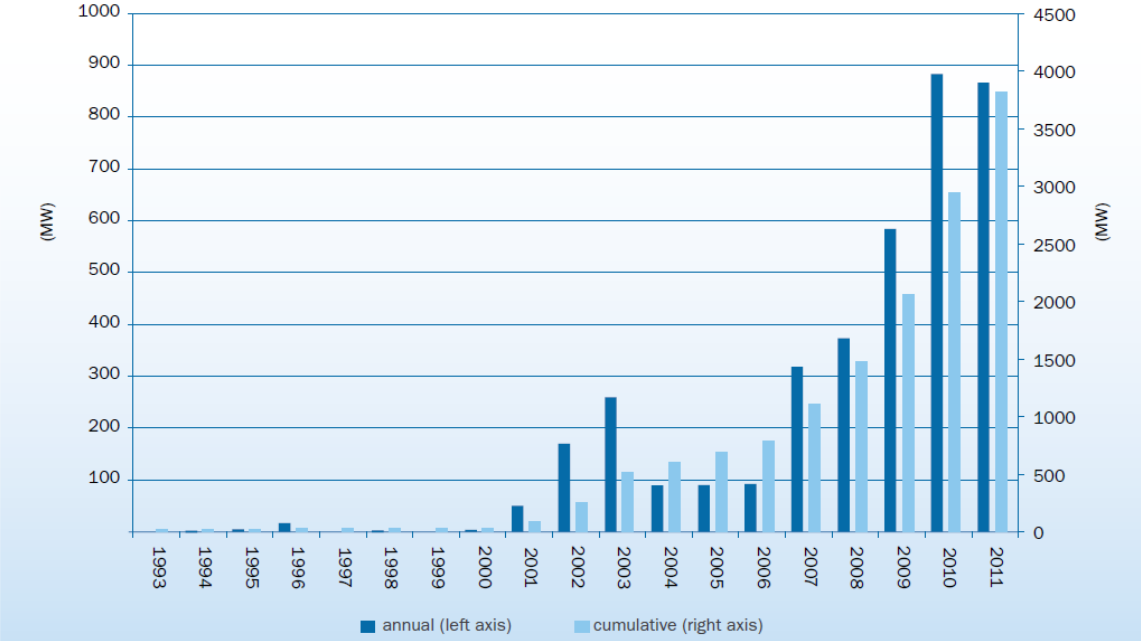


Figure 1-1 Cumulative and annual offshore installations [2]

Today there are numerous floating support platform concepts for offshore wind turbines under development. Some of the different concepts are shown in figure 1-2. The catenary moored spar-buoy concept (CMS) achieves stability by using ballast to lower the centre of mass below the centre of buoyancy. The tension-leg platform (TLP) concept achieves stability through the use of mooring-line tension caused by excess buoyancy in the tank. Semisubmersibles achieve stability through water plane area. From these three basic concepts there have been made modifications and variations where one concept build on the next one. Examples on concepts which are under development and production today are Hywind (spar-type), WindFloat (semi-sub), SWAY (spar-type), Njord (spar-type) and WindSea (semi-sub). To prepare these concepts for the harsh offshore environment a lot of research has to be done regarding dynamic response analysis, structural integrity, installation and optimisation of the design.

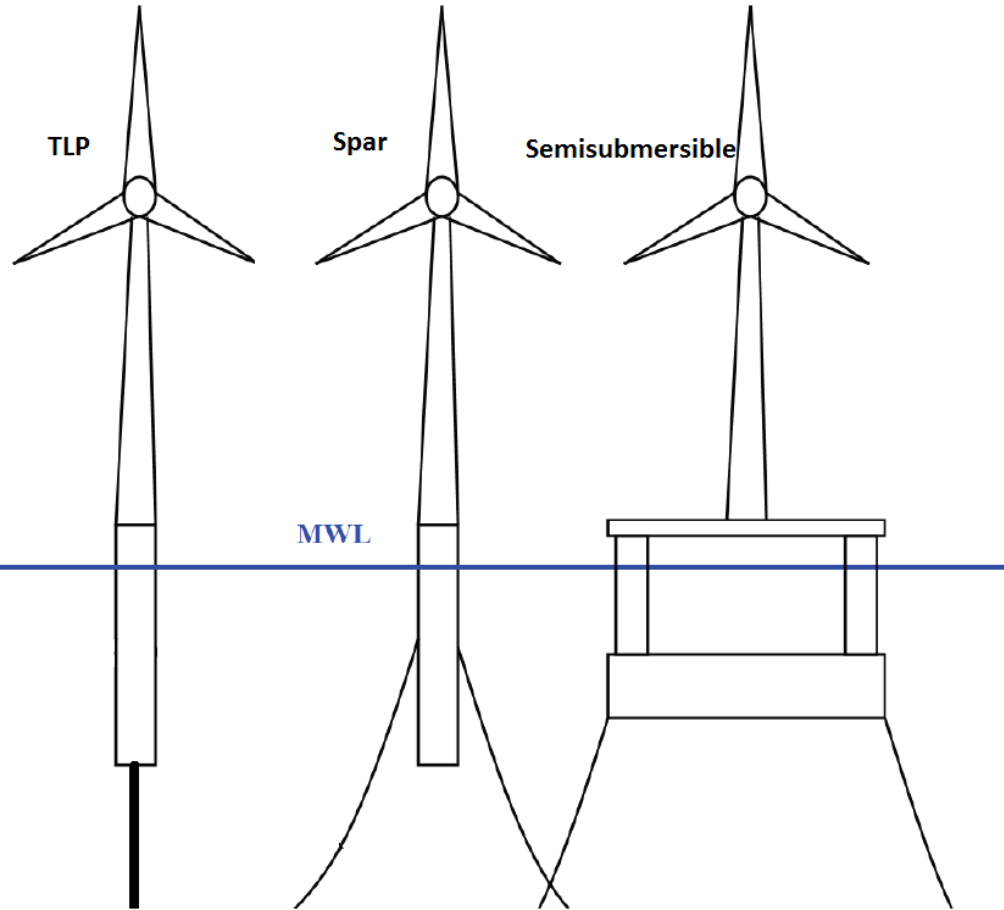


Figure 1-2 Different floating offshore wind turbine concepts [4]

1.2 Objectives and scope of the thesis

The first objective of this thesis is to design a feasible spar-type support structure for a 5-MW floating wind turbine in moderate water depth. The tower and the turbine are included and the total floating wind turbine is exposed to simultaneous wind and wave conditions. The coupled dynamic response analysis is performed. The main objective is to perform fatigue damage analysis of the tower base and study which effects different wave heights and peak periods will have on the fatigue.

In chapter 1 a brief introduction is given to give the reader some insight in the development and progress of the wind turbine environment.

Chapter 2 describes the basic theory which is the background for the analysis performed in this thesis. Subjects covered in this chapter are equations of motion, linear and non-linear wave theory, wind and wave loads and fatigue.

Chapter 3 describes the modelling and programming process. Objects modelled and described in this chapter are the floating support structure, tower and wind turbine and mooring system. In addition a brief description of different types of mooring system and mooring lines is given. The software used in this thesis is described together with the TDHmill extension.

In chapter 4 the environmental conditions are described which are based on the joint distribution of simultaneous wind and waves.

Chapter 5 gives a description of the load cases used in the fatigue analyses. The load cases are chosen based on the joint distribution of simultaneous wind and waves, and which parameter it is interesting to study.

Chapter 6 describes and discusses the different analysis and the results of them. The main focus in the analysis has been on fatigue damage and which effect variation of different parameters has on fatigue.

2 Theory

2.1 Equations of Motion

The equations of motion for a floating structure can be derived from Newton's second law in the following way: $\mathbf{M}\ddot{\mathbf{x}} = \mathbf{F}_{Generalized}(t, \mathbf{x}, \dot{\mathbf{x}})$. The generalized force vector contains all forces acting on the floating body and can be expressed as:

$$\mathbf{F}_{Generalized}(t, \mathbf{x}, \dot{\mathbf{x}}) = \mathbf{F}_{Inertia} + \mathbf{F}_{Gravitational} + \mathbf{F}_{Environmental} + \mathbf{F}_{Damping} + \mathbf{F}_{Stiffness} + \mathbf{F}_{Mooring} + \dots \quad \text{Equation 2.1}$$

The stiffness and damping forces includes both aerodynamic, hydrodynamic and structural stiffness and damping forces. The mass matrix, \mathbf{M} , contains both the structural mass and the hydrodynamic mass. \mathbf{x} , $\dot{\mathbf{x}}$, and $\ddot{\mathbf{x}}$ are motion vectors, velocity vectors and acceleration vectors respectively.

The motions and loads of a floating vessel with mooring lines is analysed by a separated two step procedure: [5]

1. Compute the motions of the floating vessel based on diffraction and radiation theory, where the load effects from the mooring lines are modelled as a linear restoring force. This is a linear frequency domain procedure.
2. Apply the vessel motions computed in the frequency domain. The motions are transformed into a time domain by an inverse Fourier transformation. The dynamic motions and loads for the coupled system are computed using a non-linear time domain procedure where the total response for the vessel and mooring lines is solved simultaneously at every time step in the simulation.

The rigid body equations for a floating wind turbine without the aero dynamic effects in regular wave can be written as:

$$\mathbf{M}\ddot{\mathbf{x}} + \mathbf{C}\dot{\mathbf{x}} + \mathbf{D}_{linear}\dot{\mathbf{x}} + \mathbf{D}_{quadratic}\dot{\mathbf{x}}|\dot{\mathbf{x}}| + \mathbf{K}\mathbf{x} = \mathbf{F}(t, \mathbf{x}, \dot{\mathbf{x}}) \quad \text{Equation 2.2}$$

The frequency-dependent mass matrix can be written as $\mathbf{M} = \mathbf{m} + \mathbf{A}(\omega)$, where \mathbf{m} is the structural mass and $\mathbf{A}(\omega) = \mathbf{A}_{\infty} + \mathbf{a}(\omega)$ is the frequency-dependent added mass matrix. \mathbf{C} is the frequency-dependent potential damping matrix given by $\mathbf{C}(\omega) = \mathbf{C}_{\infty} + \mathbf{c}(\omega)$. \mathbf{D}_{linear} is the linear viscous hydrodynamic damping matrix and $\mathbf{D}_{quadratic}$ is the quadratic viscous hydrodynamic damping matrix. \mathbf{K} is the hydrostatic stiffness matrix and the position vector \mathbf{x} contains both translation and rotation. The exciting forces of the system are given by the force vector: $\mathbf{F}(t, \mathbf{x}, \dot{\mathbf{x}}) = \mathbf{F}_{Hydrodynamic} + \mathbf{F}_{Current} + \mathbf{F}_{Mooring} + \mathbf{F}_{Gravitational}$. The forces depend on the environment the structure is exposed to.

To solve the equations of motion in a non-linear time domain we have to transform the frequency-dependent terms into time domain. This can be solved by introducing a convolution integral and applying an inverse Fourier transformation on the radiation part. The retardation function can be calculated using the added mass or the potential damping. [6] The equation of motion with the retardation function becomes:[7]

$$M\ddot{x} + C\dot{x} + D_{linear}\dot{x} + D_{quadratic}\dot{x}|\dot{x}| + Kx + \int_0^t R(t - \tau)\dot{x}(\tau)d\tau = F(t, x, \dot{x}) \quad \text{Equation 2.3}$$

The retardation function from the potential damping or the added mass is given by equation 2.4.

$$R(t) = \frac{2}{\pi} \int_0^\infty [c(\omega) - C_\infty] \cos(\omega t) d\omega = -\frac{2}{\pi} \int_0^\infty \omega [a(\omega) - A_\infty] \sin(\omega t) d\omega \quad \text{Equation 2.4}$$

For large-volume structures, such as ships and semisubmersibles, the potential damping and added mass are highly frequency dependent and the radiation will play a significant part. However, for a spar type structure, the retardation function converges to zero (see figure 2-1) since the potential damping and added mass is almost frequency-independent.

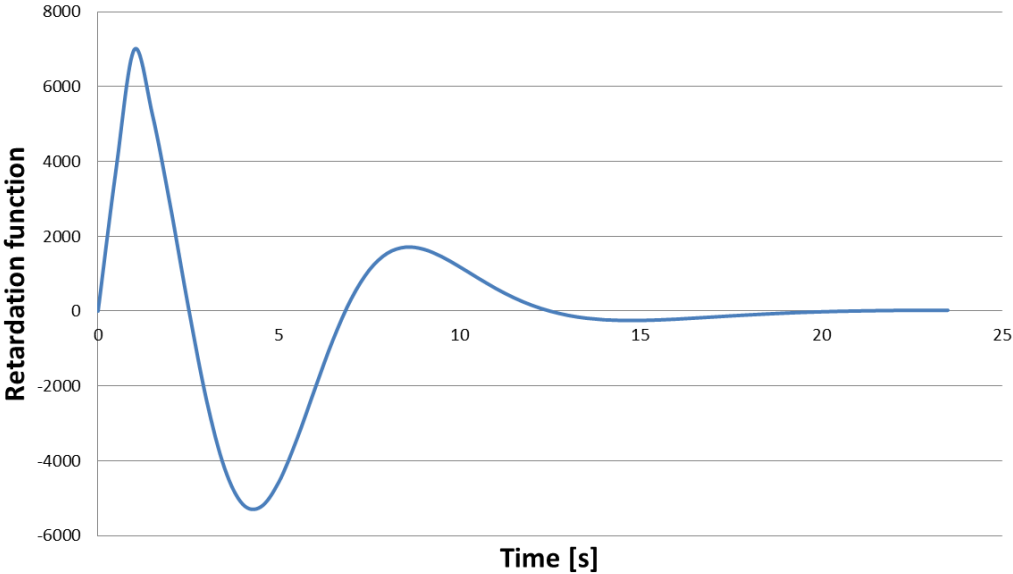


Figure 2-1 Retardation function for spar type structure

2.2 Linear Wave Potential Theory

Linear wave potential theory is based on wave potential for an incoming undisturbed regular sinusoidal wave with constant wave amplitude, wave length and amplitude. The wave potential ϕ_0 for a regular wave is, according to Airy's theory expressed by equation 2.5.

$$\phi_0 = \frac{\zeta_a g \cosh k(z+d)}{\omega \cosh kd} \cos(\omega t - kx \cos \beta - ky \sin \beta + \phi_\zeta) \quad \text{Equation 2.5}$$

where

ζ_a wave amplitude

g acceleration of gravity

k wave number , $k = \frac{\omega^2}{g}$

β direction of wave propagation. In this thesis $\beta = 0$.

In Airy's theory the sea water is assumed incompressible and inviscid and the fluid motion is assumed to be irrotational. From the wave potential we can find the water particle velocity (eq. 2.6) and acceleration (eq. 2.7) in the wave propagating direction and the dynamic pressure (eq. 2.8).

$$u = \omega \zeta_a \frac{\cosh k(z+h)}{\sinh kh} \sin(\omega t - kx) \quad \text{Equation 2.6}$$

$$a_x = \omega^2 \zeta_a \frac{\cosh k(z+h)}{\sinh kh} \cos(\omega t - kx) \quad \text{Equation 2.7}$$

$$P_D = \rho g \zeta_a \frac{\cosh k(z+h)}{\cosh kh} \sin(\omega t - kx) \quad \text{Equation 2.8}$$

In figure 2-2 and figure 2-3 you can see how the horizontal velocity and the dynamic pressure decreases with depth in regular wave theory under a wave crest and wave trough. [8]

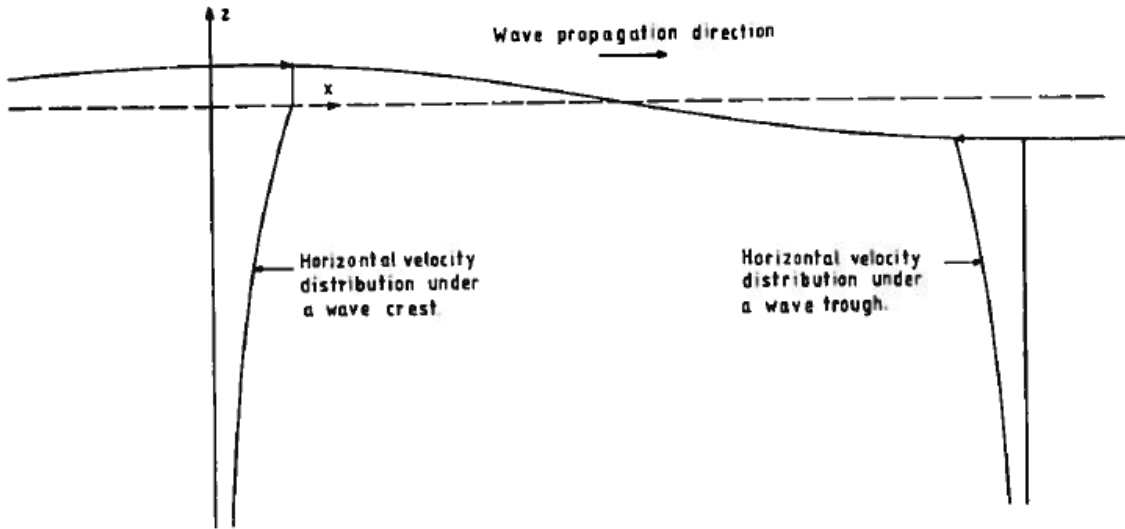


Figure 2-2 Horizontal velocity distribution under a wave crest and wave trough [8]

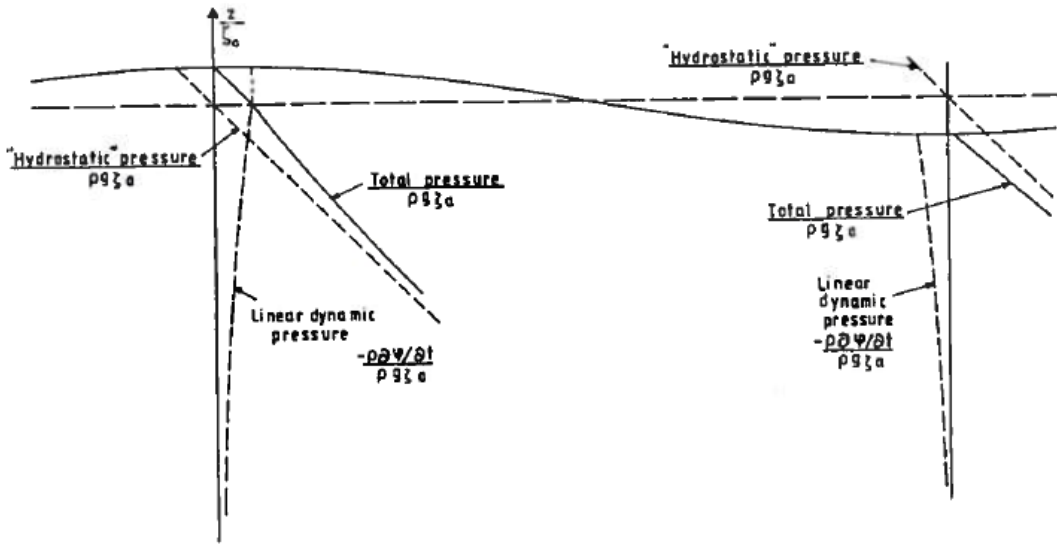


Figure 2-3 Pressure variation under a wave crest and wave trough [8]

The movement of the water particles depends on the water depth. In deep water the water particle move in a circular motion according to the harmonic wave, while in shallow water the water particle will move in an elliptic motion (See figure 2-4). Deep water is defined as where the water depth is greater than half of the wave length, $h \geq \frac{\lambda}{2}$. [9]



Figure 2-4 Motion of water particles in deep water (left) and shallow water depth (right) [8]

2.3 Irregular Wave Theory

An irregular sea condition consists of many different regular waves merging together creating a disturbed wave picture. If we consider a sea state where the surface is build-up of a number of long-crested waves with different wave amplitude and frequency then we can express the surface elevation as:[10]

$$\zeta(x, t) = \sum_{n=1}^N \zeta_{An} \cos(\omega_n t - k_n x + \varepsilon_n) \quad \text{Equation 2.9}$$

In equation 2.9 N is the total number of regular waves and n is the individual wave number. The phase angle ε_n is considered as a stochastic variable which are statistically independent and identically rectangular distributed between 0 and 2π . Further we assume that the wave process within a short term perspective (30 min – 3 hours) is stationary with constant mean value and standard deviation. The surface elevation is assumed to be normally distributed with mean value equal to zero and a standard deviation σ^2 . The wave process is also assumed to be ergodic, which means that a single wave time series is representative for the whole wave process. If we consider a single regular wave, then the energy per unit is given by:

$$E_n = \frac{1}{2} \rho g \zeta_{An}^2 \quad \text{Equation 2.10}$$

Equation 2.10 represents the energy within one wave component in a wave process, so if we sum up all the energy components in an irregular sea state we get the total energy for that sea state (eq. 2.11).

$$\frac{E}{\rho g} = \sum_{n=1}^N \frac{1}{2} \zeta_{An}^2(\omega_n) \quad \text{Equation 2.11}$$

$\zeta_{An}^2(\omega_n)$ is the wave amplitude with corresponding wave frequency ω_n . If we now introduce the wave spectrum, $S(\omega_n)$, to the wave elevation we can express the energy within a frequency interval $\Delta\omega$ by equation 2.12.

$$\frac{1}{2} \zeta_{An}^2 = S(\omega_n) \Delta\omega \quad \text{Equation 2.12}$$

By combining equation 2.11 and 2.12 we can express the total energy within a wave process as:

$$\frac{E}{\rho g} = \sum_{n=1}^N \frac{1}{2} \zeta_{An}^2 = \sum_{n=1}^N S(\omega_n) \Delta\omega \quad \text{Equation 2.13}$$

If we now let the total number of wave component go to infinity, $N \rightarrow \infty$, so that the frequency interval goes to zero, $\Delta\omega \rightarrow 0$, then the total energy becomes:

$$\frac{E}{\rho g} = \frac{1}{2} \zeta_A^2 = \int_0^{\infty} S(\omega) d\omega \quad \text{Equation 2.14}$$

If we solve equation 2.12 with respect to the wave amplitude and insert the expression in equation 2.9 we get the total wave elevation expressed with the wave spectrum (eq. 2.15).

$$\zeta(x, t) = \sum_{n=1}^N \sqrt{2S(\omega_n)\Delta\omega} \cos(\omega_n t - k_n x + \varepsilon_n) \quad \text{Equation 2.15}$$

There exist several spectrums to describe different sea states. Since we do not have access to the real wave spectrum for the real sea state, we have to use standardized wave spectrums. Two examples of wave spectrum are Pierson-Moskowitz and JONSWAP spectrum. The Pierson-Moskowitz spectrum is based on wave measurements from the North Atlantic Ocean while the JONSWAP spectrum is based on measurements from the south-eastern part of the North Sea. In this thesis I have used a JONSWAP spectrum given by equation 2.16.[11]

$$S(\omega) = \frac{\alpha g^2}{\omega^5} \exp\left(-\beta \left(\frac{\omega_p}{\omega}\right)^4\right) \gamma \exp\left(-\frac{1}{2} \left(\frac{\omega - \omega_p}{\sigma \omega}\right)^2\right) \quad \text{Equation 2.16}$$

where

- α spectral parameter
- ω_p peak frequency, $\omega_p = 2\pi/T_p$
- γ peakedness parameter
- β form parameter, default value $\beta = 1.25$
- σ spectral parameter with default values
 - $\sigma = 0.07$ for $\omega < \omega_p$
 - $\sigma = 0.09$ for $\omega > \omega_p$

2.4 Wave loads

The wave exciting forces and moments on a structure are the loads when we have an incident wave and the structure is restrained from oscillating.[8] If we assume that we have a regular sinusoidal wave, the unsteady fluid pressure can be divided into two effects. The first effect is that the undisturbed incoming wave will induce an unsteady pressure field. This unsteady pressure field creates a force called the Froude-Kriloff force. The second effect is a force created because the structure changes the unsteady pressure field around the structure. This force is called the diffraction force. To find this diffraction force one have to solve the boundary value problem for the velocity potential. For a cylindrical structure the Froude-Kriloff force and the diffraction force is the mass force in Morison's equation (eq. 2.17). Morison's equation can be modified for a floating cylinder. If a strip dz of the cylinder has a velocity $\dot{\eta}$ and acceleration $\ddot{\eta}$ then the hydrodynamic force on the strip will be:

$$dF = \rho \frac{\pi D}{4} C_M a_x dz - \rho \frac{\pi D^2}{4} (C_M - 1) \dot{\eta} dz + \frac{1}{2} \rho C_D (u - \dot{\eta}) |u - \dot{\eta}| dz \quad \text{Equation 2.17}$$

In equation 2.17 a_x is the water particle acceleration, C_M is the added mass coefficient, C_D is the quadratic drag coefficient, ρ the water density and D is the cylinder diameter. The last term in equation 2.17 is the quadratic viscous drag force. In general we can introduce a linear drag force in Morison's equation, but for a floating cylinder structure the quadratic drag force will dominate and the linear term will not be included.

In equation 2.17 the small body assumption has been applied. That means that the structure is small compared to the wave length, $\lambda > 5D$. In figure 2-5 you can see which forces that dominates for different wave length – diameter ratios. We see from the figure that for large structure, $\lambda < 5D$, the diffraction force becomes important while for smaller structures the viscous and mass forces are the dominating forces.

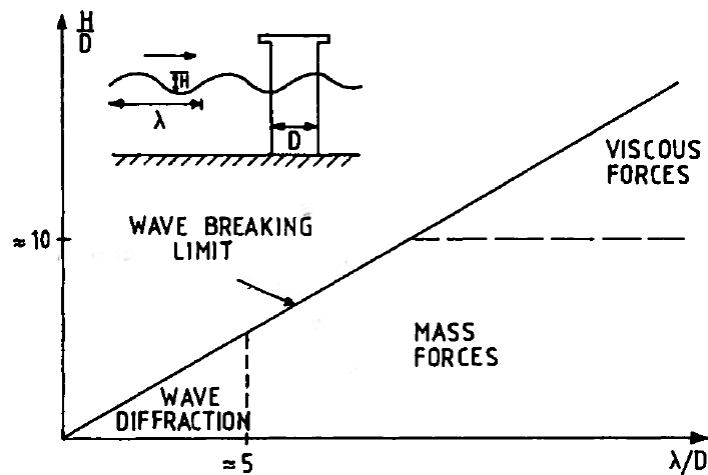


Figure 2-5 Dominating forces on marine structures [8]

2.5 Wind Theory

The wind varies both over space and time. When you are considering a location for offshore wind turbine it is important to know these variations to get an overview over the energy resources of the location. The variations of wind over space and time are listed below: [7]

Space variations:

- Trade winds emerging from subtropical, anticyclonic cells in the north and southern hemisphere.
- Difference in temperature between land and sea generates seasonal winds such as monsoons.

- Sub-polar flows and westerlies.
- Synoptic-scale motions.
- Differential heating of cold breezes and topological features causes mesoscale wind systems.

Time variations:

- Annual variations of wind in a special site.
- Diurnal and semidiurnal variations.
- Seasonal and monthly variability.
- Turbulence, variations in the range from seconds to minutes.

The variation of the wind over time is usually represented by the energy spectrum of the wind. Most of the wind energy is concentrated around two separated time periods, namely diurnal and 1 minute periods. As a result of this we can split the wind speed into two terms. The first term is the quasi-static wind speed which often is referred to as mean wind speed. The second term is the turbulent wind which is the dynamic part of the wind speed. With these two parts the time-varying wind speed becomes a combination of mean wind speed and fluctuations around the mean wind speed. The mean wind speed is a function of height above mean sea level and a height coefficient (often referred to as roughness parameter).(eq. 2.18)[11]

$$\bar{u}(z) = \bar{u}_r \left(\frac{z}{z_r} \right)^\alpha \quad \text{Equation 2.18}$$

where

- z height above water plane
- z_r reference height, normally 10 m
- \bar{u}_r average velocity at a height z_r above surface
- α height coefficient (0.10 – 0.14)

The wind turbulence varies much over a short period of time (seconds to minutes) and can be described in a given point in space using a wind power spectrum. Equation 2.19 shows the Kaimal wind spectrum.

$$S_{Kaimal}(f) = 4\sigma_u^2 \cdot \frac{L_k}{U_m} \cdot \frac{1}{\left(1 + 6f \cdot \frac{L_k}{U_m}\right)^{\frac{5}{3}}} \quad \text{Equation 2.19}$$

where

$$\sigma_u = T_I \cdot (U_m \cdot 0.75 + 5.6)$$

$$L_k = 8.1 \cdot \lambda$$

and

- λ Spectral parameter
- U_m mean wind speed at height above water plane
- T_I turbulence intensity.

2.6 Fatigue

Fatigue is caused by cycle loading and is an important design criterion for a floating wind turbine because of the cyclic wind and wave loading the structure is exposed to throughout the service life. Fatigue damage is based on the structural response of a structure. The response can either be represented in the frequency domain or in the time domain. In the frequency domain the response is represented by a response spectrum while in the time domain the response is represented as a time series. If the response in the frequency domain can be described by a Rayleigh distribution, then the Rayleigh approximation for damage can be applied (eq. 2.20). This holds for narrow banded Gaussian response. Standard deviation σ_s and mean upcrossing rate ν_0 is then based on the solution of the equation of motion in frequency domain. [12]

$$D = \frac{\nu_0 T}{K} (2\sqrt{2} \sigma_s)^m \Gamma\left(1 + \frac{m}{2}\right) \quad \text{Equation 2.20}$$

where K is a material parameter, m is the slope of the SN-curve and T is total time.

From the stochastic time domain response it is possible to calculate the short-term fatigue damage in two different ways:

- Direct use of the calculated stress-cycle distribution from rainflow counting.
- Select a relevant probability distribution and estimate the parameter of the distribution based on the time series. The fatigue damage is calculated by integrating the probability distribution versus the SN-curve.

Rainflow counting is the most commonly used cycle counting method and was introduced by Matsuishi and Endo in 1968. The definition of the rainflow algorithm is as follows [13]: *From each local maximum M_k one shall try to reach above the same level, in the backward and forward directions, with an as small downward excursion as possible. The minima on each side are identified. The minimum that represents the smallest deviation from the maxima is defined as the corresponding rainflow minimum m_k^{RFC} .* See figure 2-6 for illustration.

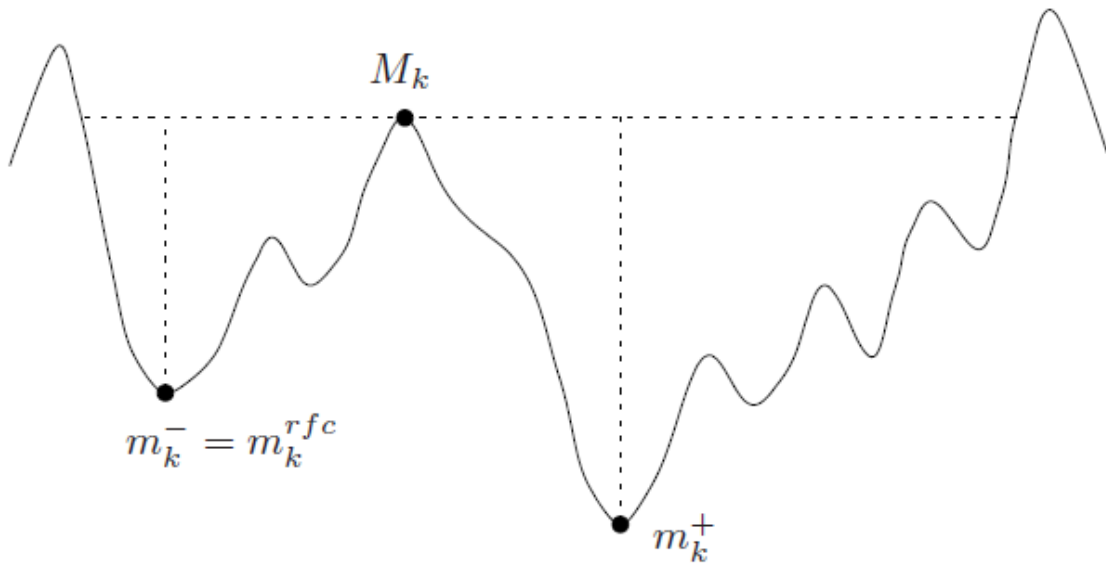


Figure 2-6 Definition of the rainflow cycle [13]

If you assume a given number of cycles to failure for a given stress range, i.e. SN-curves, the Palmgren-Miner sum (eq. 2.21) can be used to calculate fatigue damage for a single time series.

$$D = \sum_{i=1}^n \frac{n_i}{K} S_i^m \quad \text{Equation 2.21}$$

where n_i is the number of cycles counted for stress range S_i , K is material parameter and m is slope of SN-curve. For several time series fatigue damage calculations can follow the following procedure:

- The environmental conditions are divided into a number of representative blocks.
- Each block represents a single environmental load condition for which the probability of occurrence is calculated.
- The fatigue damage is computed for each single environmental condition with Palmgren-Miner summation.
- The accumulated fatigue damage from all the environmental conditions is calculated from equation 2.22.

$$D_{Tot} = \sum_{i=1}^{N_s} D_i P_i \quad \text{Equation 2.22}$$

where D_{Tot} is the total damage from all the environmental conditions, N_s is the total number of environmental conditions, D_i is the damage from Palmgren-Miner sum and P_i is the probability of occurrence of each individual environmental condition.

In fatigue damage calculations it is very important that the stresses are calculated in agreement with the definition of the stresses to be used together with a particular SN-curve. In the DNV standard for fatigue calculations three different concepts of SN-curves are defined:[14]

- Nominal stress SN-curve. Nominal stress is stress in a component that can be derived by classical theory such as beam theory. Nominal stress is often taken as the membrane stress.
- Hot spot stress SN-curve. Hot spot stress is the geometric stress created by the considered detail.
- Notch stress SN-curve. The notch stress is defined as the total stress resulting from the geometry of the detail and the non-linear stress field due to the notch at the weld toe

The three stress concepts are illustrated in figure 2-7 for a simple plate specimen with an attachment.

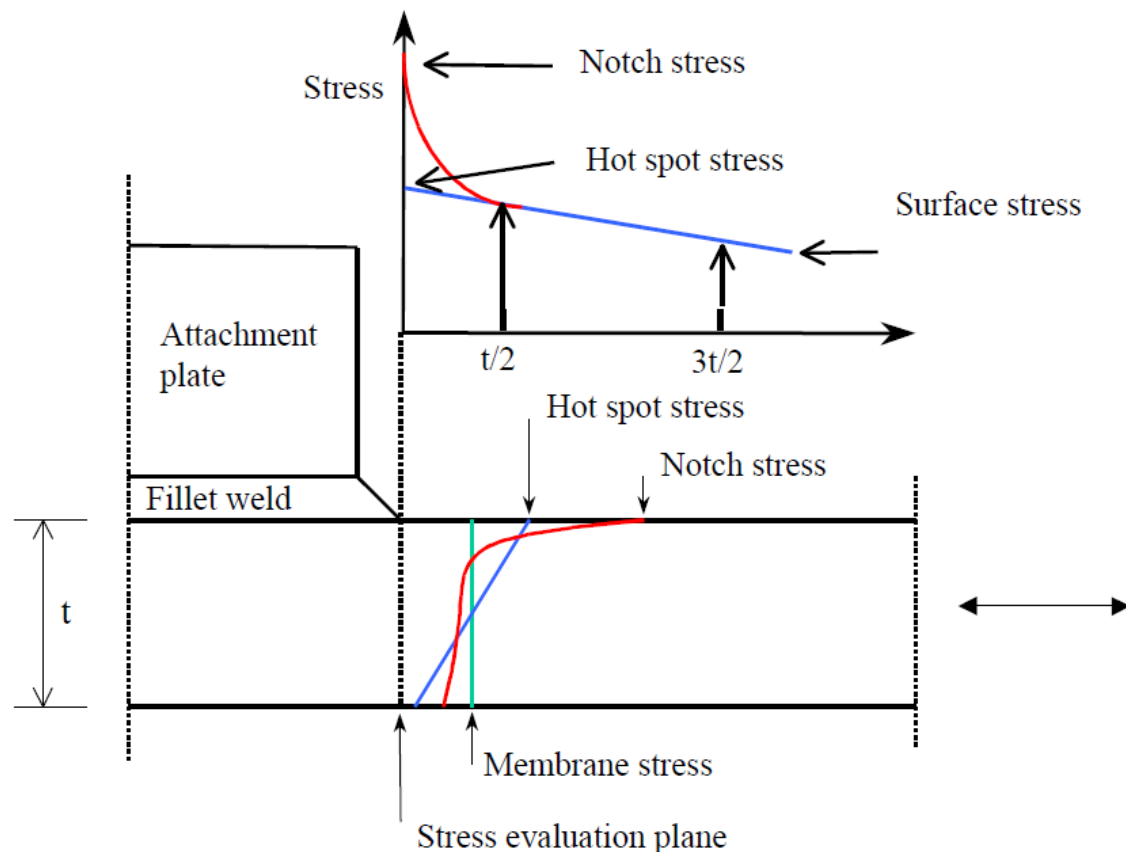


Figure 2-7 Stress concepts for welded structure [14]

For plated structures using nominal stress S-N curves the joint classification and corresponding S-N curves takes into account the local stress concentrations created by the joints themselves and by the weld profile, so the nominal stress or membrane stress can be considered as the design stress. However, if the joint is located in a region of stress concentration resulting from the gross geometry of the structure, a stress concentration factor (SFC) must be included to get the correct design stress. The local design stress with the SFC is given as:

$$\sigma_{local} = SFC \cdot \sigma_{nominal} \quad \text{Equation 2.23}$$

The stress concentration factor is dependent on the geometry and may be defined as the ratio of hot spot stress range over nominal stress range.

The SN-curve gives the number of cycles to failure (N) for a given stress range (S) and are derived by fatigue testing of small specimens in test laboratories. For fatigue design, welded joints are divided into several classes, each with a corresponding design SN curve. Tubular joints are assumed to be class T, while other types of joints may fall under one of the 14 classes specified in the DNV standard.

Which joint classification the joint will fall under may depend upon:

- The geometrical arrangement of the detail
- The direction of the fluctuating stress relative to the detail
- The method of fabrication and inspection of the detail

The basic SN-curve is given by:

$$\log N = \log \bar{a} - m \log \Delta\sigma \quad \text{Equation 2.24}$$

where

N predicted number of cycles to failure for stress $\Delta\sigma$

$\Delta\sigma$ stress range

m negative inverse slope of SN-curve

$\log \bar{a}$ intercept of log N-axis by SN-curve, and is given by:

$$\log \bar{a} = \log a - 2 \cdot S_{\log N} \quad \text{Equation 2.25}$$

where

$\log a$ intercept of mean SN-curve with the log N-axis

$S_{\log N}$ standard deviation of logN

The fatigue strength may be dependent on the plate thickness. This thickness effect is considered through a thickness exponent. There are given different SN-curves for which environmental condition the material is subjected for, namely SN-curves for air, sea water with cathodic protection and sea water without cathodic protection. Figure 2-8 shows the SN-curve for the different joint classification in sea water with cathodic protection.

The axial stress (equation2.26) is calculated in this thesis. It is uncertainties regarding if von Mises stresses can be used in fatigue calculations. The DNV fatigue standard claims that stress ranges calculated based on von Mises stress can be used for fatigue analysis of notches in base material where initiation of a fatigue crack is a significant part of the fatigue life. The von Mises stress will always be positive which halves the actual stress range. They are also unidirectional, while fatigue cracks are directional, so this suggests that von Mises stresses are not recommended for fatigue analysis. The axial stress together with nominal stress SN-curve is used to calculate the damage from the Palmgren-Miner sum.

$$\sigma_x = \frac{N_x}{A} + \frac{M_z}{I_z} y + \frac{M_y}{I_y} z \quad \text{Equation 2.26}$$

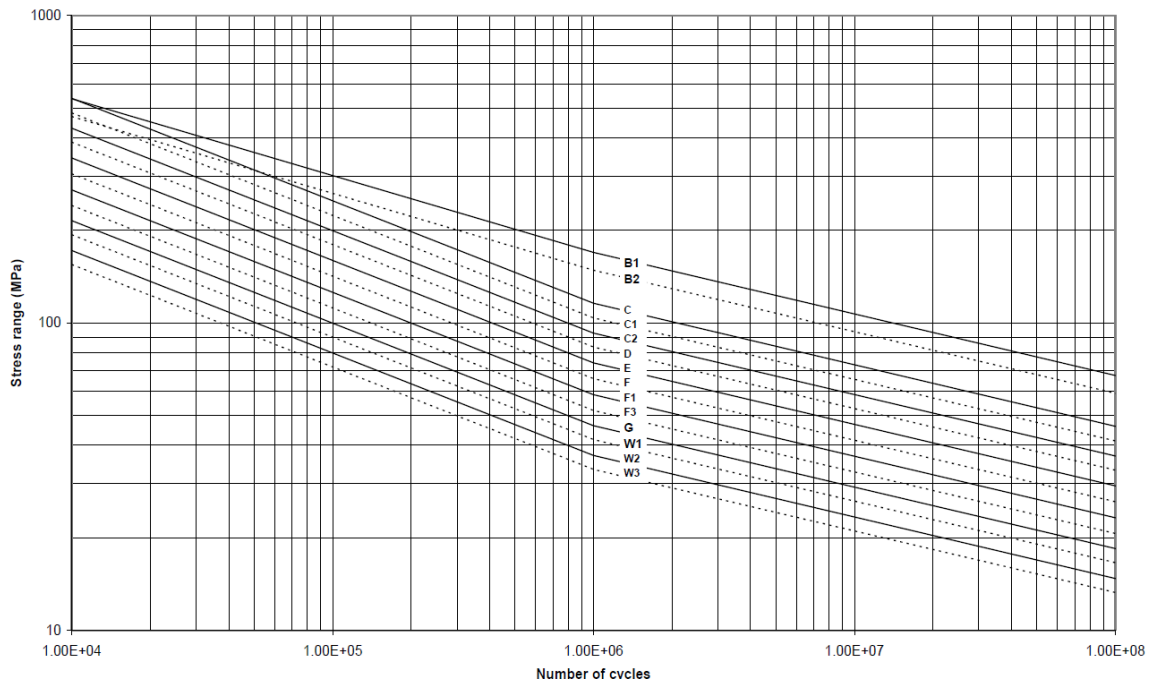


Figure 2-8 SN-curve in sea water with cathodic protection [14]

3 Modelling and Programming

3.1 General

The design and modelling of the floating support structure was performed in my pre-project [15] and has been modified in this thesis to include the NREL 5-MW wind turbine. The design of the floating support structure is based on previous designs of spar-type structures with minor modifications to fulfil the design criteria in this thesis. The main design criteria for the floater are total displacement of the submerged spar of 8016 m^3 and total draft of the spar of 80 m . In addition the following criteria must be fulfilled:

- Based on the weight of the structure and mooring system the structure must remain in static vertical equilibrium.
- Natural pitch period $T_{n,pitch}$ must be larger than the wave period range. Limit is set to be: $T_{n,pitch} > 27 \text{ s}$
- Natural heave period $T_{n,heave}$ must be larger than the wave period range. Limit is set to be: $T_{n,heave} > 28 \text{ s}$
- Vertical stability requirement must be fulfilled.

It is important to have natural periods which do not counteract with wave periods to avoid large resonance motions.

3.2 Floating Support Structure

The floating support structure has a displacement of 8016 m^3 , total length of 90 m and draft of 80 m (figure 3-1). The cross-section of the spar is cylindrical shaped and double-symmetrical. The support structure consists of two sections, one above mean water level (MWL) and one below MWL. The section above MWL is 10 m high and shaped as a cone with lower diameter of 6.5 m and upper diameter of 6 m . The upper part of this section is connected to the base of the wind turbine tower. The section below MWL consists of one cone section, one upper cylindrical section and one lower cylindrical section. The upper cylindrical section is 14 m long with a diameter of 6.5 m and ranging from MWL to 14 m below MWL. The reason for the relatively small diameter of the upper cylinder is because it is desirable to have a slender structure near the MWL to reduce the hydrodynamic loads on the structure. The lower cylindrical section is 60 m long with a diameter of 12.3 m . The cone section is 6 m high and connects the two cylindrical sections. The properties of the floating support structure are summarized in table 3-1.

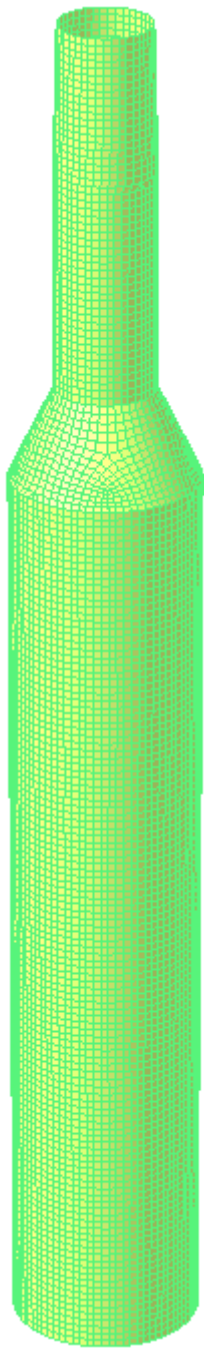


Figure 3-2 Model of floating support structure from HydroD

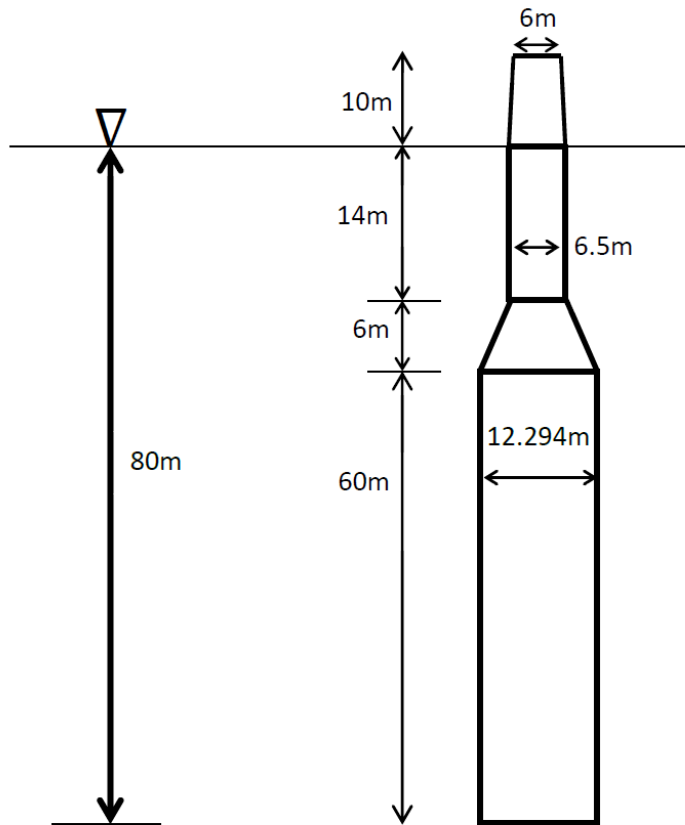


Figure 3-1 Dimension of floating support structure

The modelling of the structure is performed in three steps. First a 3D panel model of the floating structure is modelled and meshed in the computer software GeniE. Due to double-symmetry of the cross section we only have to model one quarter of the spar. The model consists of 12000 second order rectangular elements (or panels) with a mesh size of 0.5 meter. Sufficiently small panel sizes are needed to capture the impact from smaller waves. GeniE creates a finite element file which is input to HydroD. HydroD is an interactive application for computation of hydrostatic and stability, wave loads and motion response for ships and offshore structures. [16] HydroD is used to solve the hydrodynamic linear potential flow problems of radiation and diffraction by utilizing the Wadam code which solves the hydrodynamic problems in the frequency domain. The solution of the diffraction problem gives out the frequency dependent force and moment transfer functions, while the solution to the radiation problem gives out the frequency dependent added mass and damping matrices. For this model Wadam executes the analysis in one direction and for 40 frequencies ranging from 0.01 rad/s

to 2.00 rad/s with frequency interval of 0.05 rad/s. Figure 3-2 shows the model from HydroD. The hydrodynamic results from HydroD together with the finite element file from GeniE are imported into DeepC. DeepC is a software program used to model floating vessels connected to the seabed through mooring lines, tension legs and risers. [5] DeepC consist of the two Marintek developed programs SIMO and Reflex which perform the non-linear time domain finite element simulations. SIMO simulates the motion and station-keeping behaviour of a complex system of floating vessels and suspended loads [11] while Reflex executes the analysis of slender structures like risers, mooring lines, umbilicals and steel pipelines. [17]

Total Draft of the Floating Support Structure	80 m
Elevation from Floating Support Structure to tower base	10 m
Depth to the top of lower cone	14 m
Depth to the top of lower cylinder	20 m
Diameter upper cylinder	6.5 m
Diameter tower base	6.0 m
Diameter lower cylinder	12.3 m
Floating support structure mass, included ballast	7,519,100 kg
Displacement	8016 m ³
Centre of Gravity of support structure only	- 61.3 m
Centre of Gravity of support included tower and turbine	- 49.3 m
Centre of Buoyancy	- 45.7 m
Pitch Moment of Inertia about CG, support only	1,689,695,022 kgm ²
Roll Moment of Inertia about CG, support only	1,689,695,022 kgm ²
Yaw Moment of Inertia about CG, support only	50,293,217 kgm ²

Table 3-1 Properties of Floating Support Structure

3.3 Tower and Turbine System

The wind turbine used in this thesis is the NREL offshore 5-MW baseline wind turbine. [18] This turbine was developed by the National Renewable Energy Laboratory (NREL) to support concept studies aimed at assessing offshore wind technology. This wind turbine is a conventional three-blade upwind variable-speed variable blade-pitch-to-feather-controlled turbine. The main properties of the tower and wind turbine are listed in table 3-2.

Rating	5 MW
Rotor Orientation, Configuration	Upwind, 3 Blades
Control	Variable Speed, Collective Pitch
Drivetrain	High Speed, Multiple-Stage Gearbox
Rotor, Hub Diameter	126 m, 3 m
Hub Height	90 m
Cut-In, Rated, Cut-Out Wind Speed	3 m/s, 11.4 m/s, 25 m/s
Cut-In, Rated Rotor Speed	6.9 rpm, 12.1 rpm
Rated Tip Speed	80 m/s
Overhang, Shaft Tilt, Precone	5 m , 5°, 2.5°
Rotor Mass	110,000 kg
Nacelle Mass	240,000 kg
Tower Mass	347,460 kg
Coordinate Location of Overall CM	(-0.2 m, 0.0 m, 64.0 m)
Length of blade	61.5 m
Blade Mass Moment of Inertia (w.r.t Root)	11,776,047 kgm ²
Hub Mass Moment of Inertia about Low-Speed Shaft	115,926 kgm ²
Nacelle Mass Moment of Inertia about Yaw Axis	2,607,890 kgm ²
Tower Mass Moment of Inertia about Yaw Axis	2,265,257 kgm ²

Table 3-2 Tower and Wind Turbine Properties [18]

The tower has a length of 87.6 m where the diameter linearly decreases with height. The diameter at tower base is 6 m and 3.87 m at the tower top. Total weight of the tower is 347,433 kg. The modelling of the tower and turbine is performed directly in DeepC as flexible elements and are based

on the model from Chenyu Luan (see figure 3-3). The tower is divided into eighteen steel pipe sections with individual diameter and wall thickness for each element. The three blades are modelled as massless lines with a clump weight of 17740 kg located at the total centre of gravity of the blades. The weight of the clump weight equals the total mass of one blade. The hub is modelled as a clump weight with volume of 8 m³ and weight of 56780 kg, while the nacelle and shaft are modelled as lines with a total length of 13.2 m and a unit mass of 17391 kg/m. The tower structure is connected to the floating support structure through fairleads.

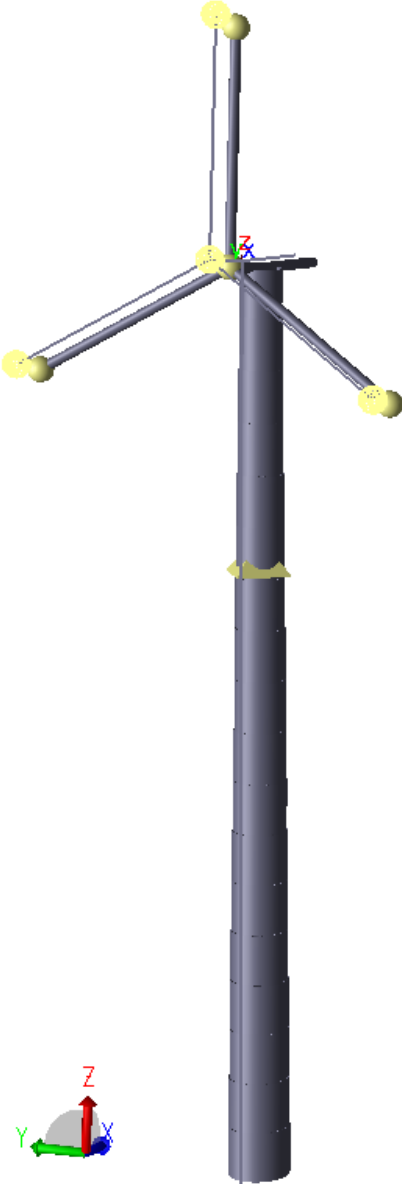


Figure 3-3 Model of Tower and Turbine from DeepC

3.4 Mooring system

A mooring system is designed to prevent a floating structure to move under wind, waves and current. The mooring system (often referred to as stationkeeping system) of a floating structure basically consists of some kind of mooring line connected to the floating structure and to the sea bed. It can either be a single point mooring system or a spread mooring system.

3.4.1 Types of mooring system

The single point mooring systems are primarily used for ship shaped vessels. They allow the vessel to weathervane, which is necessary to minimize the environmental loads on the vessel. The most used single point moorings is turret mooring, CALM (Catenary Anchor Leg Mooring) and SALM (Single Anchor Leg Mooring).[19]

A turret mooring system contains of a number of catenary mooring legs which are connected to a turret, which includes bearings to allow the vessel to rotate around the anchor legs. This property makes turret mooring very beneficial for e.g. a FPSO vessel which allows the vessel to weathervane around the turret.

The CALM system consists of a large buoy supported by a number of catenary chains anchored to the sea bed. Risers and flow lines emerge from the sea floor and are attached to the underside of the CALM buoy. This system is limited to certain environment condition since the buoy has totally different response than the vessel. A solution to this problem is to connect the buoy to the vessel by a rigid structural link which virtually eliminates horizontal motions between the vessel and the buoy.

The SALM system uses a buoy section with large amount of buoyancy which is held steady with a vertical pre-tensioned riser. The vessel is typically connected to the buoy section with a rigid connection. The riser-buoy system will act like a pendulum which will force the system back to equilibrium position when the system is displaced to one of the sides.

Spread mooring system is a group of mooring lines located at the corners of the vessel to keep it in a stable position. The mooring line can be chain, wire rope, fibre rope, or a combination of the three. For double-symmetrical floating structures, such like semi-submersibles and spar, the environmental force acting on the structure will not depend very much on the direction, so the mooring system can

be double-symmetrical designed. The two most used mooring systems for spar and semi-submersibles are catenary mooring and tension legs, or a combination. For a CMS (Catenary Moored Spar) the most commonly used mooring system consist of axisymmetric system with catenary mooring lines in three directions. Each mooring line is connected to the spar through two delta lines (see figure 3-8). In the tension leg concepts (TLP or TLS) the bottom of a platform or a spar is connected to sea floor through a pre-tensioned leg. A single-symmetrical floating structure, e.g. ship, is more sensitive to the environmental directions, so the mooring system becomes more complex. A widely used spread mooring system for ships is the Differentiated Compliance Anchoring System (DICAS). This system operates with different mooring stiffness at the bow and stern of the ship allowing the ship to weathervane. The majority of the restoring force is provided by the mooring group in the bow, but the system stiffness is also dependent on the mooring stiffness at the stern mooring group. As the stiffness of the stern mooring groups decrease, the capability of the vessel to weathervane increase.

3.4.2 Types of mooring lines

Mooring lines for moored floating structures can consist of chain, wire rope, synthetic rope or a combination. In addition to the lines, clump masses and buoys can be used to achieve the required performance of the mooring system. The typical mooring line systems which are used in the industry are all wire rope system, all chain system or a combination system [19].

The mooring line which is most frequently used in the industry throughout the offshore history is chain mooring line. Chain has shown great durability in offshore operations, both due to its resistance capability against bottom abrasion and its contribution to the anchor holding capacity. On the other hand chain is very heavy and for deep water operations the weight of the chain will decrease the vessel's load carrying capacity.

The material choice of large diameter chain should carefully evaluated before fabrication. It is desirable to have the chain manufactured in continuous lengths for each mooring line to avoid chain connection links which can result in fatigue. The steel material used in offshore mooring lines is defined in the DNV Standard for offshore mooring chain [20] and are classified by specified minimum ultimate tensile strength into five grades (See table 3-3).

Steel Grade	Yield Stress	Tensile Strength
	R_e N/mm^2	R_m N/mm^2
R3	410	690
R3S	490	770
R4	580	860
R4S	700	960
R5	760	1000

Table 3-3 Minimum mechanical properties for chain cable materials [20]

For more than 30 years stud chain has been used in offshore industry. Studs are welded on the opposite side to the flash weld and are normally not used for steel grade higher than R3 (Figure 3-4). The industry has experienced some problems with the use of studs, such as fracture at the stud weld, fatigue crack and loose stud. To solve these problems there were produced a new studless chain (see figure 3-4) which has the same breaking strength as stud chain but is 10 % lighter. [19]

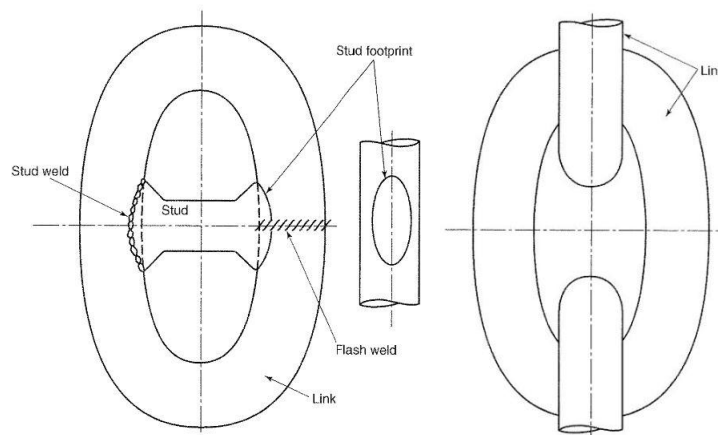


Figure 3-4 Stud chain (left) and studless chain (right) [19]

Wire rope mooring lines provides a greater restoring force than chain for a given pre-tension. This is because wire rope is much lighter than chain. Due to this restoring force for an all wire system, much longer line length is required. Another problem with all wire mooring system is wear due to long term abrasion when the wire is in contact with seabed. For these reasons wire mooring line are used together with other types of mooring lines, such as chain.

The wire rope structure can come in many different variants, but the main concept of a wire rope consist of a number of strands wound in the same rotational direction around a centre core to form a rope. This rotational structure generates torque as tension increases. Some variants of wire rope structure are shown in figure 3-5.

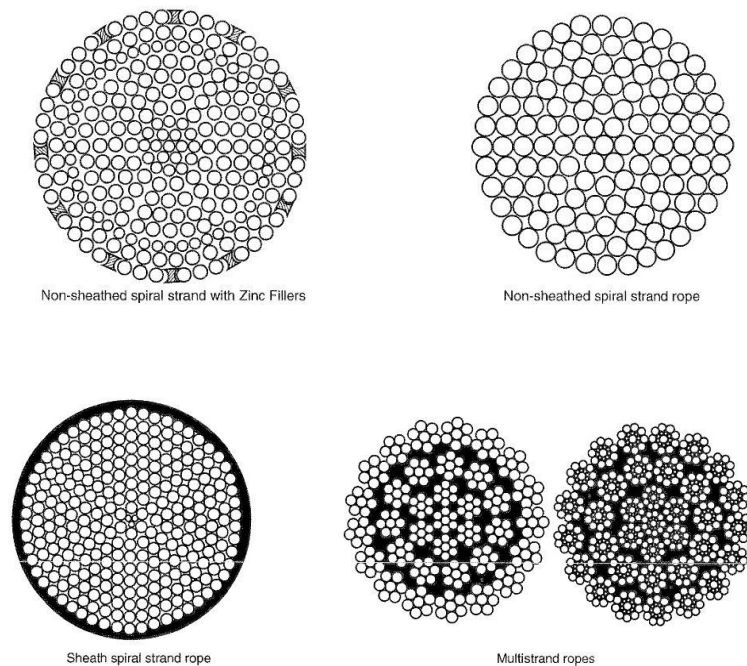


Figure 3-5 Wire Rope Structure [19]

Fibre rope can be used in mooring systems in combination with wire or chain lines. Fibre rope is not very resistant to wear in contact with external object, such as seabed and winching equipment. The most common practice for usage of fibre ropes is to place it in the catenary part of the mooring line or in taut leg systems. The main differences between fibre rope and wire/chain mooring line are that with fibre rope we have to include the non-linear stiffness of the rope, the location of the fibre rope segment must be away from the seabed and fairlead, creep phenomenon and minimum tension requirements has to be taken into account, and the fibre rope require different handling procedures. Fibre rope stiffness increases with mean load, and decreases with cyclic load range over time. Over some time the stiffness of the fibre rope tends go towards a linear function of load range and mean load. Fibre rope can be exposed to certain factors which may limit the service life. These factors can be heating and internal abrasion, hydrolysis, creep rupture, axial compressive fatigue and tension-tension fatigue.

The different fibre types which are considered for usage in mooring lines are polyester, aramid, HMPE (high modulus polyethylene) and nylon.[19] The best fibre rope candidate for offshore mooring system is considered to be polyester. Properties like low cost, good resistance to axial compression fatigue, good strength to weight ratio, good creep resistance and low stiffness which induces less dynamic tension makes polyester suited for offshore mooring systems. Nylon has been

used for hawsers, but it requires frequently inspections and replacements due to abrasion. Nylon can also be used in segments for shallow water mooring lines to absorb the energy from vessel dynamics.

The most common rope construction types are WRC (wire-rope construction) and parallel strand. WRC follow the same concept which is used in wire rope with a braided jacket to protect the strands from abrasion, soil ingress, marine growth and fish bite (see figure 3-6). [21] Parallel strands needs outer jackets to keep the strength core strands together (See figure 3-7).

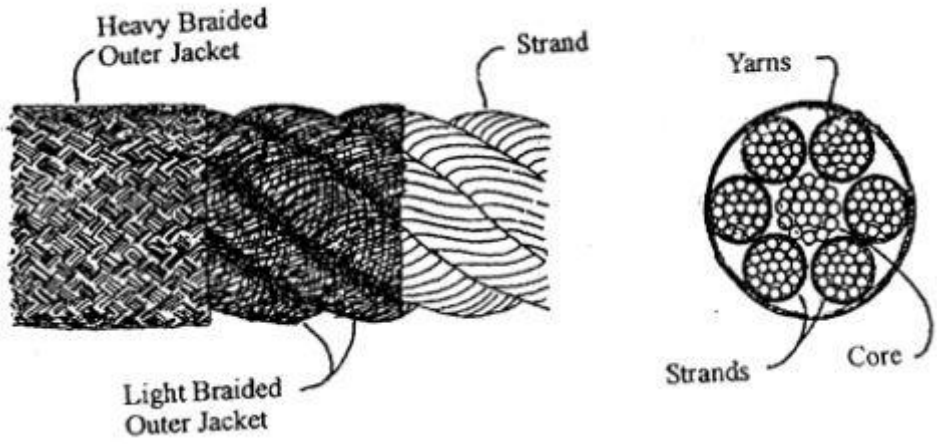


Figure 3-6 Six-strand wire rope construction [21]

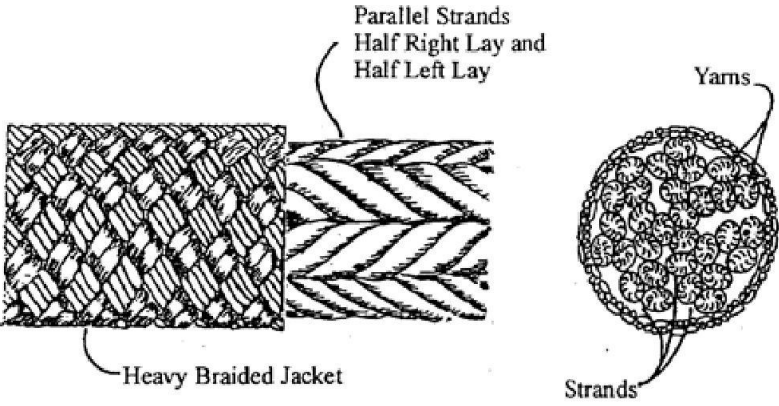


Figure 3-7 Parallel rope construction [21]

3.4.3 Design of mooring system

The mooring system used for the floating wind turbine consists of an axisymmetric system with catenary mooring lines in three directions (See figure 3-8). There are four mooring lines in each direction; two delta lines, one upper line above the clump mass and one lower line below the clump

mass. The delta lines are connected to the floating support structure through fairleads at 40 m below MWL. Clump masses are introduced to the system to increase the system yaw stiffness. The mooring system properties are listed in table 3-4. The mooring lines are modelled directly in DeepC as flexible elements.

Segment	Length [m]	Diameter [m]	Mass/Length [kg/m]	Axial stiffness [kN]
Delta line	12	0.09	77.7066	384243
Upper line	73	0.09	77.7066	384243
Lower line	345	0.09	77.7066	384243
Clump mass	2	2	32500	

Table 3-4 Properties of mooring system

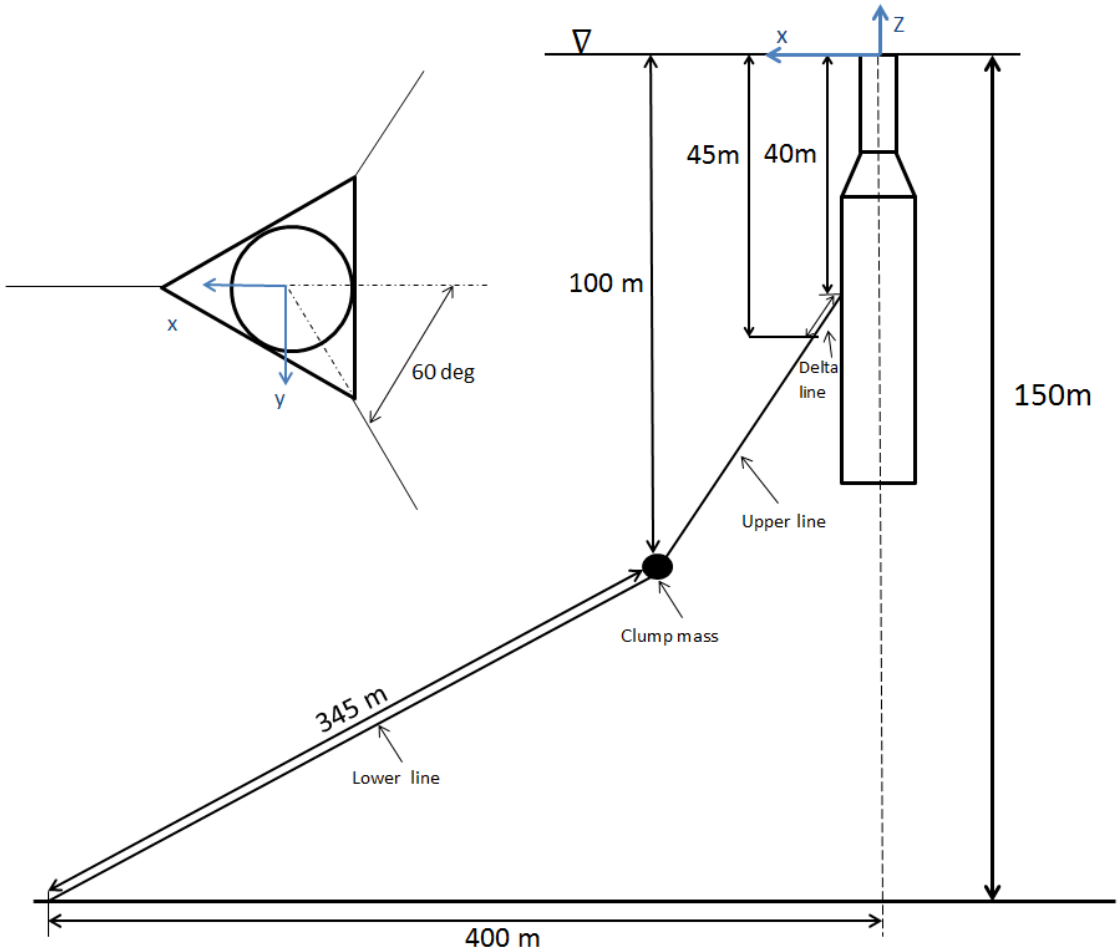


Figure 3-8 Design of mooring system

3.5 SIMO/RIFLEX

The floating support structure, the tower and turbine and the mooring system are coupled and connected through fairleads to create the total floating wind turbine system. Figure 3-9 shows the coupled model from DeepC.

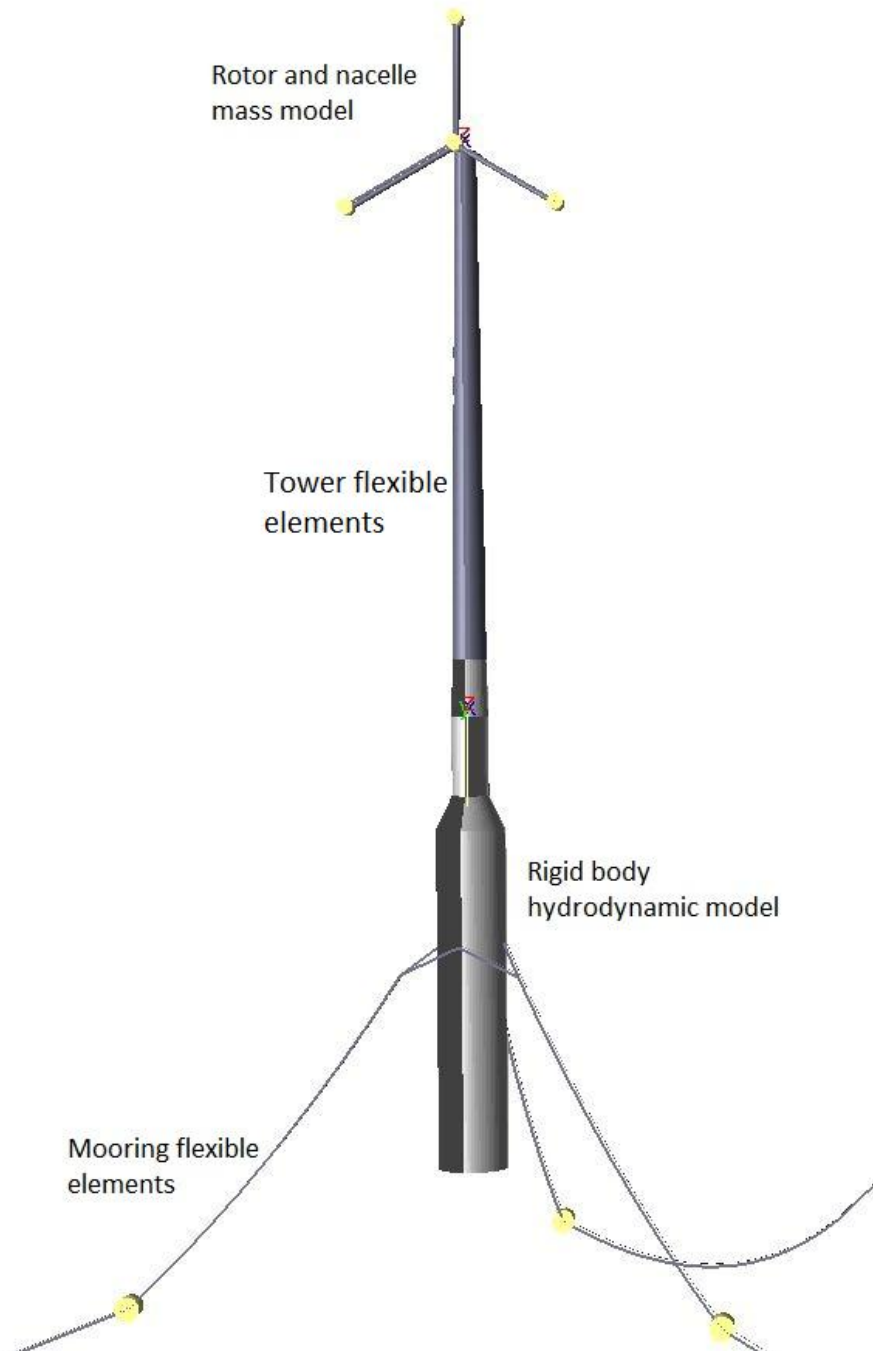


Figure 3-9 Model of the catenary moored floating wind turbine

The analysis of the catenary moored floating wind turbine is performed in the batch mode of SIMO and RIFLEX and not in the DeepC graphical user interface. When performing thousands of analysis it is not beneficial to use DeepC, because it is very time consuming to create load conditions and

execute every single analysis in DeepC. And since the TDHmill extension had to be included, the system input file for SIMO had to be manually changed for each simulation. DeepC is only used for modelling and SIMO/RIFLEX input generation. The procedure of the analysis is as follows:

1. Generate input files for SIMO and RIFLEX from DeepC.
2. Make templates out of the input files. In these templates the relevant parameters are set to be variables. Relevant parameters are e.g. wave height, wave period and simulation length. See example in appendix A
3. Use the template files to mass produce input files for different load cases. This is executed from a Python script where the wanted load cases, simulation length and integration time steps are given. See example in appendix B1
4. Run multiple analyses in batch mode executed from a Python script. See example in appendix B2
5. The results from the analysis are extracted by batch files executing outmod in RIFLEX and s2xmod in SIMO. See example in appendix C
6. Matlab with the WAFO extension is used to process the results. Examples of Matlab codes are shown in appendix E

3.6 Free Decay Test

To find the natural periods of the floating wind turbine, free decay tests are performed in DeepC. Decay tests are performed by moving the system out of its equilibrium position in one of its degrees of freedom and release it when the system has stabilized in the new position. The system will then oscillate around its equilibrium position with the damped natural period until the system has stabilized. The damping ratio and the undamped natural frequency can then be found by using logarithmic decrement. The logarithmic decrement is given by:

$$\delta = \frac{1}{n} \ln \left(\frac{x_0}{x_n} \right) \quad \text{Equation 3.1}$$

where x_0 is the initial amplitude and x_n is the amplitude n peaks away. The damping ratio is found from equation 3.2.

$$\zeta = \frac{1}{\sqrt{1 + \left(\frac{2\pi}{\delta} \right)^2}} \quad \text{Equation 3.2}$$

When the damping ratio and damped natural frequency is found we can use the following relation to find the undamped natural frequency:

$$\omega_n = \frac{\omega_d}{\sqrt{1 - \zeta^2}} \quad \text{Equation 3.3}$$

where ω_d is the damped natural frequency and ω_n is the undamped natural frequency of the floating wind turbine. The natural periods found from the decay tests are given in table 3-5.

Mode	Natural period [s]	Natural frequency [rad/s]
Surge	137	0.045
Sway	137	0.045
Heave	31,8	0.197
Pitch	27,8	0.226
Roll	27,8	0.226
Yaw	5,8	1.083

Table 3-5 Natural periods and frequencies from decay tests

3.7 TDHmill

In order to simulate the dynamic behaviour of the floating offshore wind power facilities using SIMO, a model for the aerodynamic load and gyro moment from the wind has been established separately as a dynamic linked library (DLL) to be called by SIMO. This is performed by the external extension TDHmill. TDHmill is developed by Marintek and Statoil and is a numerical model of thrust from a wind turbine rotor onto the nacelle. [22] The model consists of thrust coefficients tabulated as a function of relative velocity between wind and rotor. The thrust coefficients also include the effect of pitch control above rated wind speed. The gyro moment from the rotor is calculated based on RPM. The turbulent wind at hub height is given as a time series. The TDHmill extension files are shown in appendix A. For wind speeds above rated wind speed, an instability effect will occur since the thrust coefficients are used in the dynamic analysis. Due to forward and backward motions of the rotor, the relative wind speed will change and the negative slope of the thrust force curve (see figure 3-12) as a function of the wind speed increase the motion. By utilising the notch filter in the TDHmill extension the negative damping from the thrust force can be removed.

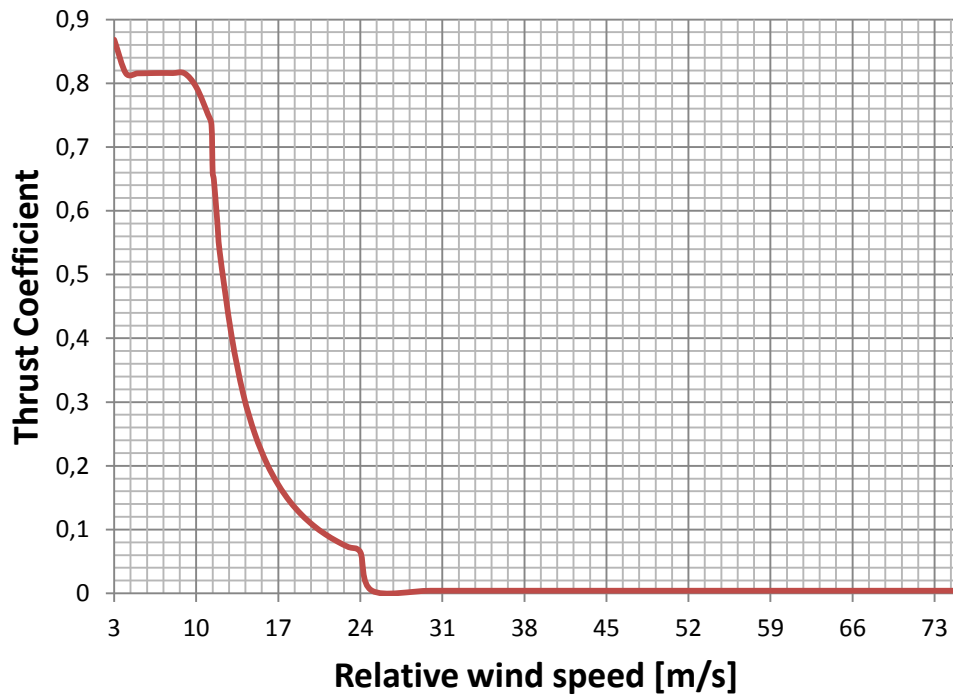


Figure 3-10 Thrust Coefficient as a function of relative wind speed

4 Environmental conditions

4.1 General

To find relevant combination of wind and waves for the analysis the joint distribution for wind and waves in the North Sea was used. [23] The distribution is a joint probabilistic model of mean wind speed, significant wave height and spectral peak period and is based on simultaneous wind and wave measurements from the North Sea in the period 1973 – 1999. In this distribution the wind speed is assumed to have the greatest influence on the loads on the structure, and is therefore chosen as the primary parameter. The significant wave height is chosen as the secondary parameter while the spectral peak period is assumed to be the parameter to have the least influence on the loads. The probabilities are calculated based on bins of 1 m for H_{m0} , 1 s for T_p and 1 m/s for the wind speed.

4.2 Joint Distribution of Simultaneous Wind and Waves

The joint distribution of simultaneous wind and waves is given by equation 4.1.

$$f_{WH_{m0}T_p}(w, h, t) = f_W(w) \cdot f_{H_{m0}|W}(h|w) \cdot f_{T_p|H_{m0}W}(t|h, w) \quad \text{Equation 4.1}$$

The marginal distribution for the mean wind speed, $f_W(w)$, is described by the 2-parameter Weibull distribution (eq. 4.2) and are shown in figure 4-1 for wind speeds in the range 1 – 24 m/s.

$$f_W(w) = \frac{\alpha}{\beta} \left(\frac{w}{\beta}\right)^{\alpha-1} \cdot e^{-\left(\frac{w}{\beta}\right)^\alpha} \quad \text{Equation 4.2}$$

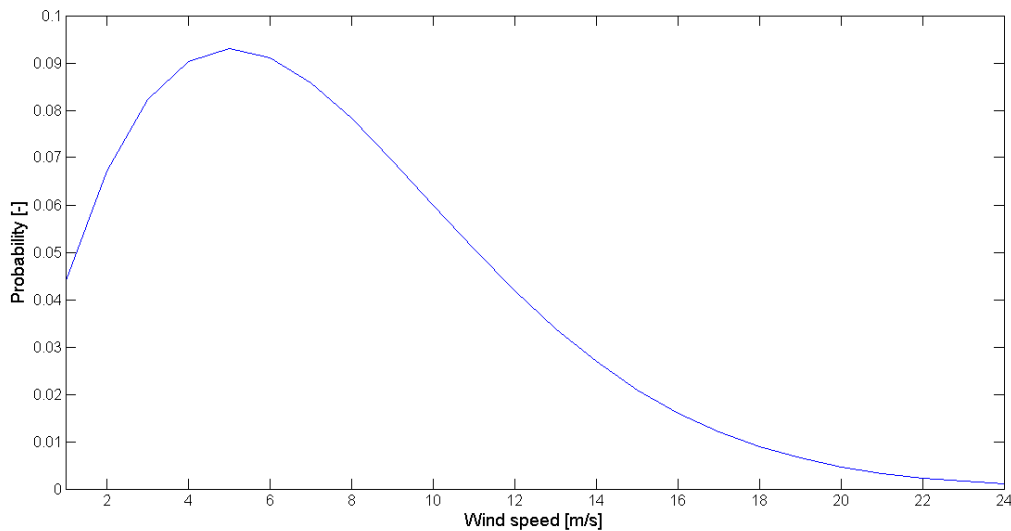


Figure 4-1 Marginal distribution of the mean wind speed

In equation 4.2 the parameters α and β are based on the measurements from the North Sea and have the following values: $\alpha = 1.708$, $\beta = 8.426$. The conditional distribution of the significant wave

height for given mean wind speeds, $f_{H_{m0}|W}(h|w)$, will also be described by the 2-parameter Weibull distribution and the parameter α and β will be depended on the mean wind speed (equation 4.3).

$$f_{H_{m0}|W}(h|w) = \frac{\alpha}{\beta} \left(\frac{h}{\beta}\right)^{\alpha-1} \cdot e^{-\left(\frac{h}{\beta}\right)^\alpha}$$

Equation 4.3

$$\alpha = 2.0 + 0.135 \cdot w$$

$$\beta = 1.8 + 0.1 \cdot w^{1.322}$$

In figure 4-2 the conditional distribution of the significant wave height is plotted for increasing mean wind speeds. We can see from figure 4-2 that the probability peak of the wave height decreases as the wind speed increases while the width of the probability distribution increases as the wind speed increases.

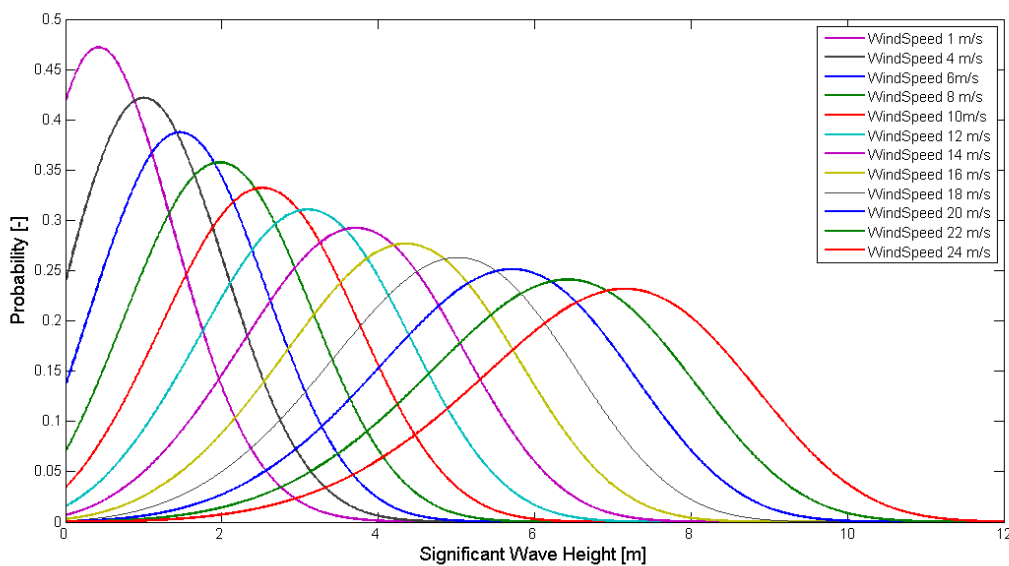


Figure 4-2 Conditional Distribution of Significant Wave Height for given wind speeds

The constant values in equation 4.3 are estimated from regression analysis. The conditional distribution of the peak period for given wind speeds and wave heights, $f_{Tp|H_{m0}W}(t|h,w)$, is described by the log-normal distribution (equation 4.4). Figure 4-3 and 4-4 shows a surface plot and a contour plot of the conditional distribution of the peak period for selected wind speeds, wave heights and peak periods. From figure 4-3 we can see how the probability increases as the wave height and peak period increases. As the wind speed increases, a peak in the distribution occurs for small peak periods and wave heights. This can also be seen from figure 4-4 where the contours increase for small peak period and wave height as the wind speed increases. The width of the distribution becomes narrower as the wind speed increases.

$$f_{T_p|H_{mo}W}(t|h, w) = \frac{1}{t \cdot \sigma_{\ln(T_p)} \cdot \sqrt{2\pi}} \cdot \exp \left[-\frac{1}{2} \cdot \left(\frac{\ln(t) - \mu_{\ln(T_p)}}{\sigma_{\ln(T_p)}} \right)^2 \right] \quad \text{Equation 4.4}$$

The mean value and standard deviation of $\ln(T_p)$ are given by equation 4.5 and 4.6 respectively.

$$\mu_{\ln(T_p)} = \ln \left[\frac{\mu_{T_p}}{\sqrt{1 + v_{T_p}^2}} \right] \quad \text{Equation 4.5}$$

$$\sigma_{\ln(T_p)}^2 = \ln[v_{T_p}^2 + 1] \quad \text{Equation 4.6}$$

where

$$v_{T_p} = \frac{\sigma_{T_p}}{\mu_{T_p}} \quad \text{Equation 4.7}$$

$$\mu_{T_p} = (4.883 + 2.68 \cdot h^{0.529}) \cdot \left[1 - 0.19 \cdot \left(\frac{w - (1.764 + 3.426 \cdot h^{0.78})}{1.764 + 3.426 \cdot h^{0.78}} \right) \right]$$

$$\sigma_{T_p} = [-1.7 \cdot 10^{-3} + 0.259 \cdot \exp(-0.113 \cdot h)] \cdot \mu_{T_p}$$

The constants in equation 4.7 are estimated from regression analysis where all the points from the measurements were included.

The combination of equation 4-2 to 4-7 gives the total joint distribution of simultaneous wind and waves. The distribution is plotted for selected wind speeds as a surface plot in figure 4-5 and as a contour plot in figure 4-6. From these figures we can see how the probability distribution develops as the wind speed increases. The shape of the distribution is almost the same for different wind speeds, while the probability peak decreases as the wind speed increases. In appendix D the distribution is plotted for all the mean wind speeds.

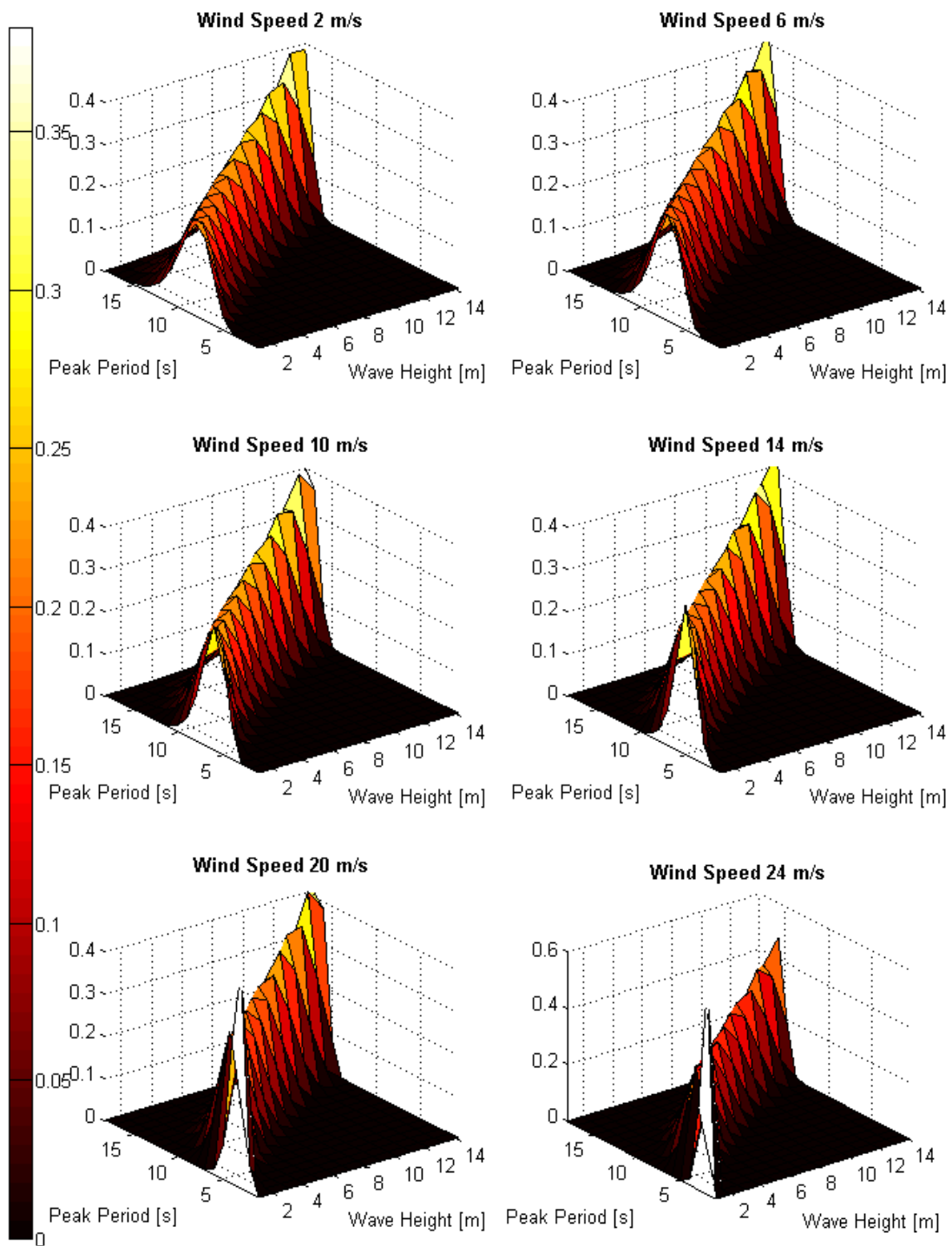


Figure 4-3 Surface plot of the conditional distribution of peak period for given wind speed and wave height

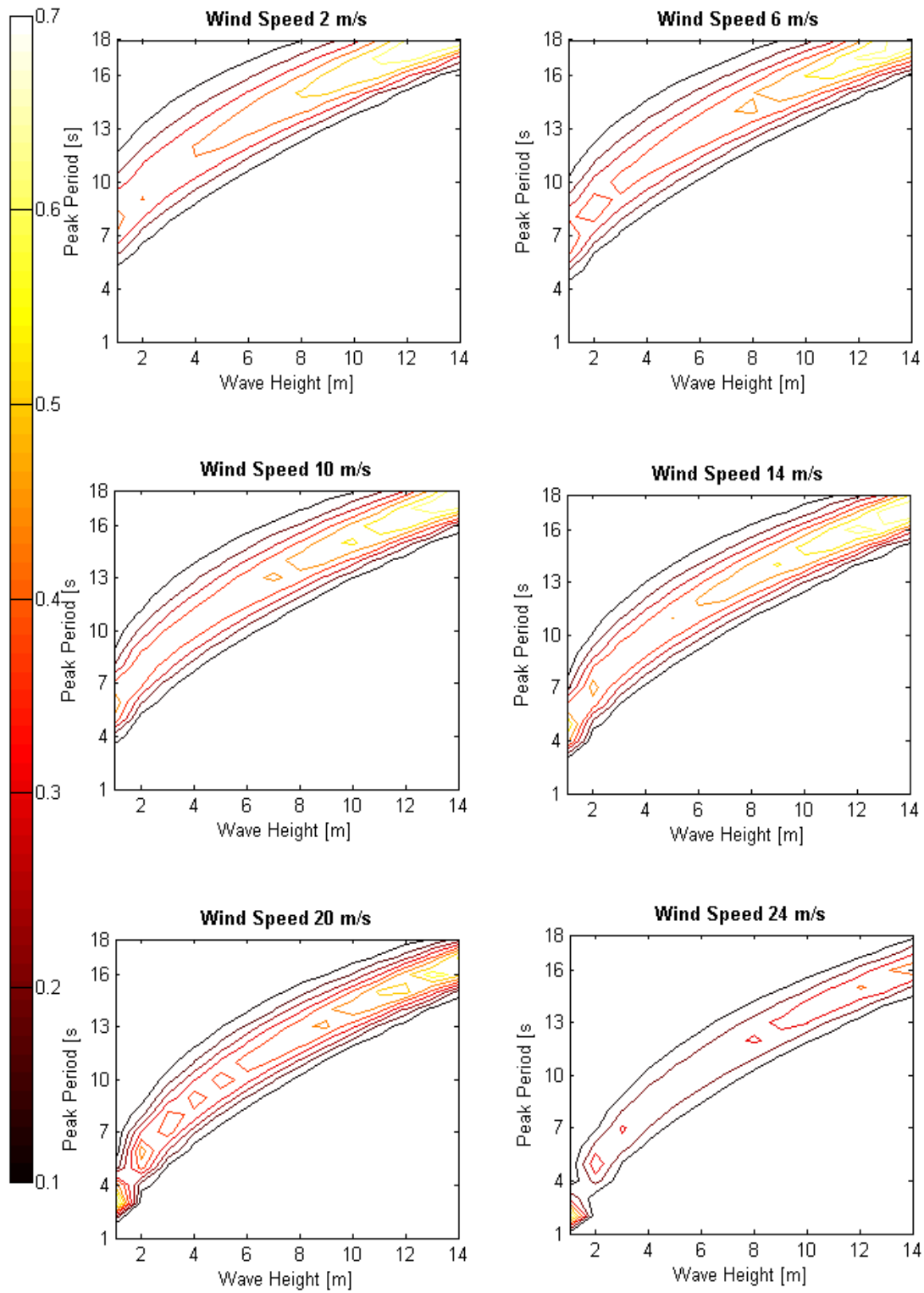


Figure 4-4 Contour plot of the conditional distribution of peak period for given wind speed and wave height

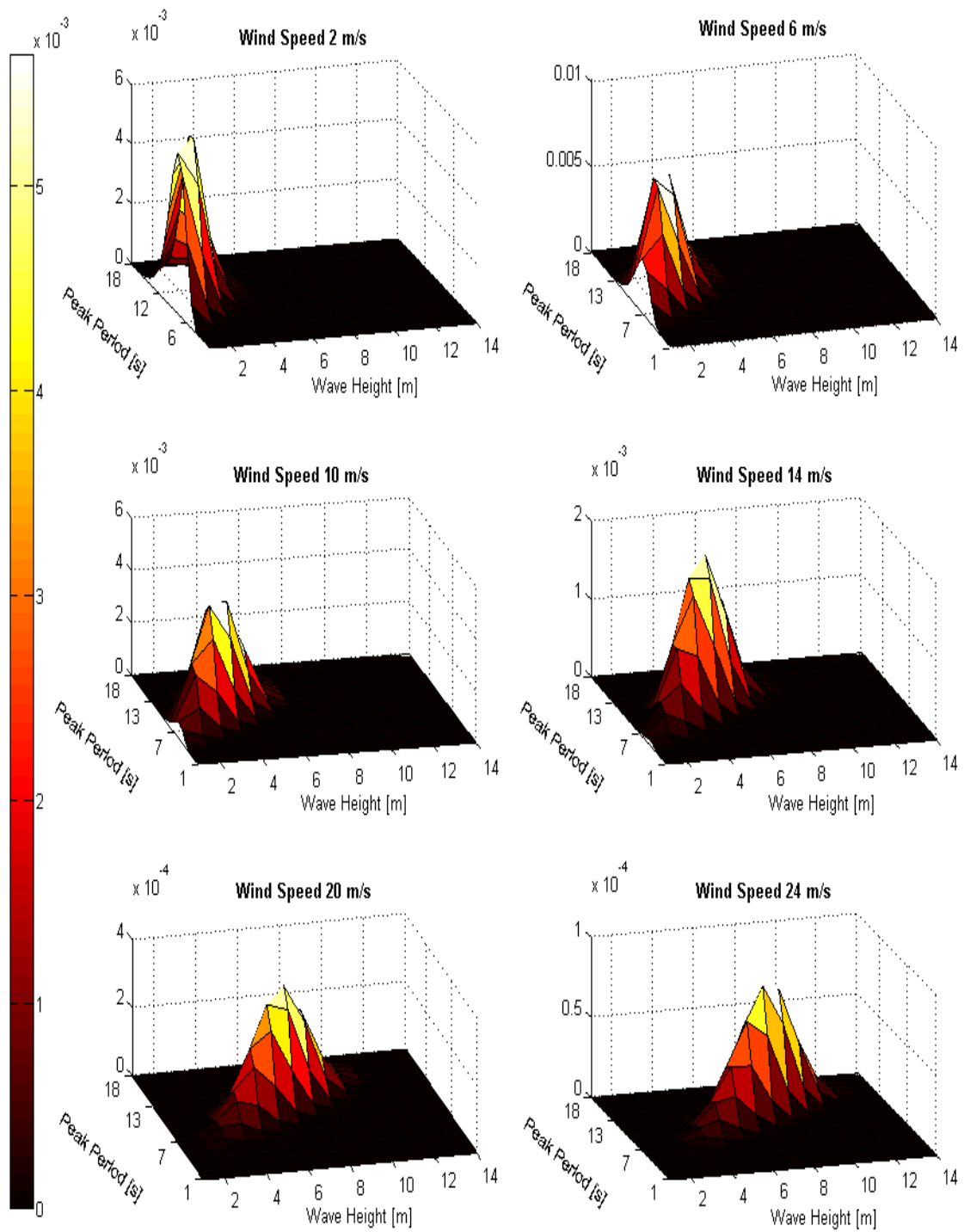


Figure 4-5 Surface plot of the joint distribution of simultaneous wind and waves for selected wind speeds

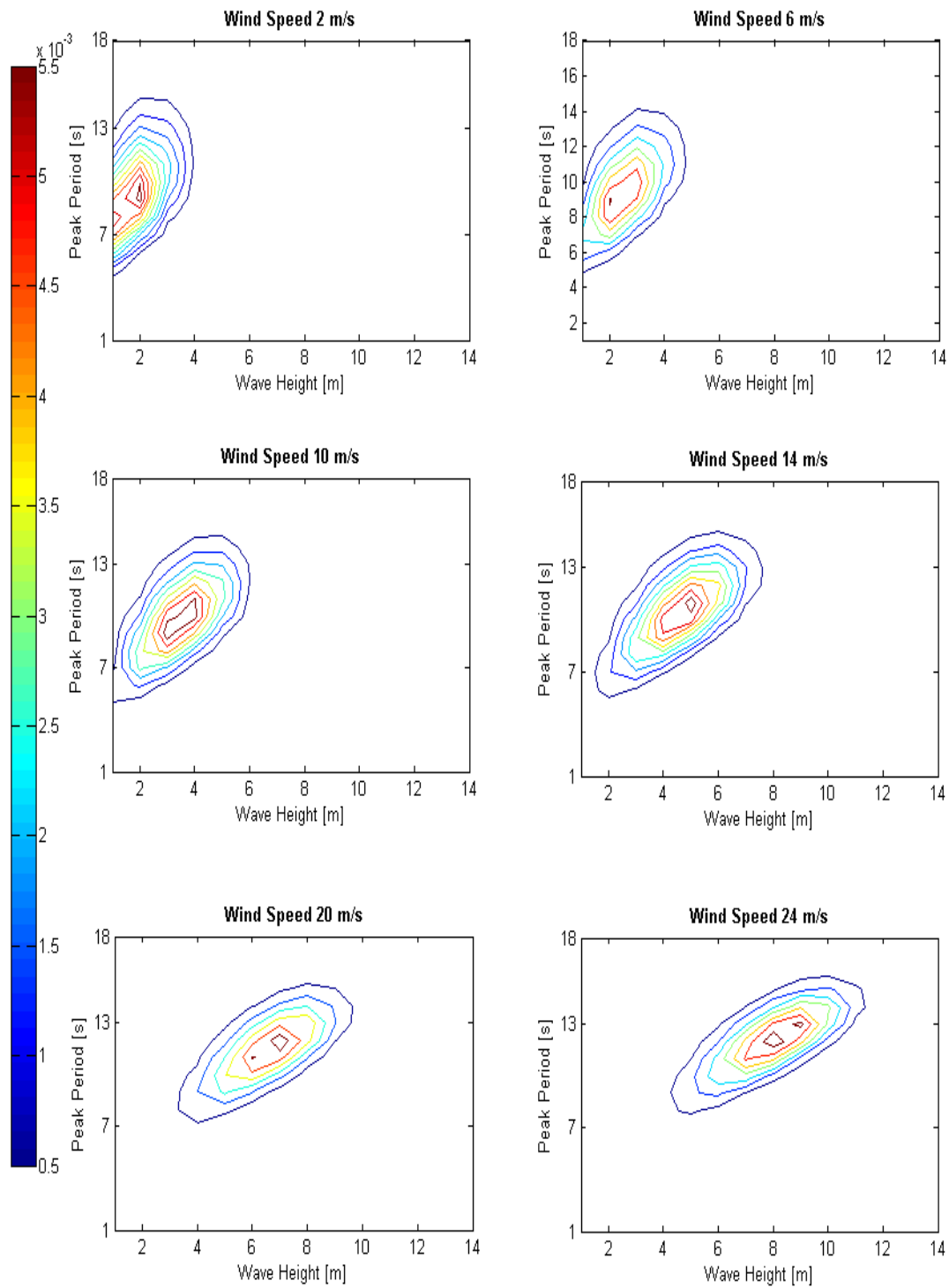


Figure 4-6 Contour plot of the joint distribution of simultaneous wind and waves for selected wind speeds

5 Load Cases

When performing a total fatigue damage analysis of a floating structure, all the different load conditions throughout the service life of the structure should be included. With combinations of wind and wave the number of load cases will reach tens of thousands throughout the service life. In the design phase it is not realistic to perform simulations for all the different load cases.

Based on chapter 4 and appendix D the most probable environmental load cases for each wind speed are picked. In the next chapters a description of the load cases which was used in the fatigue damage analysis is given.

5.1 Load Cases for Sensitivity of Fatigue to Simulation Length

The load cases used in the fatigue analysis of different simulation length consists of twelve load cases with mean wind speed within the operation range of the 5 MW turbine, i.e. 1-24 m/s. The load cases are listed in table 5-1 with the corresponding probability of occurrence. Figure 5-1 shows the probability distribution of the load cases.

Most Probable Load Cases For Simulation Length Analysis

Load Case	Mean Wind Speed [m/s]	Significant Wave Height [m]	Peak Period [s]	Probability of occurrence [-]
1	2	2	9	0,0056
2	4	2	9	0,0082
3	6	2	9	0,0071
4	8	3	9,5	0,0061
5	10	3,5	10	0,005
6	12	4	10	0,0031
7	14	5	11	0,0019
8	16	5,5	11	0,001
9	18	6	11	0,00064147
10	20	7	12	0,00033391
11	22	7,5	12	0,00015424
12	24	8	12	0,000079099

Table 5-1 Most Probable Load Cases for given wind speed

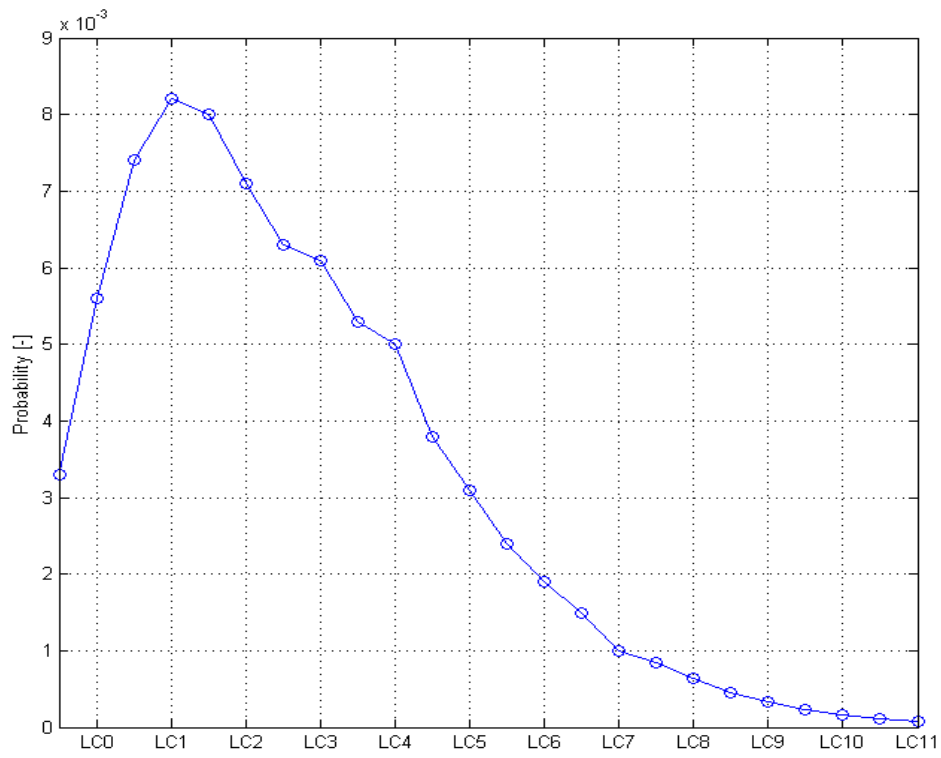


Figure 5-1 Probability distribution of the load cases

5.2 Load Cases for Sensitivity of Fatigue to Peak Period

In this analysis the sensitivity of the peak period for variation of significant wave height with constant wind speed is investigated. The wind speed is kept constant equal to 4 m/s for all the load cases. The load cases are divided into three blocks where the peak period varies from 8 to 10 seconds and significant wave height varies from 1 to 15 m. The wind speed is held constant to give a clearer view on the effect of varying wave height and the value is chosen based on the marginal distribution of the mean wind speed. Total number of load cases in this sensitivity study is 45. The load cases with the corresponding marginal probability are listed in table 5-2 to 5-4. Figure 5-8 shows the marginal probability of the different load cases. We can see from the figure and the tables how the probability goes towards zero for wave heights above 5 m.

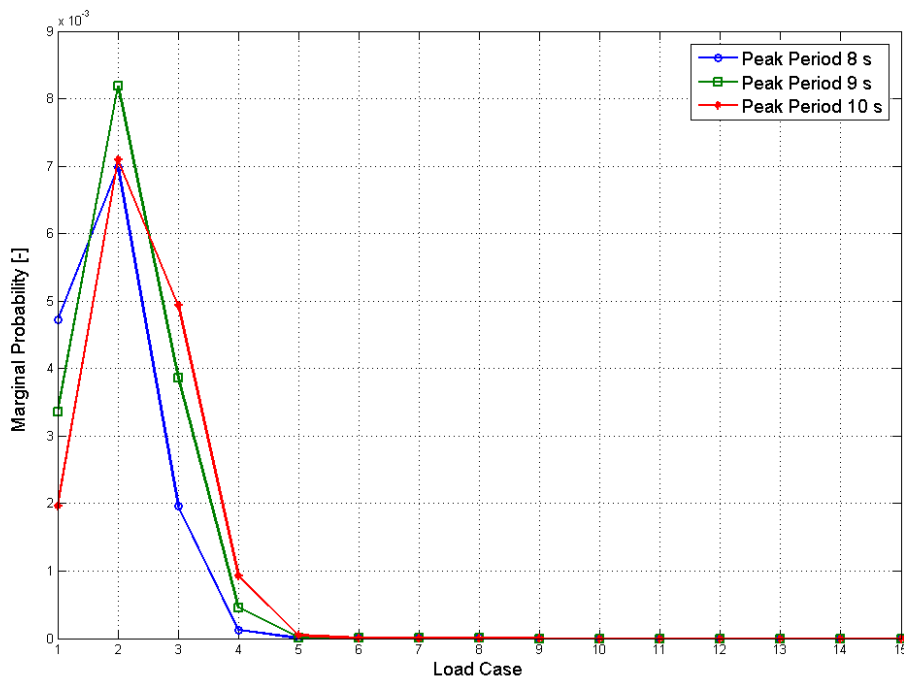


Figure 5-2 Marginal probability of the different load cases in the peak period sensitivity analysis

Load Cases Block 1

Load Case	Wind Speed [m/s]	Significant Wave Height [m]	Peak Period [s]	Probability of occurrence [-]
1	4	1	8	0,00471948
2	4	2	8	0,00697833
3	4	3	8	0,00196222
4	4	4	8	0,00012443
5	4	5	8	1,51E-06
6	4	6	8	2,63E-09
7	4	7	8	4,58E-13
8	4	8	8	4,98E-18
9	4	9	8	1,89E-24
10	4	10	8	1,18E-32
11	4	11	8	4,72E-43
12	4	12	8	3,52E-56
13	4	13	8	1,01E-72
14	4	14	8	1,41E-93
15	4	15	8	6,62E-120

Table 5-2 Load Cases Wave Height Sensitivity Block 1

Load Cases Block 2

Load Case	Wind Speed [m/s]	Significant Wave Height [m]	Peak Period [s]	Probability of occurrence [-]
1	4	1	9	0,00335019
2	4	2	9	0,00818677
3	4	3	9	0,00385776
4	4	4	9	0,00045435
5	4	5	9	1,20E-05
6	4	6	9	5,72E-08
7	4	7	9	3,65E-11
8	4	8	9	2,15E-15
9	4	9	9	7,32E-21
10	4	10	9	7,91E-28
11	4	11	9	1,27E-36
12	4	12	9	1,15E-47
13	4	13	9	1,65E-61
14	4	14	9	7,34E-79
15	4	15	9	1,18E-100

Table 5-3 Load Cases Wave Height Sensitivity Block 2

Load Cases Block 3

Load Case	Wind Speed [m/s]	Significant Wave Height [m]	Peak Period [s]	Probability of occurrence [-]
1	4	1	10	0,00196151
2	4	2	10	0,00709634
3	4	3	10	0,00493965
4	4	4	10	0,00092494
5	4	5	10	4,39E-05
6	4	6	10	4,45E-07
7	4	7	10	7,60E-10
8	4	8	10	1,62E-13
9	4	9	10	2,94E-18
10	4	10	10	2,83E-24
11	4	11	10	7,91E-32
12	4	12	10	2,94E-41
13	4	13	10	5,33E-53
14	4	14	10	1,28E-67
15	4	15	10	7,33E-86

Table 5-4 Load Cases Wave Height Sensitivity Block 3

5.3 Load Cases for Sensitivity of Fatigue to Wave Height

The sensitivity of variation of the peak period for constant mean wind speed and significant wave height is also performed. The mean wind speed is held constant equal to 4 m/s for all the load cases. The load cases are divided into seven blocks where the significant wave height varies for each block but is held constant within each block. The peak period varies from 5 to 16 seconds within each block. The load cases are listed in table 5-5 to 5-11 and the probability of occurrence is shown in figure 5-9. From the figure we can see that the marginal probability is largest for wave height of 2 m and is decreasing for increasing wave heights.

Load Cases Block 1

Load Case	Wind Speed [m/s]	Significant Wave Height [m]	Peak Period [s]	Probability of occurrence [-]
1	4	1	5	0,00126
2	4	1	6	0,003503
3	4	1	7	0,005021
4	4	1	8	0,004719
5	4	1	9	0,00335
6	4	1	10	0,001962
7	4	1	11	0,001003
8	4	1	12	0,000466
9	4	1	13	0,000202
10	4	1	14	8,35E-05
11	4	1	15	3,33E-05
12	4	1	16	1,30E-05

Table 5-5 Load Cases Peak Period Sensitivity Block 1**Load Cases Block 2**

Load Case	Wind Speed [m/s]	Significant Wave Height [m]	Peak Period [s]	Probability of occurrence [-]
1	4	2	5	1,28E-04
2	4	2	6	1,14E-03
3	4	2	7	0,00387208
4	4	2	8	0,00697833
5	4	2	9	0,00818677
6	4	2	10	0,00709634
7	4	2	11	0,00494199
8	4	2	12	0,00292884
9	4	2	13	0,00153848
10	4	2	14	0,00073775
11	4	2	15	0,00033009
12	4	2	16	0,00014009

Table 5-6 Load Cases Peak Period Sensitivity Block 2

Load Cases Block 3

Load Case	Wind Speed [m/s]	Significant Wave Height [m]	Peak Period [s]	Probability of occurrence [-]
1	4	3	5	1,98E-06
2	4	3	6	6,39E-05
3	4	3	7	0,000547
4	4	3	8	0,001962
5	4	3	9	0,003858
6	4	3	10	0,00494
7	4	3	11	0,004619
8	4	3	12	0,003413
9	4	3	13	0,002108
10	4	3	14	0,001134
11	4	3	15	0,000548
12	4	3	16	0,000244

Table 5-7 Load Cases Peak Period Sensitivity Block 3

Load Cases Block 4

Load Case	Wind Speed [m/s]	Significant Wave Height [m]	Peak Period [s]	Probability of occurrence [-]
1	4	4	5	3,68E-09
2	4	4	6	5,71E-07
3	4	4	7	1,51E-05
4	4	4	8	0,000124
5	4	4	9	0,000454
6	4	4	10	0,000925
7	4	4	11	0,001222
8	4	4	12	0,001166
9	4	4	13	0,000865
10	4	4	14	0,000528
11	4	4	15	0,000276
12	4	4	16	0,000128

Table 5-8 Load Cases Peak Period Sensitivity Block 4

Load Cases Block 5

Load Case	Wind Speed [m/s]	Significant Wave Height [m]	Peak Period [s]	Probability of occurrence [-]
1	4	5	5	5,21E-13
2	4	5	6	5,85E-10
3	4	5	7	6,43E-08
4	4	5	8	1,51E-06
5	4	5	9	1,20E-05
6	4	5	10	4,39E-05
7	4	5	11	8,98E-05
8	4	5	12	0,000118
9	4	5	13	0,000111
10	4	5	14	7,93E-05
11	4	5	15	4,59E-05
12	4	5	16	2,24E-05

Table 5-9 Load Cases Peak Period Sensitivity Block 5

Load Cases Block 6

Load Case	Wind Speed [m/s]	Significant Wave Height [m]	Peak Period [s]	Probability of occurrence [-]
1	4	6	5	3,09E-18
2	4	6	6	4,33E-14
3	4	6	7	2,93E-11
4	4	6	8	2,63E-09
5	4	6	9	5,72E-08
6	4	6	10	4,45E-07
7	4	6	11	1,61E-06
8	4	6	12	3,22E-06
9	4	6	13	4,10E-06
10	4	6	14	3,63E-06
11	4	6	15	2,42E-06
12	4	6	16	1,28E-06

Table 5-10 Load Cases Peak Period Sensitivity Block 6

Load Cases Block 7

Load Case	Wind Speed [m/s]	Significant Wave Height [m]	Peak Period [s]	Probability of occurrence [-]
1	4	8	5	3,28E-34
2	4	8	6	7,39E-27
3	4	8	7	1,05E-21
4	4	8	8	4,98E-18
5	4	8	9	2,15E-15
6	4	8	10	1,62E-13
7	4	8	11	3,26E-12
8	4	8	12	2,39E-11
9	4	8	13	7,95E-11
10	4	8	14	1,41E-10
11	4	8	15	1,51E-10
12	4	8	16	1,07E-10

Table 5-11 Load Cases Peak Period Sensitivity Block 7

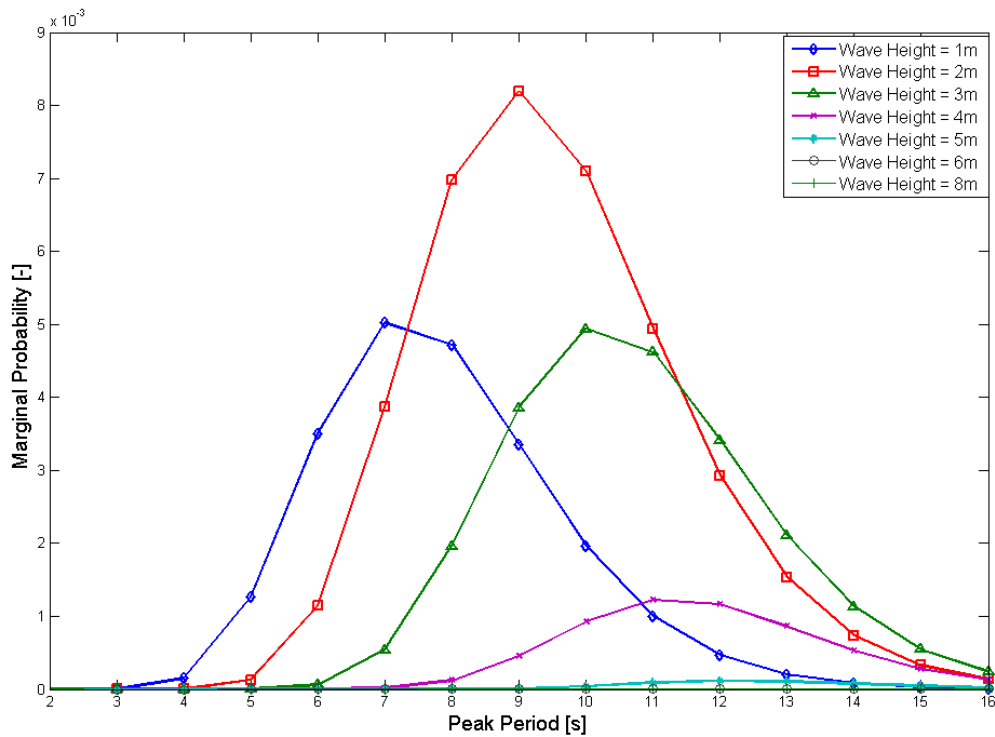


Figure 5-3 Probability of occurrence of peak period for given wave height and wind speed

6 Analysis and Results

6.1 Fatigue

In this thesis the major emphasis of the analysis has been on fatigue damage. The main objectives of the analysis was to check how sensitive the fatigue damage of the bottom tower was to simulation length and variation of significant wave and peak period relative to each other and to mean wind speed. One of the biggest challenges with fatigue damage calculation is that in order to capture all the different stress ranges throughout the service life of a floating structure, you have to simulate thousands of load cases. By investigating how sensitive the structure is to variation of different parameters it can be possible to reduce the total number of load cases. In total over 1200 simulations have been performed in this thesis.

Fatigue damage is calculated based on rainflow counting of the stress time series of axial stress, utilizing the Palmgren-Miner sum with SN-curves from the DNV fatigue standard. [14] Based on the fatigue standard the material parameter is set to $K = 1.99 \cdot 10^{-11}$ and the slope of the SN-curve $m = 3$.

To ensure acceptable statistical uncertainty each load case has to be simulated for given number of samples with different random seed number. Figure 6-1 to 6-4 shows the accumulated average standard deviation as a function of number of samples for load case 6 and 9 from chapter 5.1. The simulation length is 30 minutes and the accumulated standard deviation is plotted together with the individual standard deviations of each sample for shear force, bending moment, equivalent stress and axial stress at the base of the tower. From the figures it seems that the average accumulated standard deviation will reach a constant value after six samples which suggest that seven samples will be enough to ensure acceptable statistical uncertainty. From this conclusion seven samples per load case will be used throughout the analyses.

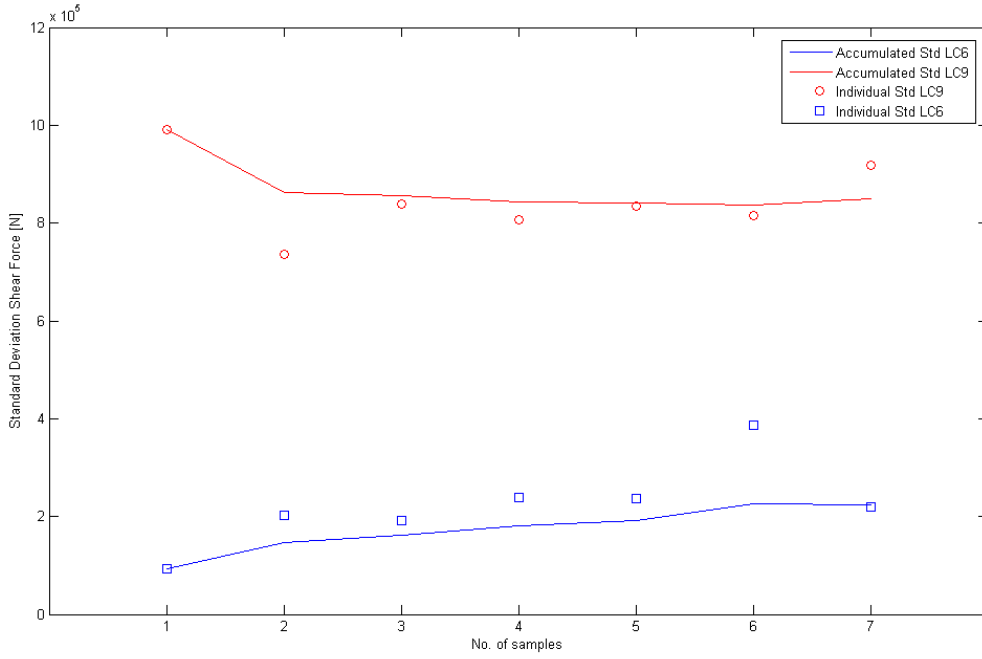


Figure 6-1 Shear force accumulated average standard deviation for LC6 and LC9

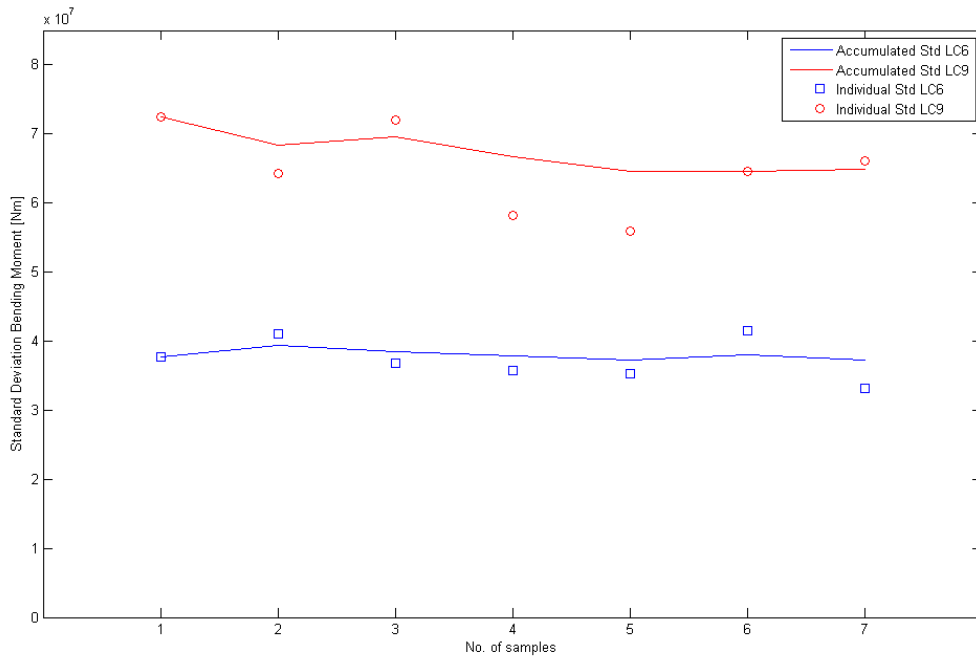


Figure 6-2 Bending moment accumulated average standard deviation for LC6 and LC9

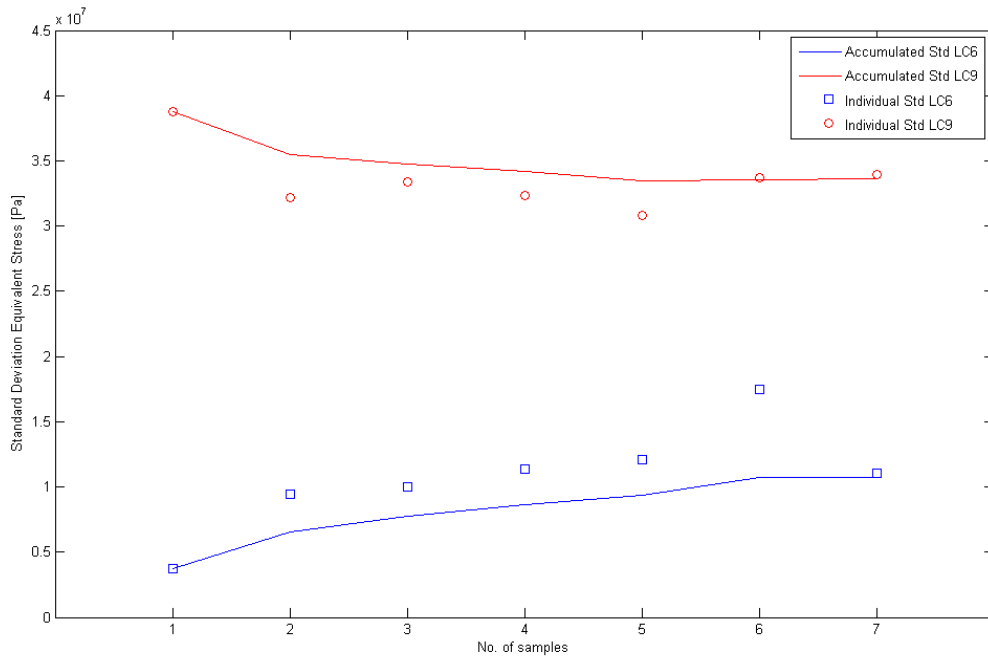


Figure 6-3 Equivalent stress accumulated average standard deviation for LC6 and LC9

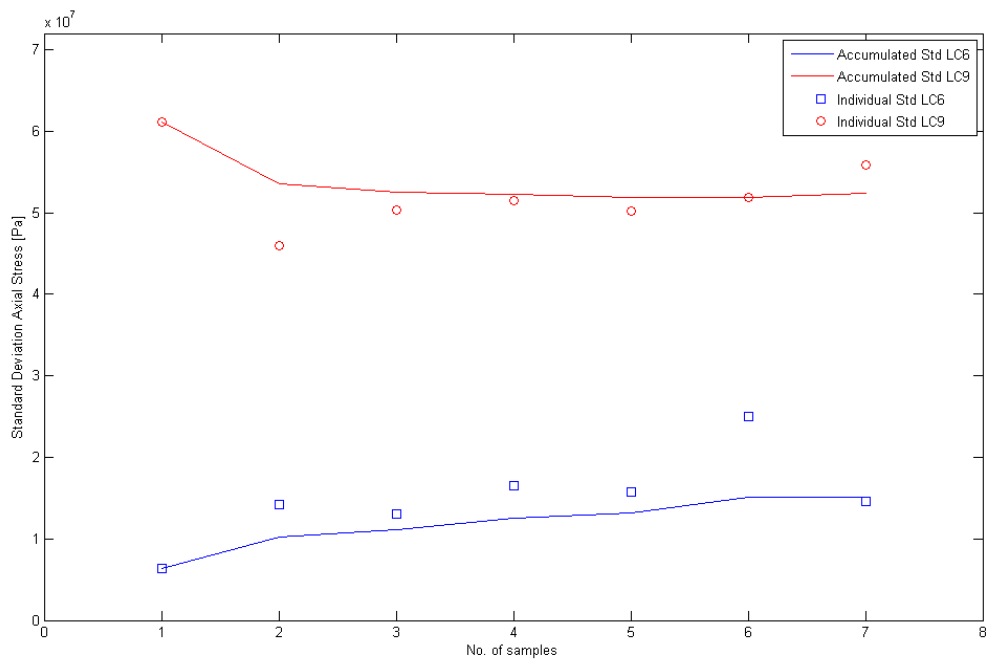


Figure 6-4 Axial stress accumulated average standard deviation for LC6 and LC9

6.2 Sensitivity of Fatigue to Simulation Length

Since fatigue damage analyses are very time consuming it becomes desirable to reduce the simulation length of each single analysis to reduce the total computational time of the analysis. The computational time has varied from 1200 seconds for some 30 minutes simulations to over 20000 seconds for some 3 hour simulations. If for example you will run 1000 analyses, the difference in total computational time will be over 200 days. So if analyses with different simulation length produce almost the same results, it becomes very profitable to use the analysis with the shortest possible simulation length. The computational time is also strongly dependent on the size of the time step in the time domain analysis. For environmental condition that gives large responses, the time step has to be smaller to ensure convergence. A result of this is that several analyses have to be executed multiple times with smaller time step until it converges.

In this analysis the statistical properties and fatigue damage of equivalent stress and axial stress has been studied for simulation length of 30 minutes, 1 hour and 3 hours. The load cases used in the analysis are described in chapter 5.1. Each load case is executed seven times with different random phase for each run. The analyses are executed in SIMO/RIFLEX with the TDHmill extension. For the 3 hours simulation only load case 1 to 6 are completed with the TDHmill extension. For load case 7 to 12 it was not possible to get convergence with the TDHmill extension included. The number of time steps in each analysis exceeded five million and total computational time was on over three weeks. A result of this is that for load case 7 to 12 with the TDHmill extension included, only the 30 minute and 1 hour simulations could be completed and compared with each other.

Table 6-1 shows the statistical properties of equivalent stress and axial stress in the tower base based on seven simulations with different random seed for each load case 1 to 6. From the table it can be seen that the only statistical property that does not change much from 30 minutes to 3 hours is the mean value. In figure 6-5 the mean values for load case 1 to 6 are shown. We can see from the figure how the differences between the mean values for different simulation lengths increase for higher load cases. For standard deviation the difference between the different simulation lengths is significant. Since fatigue analysis is related to the standard deviations for narrow banded processes we cannot use 30 minute and 1 hour simulation time based on these values. The standard deviation is shown in figure 6-6.

Time [s]	LC1	LC2	LC3	LC4	LC5	LC6
Mean [MPa]						
Equivalent Stress						
30 min	102,57	102,58	103,18	104,42	105,00	122,85
1 hour	102,59	102,68	103,23	103,54	104,18	116,06
3 hours	102,53	102,54	102,59	102,87	103,25	109,99
Axial Stress						
30 min	-102,40	-102,36	-102,28	-101,86	-100,79	-87,29
1 hour	-102,37	-102,37	-102,33	-102,11	-101,68	-92,82
3 hours	-102,37	-102,37	-102,36	-102,32	-102,22	-99,48
Standard Deviation [MPa]						
Equivalent Stress						
30 min	25,91	27,91	38,22	34,61	27,77	68,49
1 hour	17,15	20,25	27,01	22,07	17,85	57,21
3 hours	6,36	6,34	9,79	10,52	11,10	35,83
Axial Stress						
30 min	25,97	28,03	39,44	38,64	33,04	95,08
1 hour	17,32	20,60	28,30	24,53	22,47	78,48
3 hours	6,37	6,34	9,81	10,99	12,21	45,16
Skewness						
Equivalent Stress						
30 min	0,01	0,01	0,09	0,43	0,38	3,02
1 hour	0,03	0,06	0,14	0,58	1,37	4,69
3 hours	0,04	0,04	0,04	0,55	0,98	6,20
Axial Stress						
30 min	0,00	0,00	0,00	0,02	0,33	2,21
1 hour	0,01	0,00	0,00	0,09	0,39	3,71
3 hours	-0,03	-0,04	-0,01	0,16	0,34	4,68
Kurtosis						
Equivalent Stress						
30 min	2,58	2,56	2,59	4,77	7,91	28,50
1 hour	4,91	4,79	4,85	10,89	16,43	47,93
3 hours	12,92	11,91	13,49	27,35	34,08	91,23
Axial Stress						
30 min	2,58	2,57	2,69	4,95	8,13	24,82
1 hour	8,85	7,01	17,94	35,95	59,52	32,42
3 hours	12,96	11,96	13,59	28,91	37,76	101,92

Table 6-1 Statistical properties of equivalent stress and axial stress averaged over 7 simulations with different random seed number.

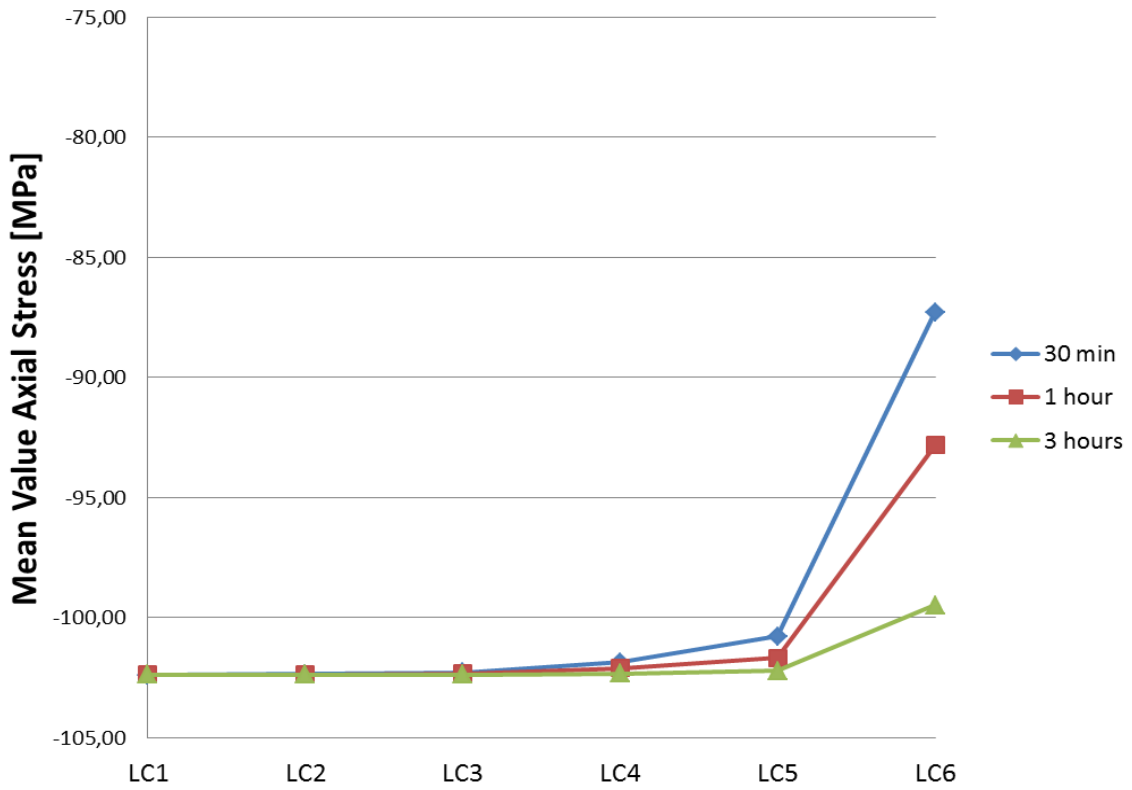


Figure 6-5 Mean Value of Axial Stress of load case 1 - 6 for different simulation lengths

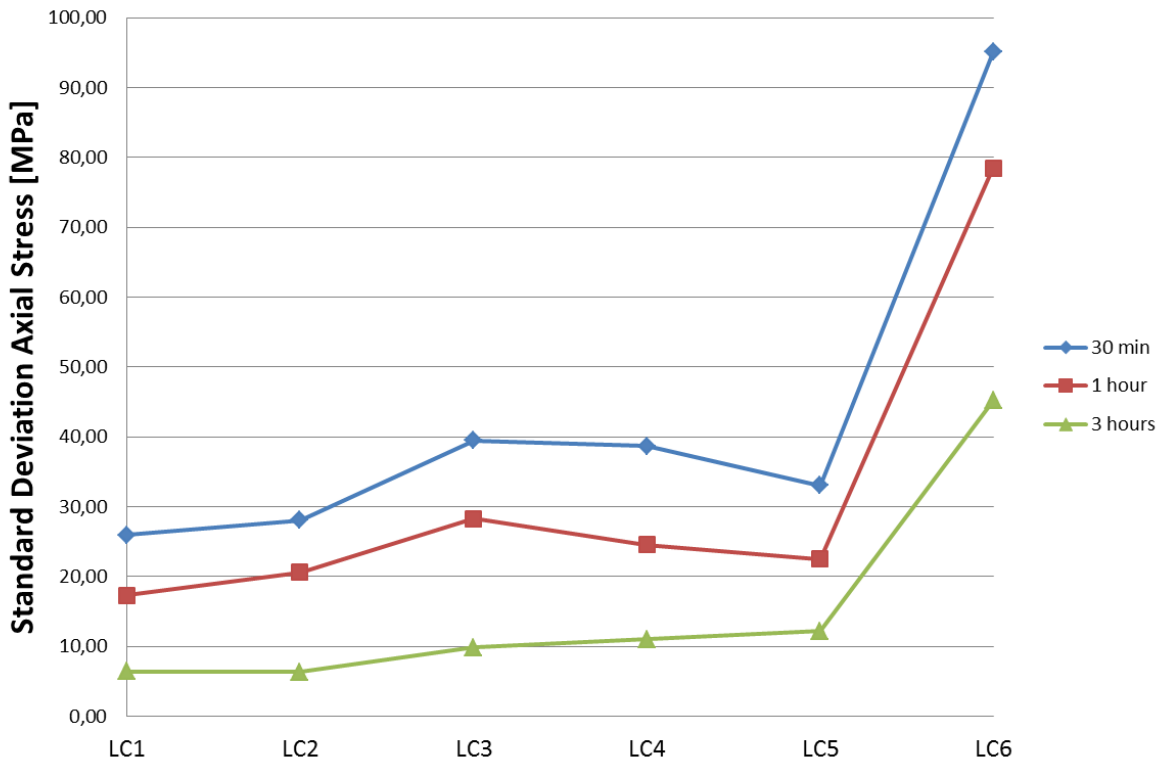


Figure 6-6 Standard Deviation of Axial Stress of LC1 –LC6 for different simulation lengths

The difference in the values of standard deviation is due to start-up transients and can be seen from the plot of time series of equivalent stress of load case 6 (figure 6-7). The figure is divided into two plots where the plot on the left hand side shows the three time series up to a simulation length of 3 hours and the plot on the right hand side shows the three time series zoomed to 30 minute simulation length. The time series are averaged over seven random seeds. From the figure we can see that the response is very large at the start of the simulation and stabilizes around 30 minutes. This is due to start-up transients and results in higher standard deviation for the analysis with shortest simulation length. The solution to this problem will be to extend all the simulation times with 30 minutes and exclude them in the post-processing. Start-up transients must be removed before post-processing, since they are not physical. In this analysis the problem with start-up transient was discovered on a very late stage in the working progress, so it was not possible to run the simulation again. Instead, I have subtracted 30 minutes from the 3 hours simulation and the 1 hour simulation, so the 3 hours simulation will be calculated as a 2.5 hours simulation and the 1 hour simulation will be calculated as a 30 minute simulation.

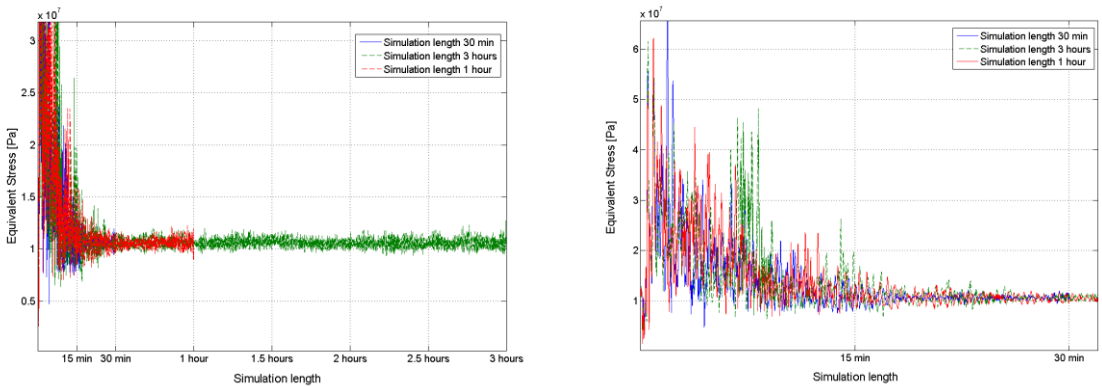


Figure 6-7 Time series of equivalent stress for load case 6 with transients

The statistical properties of axial stress for the 30 minute and 2.5 hour simulation length without the start-up transients are given in table 6-2. The standard deviation of axial stress for the 30 minute and 2.5 hours simulation without transients are shown in figure 6-8. We can see from the table and the figure that the deviation between standard deviation and the two simulation lengths are close to equal. This may indicate that 30 minute simulation length may be sufficient for fatigue analysis since fatigue can be related to the standard deviation.

Analysis	LC1	LC2	LC3	LC4	LC5	LC6
Mean [MPa]						
30 min	-102,38	-102,37	-102,35	-102,35	-102,33	-101,90
2,5 hours	-102,37	-102,37	-102,36	-102,35	-102,35	-102,06
Standard Deviation[MPa]						
30 min	2,47	2,55	2,96	3,23	3,96	8,42
2,5 hours	2,30	2,31	2,79	3,29	3,95	8,06
Kurtosis						
30 min	2,55	2,45	2,39	3,47	3,82	4,02
2,5 hours	3,02	3,12	3,41	3,55	4,01	4,32
Skewness [MPa]						
30 min	0,00	0,00	0,01	-0,01	-0,06	0,25
2,5 hours	0,00	-0,01	-0,02	0,01	-0,01	-0,02

Table 6-2 Statistical properties of axial stress for 30 minute and 2.5 hours simulation length without start-up transients

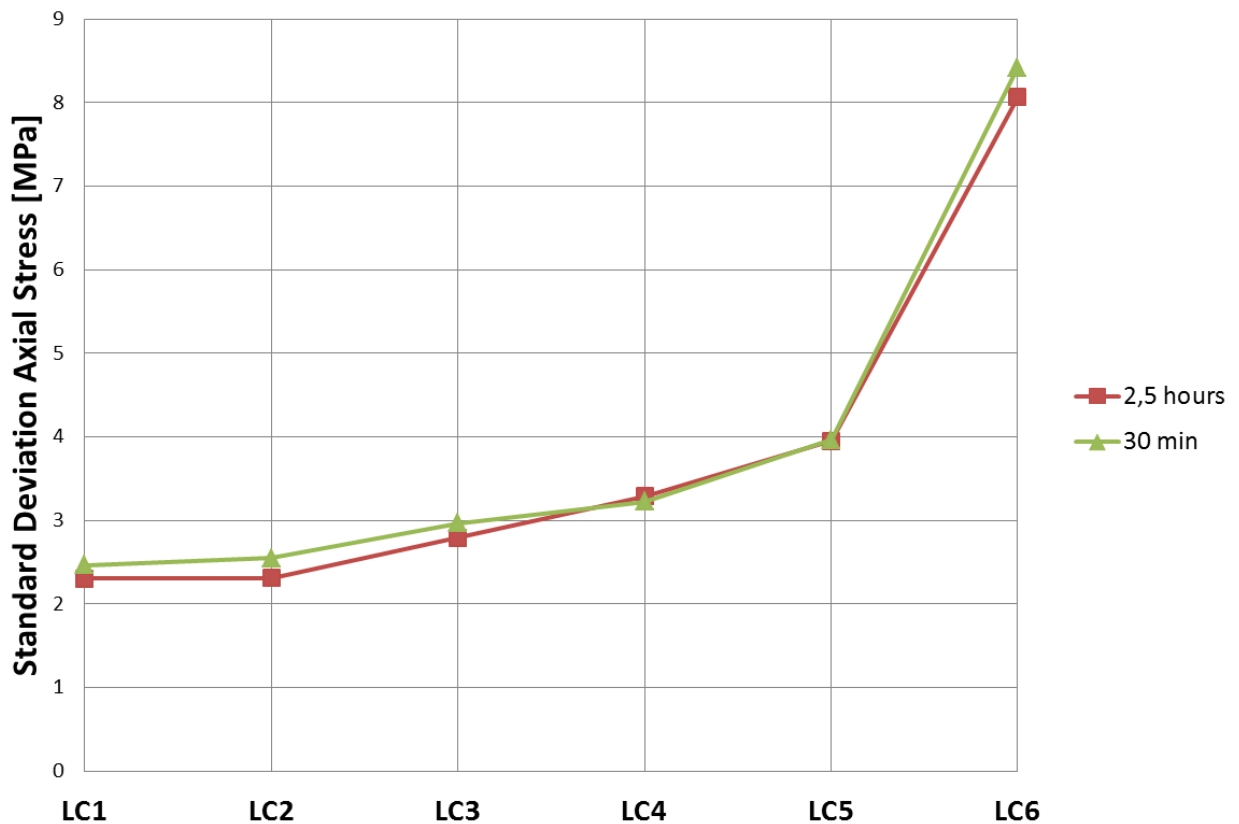


Figure 6-8 Standard deviation of axial stress for 2.5 hours and 30 min simulation length

Figure 6-9 shows the accumulated fatigue damage calculated by rainflow counting of axial stress in the tower base. The damage of the 30 minute simulation is multiplied with a factor of 5 to be comparable with the 2.5 hour simulation. From the figure we can see that the damage is close to equal for the two different simulation lengths. The damage seems to increase for each load case, and is highest for load case 6.

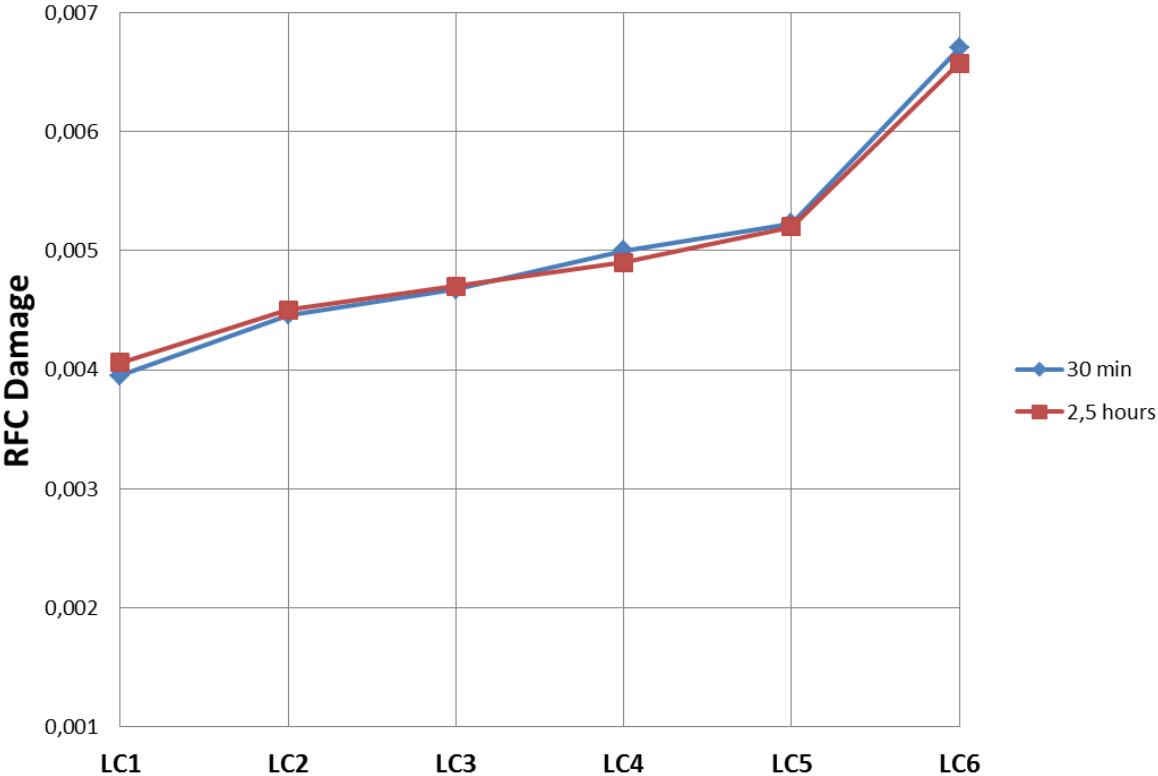


Figure 6-9 2.5 hour rainflow damage for 30 minute and 2.5 hour simulation lengths

The damage in figure 6-9 does not take the marginal probability of the load cases into account. This must be included to decide which load cases contribute most to fatigue. Figure 6-10 shows damage accumulated over one year for LC1-LC6 for the two different simulation lengths. From the figure we can see when the probability is included the dominating load case becomes LC2.

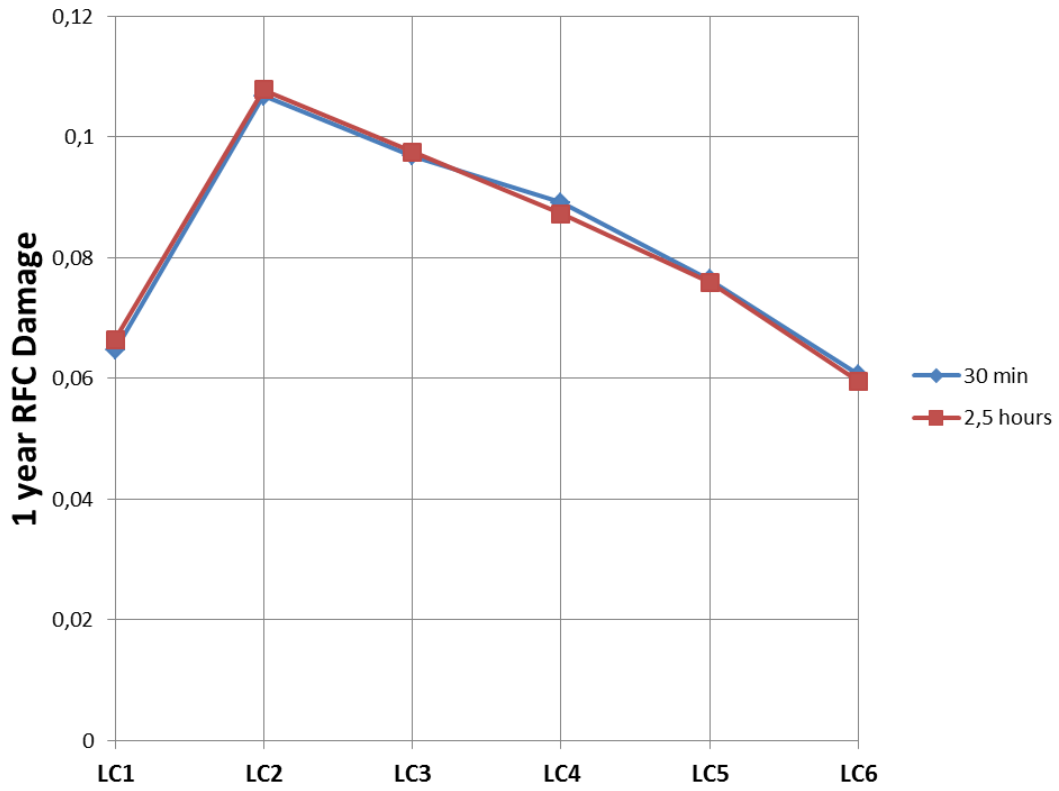


Figure 6-10 Fatigue damage accumulated over one year for different simulation lengths

6.3 Sensitivity of Fatigue to Peak Period

In this chapter the effect of varying wave height for constant peak period is studied. The wave height is kept constant to give a clearer view of the effect of varying wave height. The intention of this sensitivity study is to see if there are certain ranges of wave heights for given peak period that does not contribute to the fatigue damage. If the stresses and fatigue damage of the tower base follow some kind of pattern for certain load cases, it can be possible to reduce the total number of load cases and simulations drastically.

In this analysis a total number of 45 load cases are executed with seven random seed number for each load case, adding up to a total number of 315 simulations. Because of the time restrictions of this thesis the simulation length is chosen to be 30 minutes. The load cases used in this sensitivity analysis are described in chapter 5.2.

The statistical properties of axial stress in the tower base based on seven simulations for each load case are listed in table 6-2. The variation of the mean value and standard deviation of axial stress is shown in figure 6-13 and 6-14 respectively. From figure 6-13 it seems that the mean value of the axial stress is close to constant and equal for the chosen peak periods in the wave height range 1 m to 10 m. From wave height 11 m to 15 m the deviation between the mean values increases from the smallest value for peak period of 8 seconds up to the largest values of peak period of 10 seconds. In figure 6-14 it seems that the standard deviation of axial stress is close to equal but not constant for the same range as the mean value. The deviations and values of the standard deviation are rapidly increasing for wave height larger than 10 m for the chosen peak periods. This implies that it can be possible to exclude two of the three peak periods for wave height lower than 10 m.

Mean [MPa]								
Tp\Hs	1	2	3	4	5	6	7	8
8	-101,45	-101,41	-101,44	-101,44	-101,40	-101,38	-101,40	-101,47
9	-101,46	-101,46	-101,49	-101,48	-101,47	-101,44	-101,41	-101,32
10	-101,45	-101,47	-101,46	-101,44	-101,36	-101,30	-101,46	-101,49
Tp\Hs	9	10	11	12	13	14	15	
8	-101,50	-101,36	-100,89	-100,73	-100,87	-97,05	-97,56	
9	-101,31	-101,20	-101,02	-99,73	-97,70	-95,43	-86,94	
10	-100,87	-100,68	-97,76	-96,31	-87,22	-88,69	-86,35	
Standard Deviation [MPa]								
Tp\Hs	1	2	3	4	5	6	7	8
8	38,01	35,32	32,63	32,08	33,10	34,40	36,65	41,74
9	35,91	33,20	31,78	31,62	31,93	33,67	36,75	39,68
10	34,32	30,26	29,20	29,44	30,42	30,85	32,75	35,95
Tp\Hs	9	10	11	12	13	14	15	
8	49,28	57,59	69,43	82,86	100,22	138,42	187,71	
9	45,16	55,42	69,12	96,66	128,13	184,81	253,54	
10	49,16	64,51	98,11	136,03	218,46	274,17	350,04	
Kurtosis								
Tp\Hs	1	2	3	4	5	6	7	8
8	2,773745	4,672073	9,241201	14,35376	12,97147	10,46389	10,71686	8,478541
9	3,036457	4,989458	7,344999	10,31795	11,75104	11,04051	9,368147	8,167853
10	4,179689	12,00711	12,41246	13,72608	15,37515	16,11771	14,58766	13,26148
Tp\Hs	9	10	11	12	13	14	15	
8	6,284017	5,697832	5,89772	4,997303	4,821699	4,270573	4,11325	
9	7,590632	6,605573	5,720747	4,68196	5,914641	6,531152	4,7873	
10	8,71459	7,906559	7,480368	8,35522	7,672675	9,088785	11,03293	
Skewness								
Tp\Hs	1	2	3	4	5	6	7	8
8	0,202355	0,405537	0,817125	1,219659	1,132681	0,954641	0,930752	0,613518
9	0,251879	0,474253	0,6764	0,935317	1,066452	0,99973	0,853653	0,694447
10	0,408654	1,225798	1,138334	1,163737	1,330081	1,483767	1,162923	0,950764
Tp\Hs	9	10	11	12	13	14	15	
8	0,31	0,199681	0,199796	0,129427	0,155008	0,151634	0,057188	
9	0,509545	0,327009	0,173923	0,166659	0,175561	0,106946	0,150731	
10	0,566997	0,388653	0,442466	0,128467	0,271317	-0,07521	0,06281	

Table 6-3 Statistical properties of axial stress averaged over seven samples with different random seed number

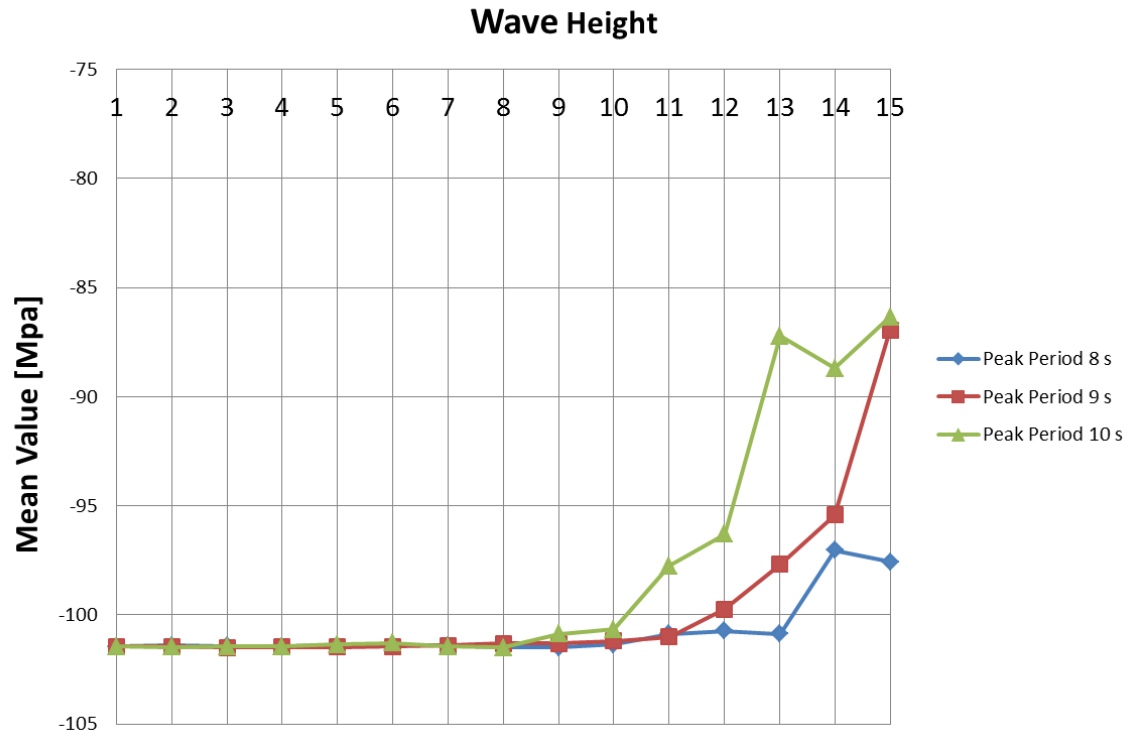


Figure 6-11 Mean Value of Axial Stress for Peak Period Sensitivity Analysis

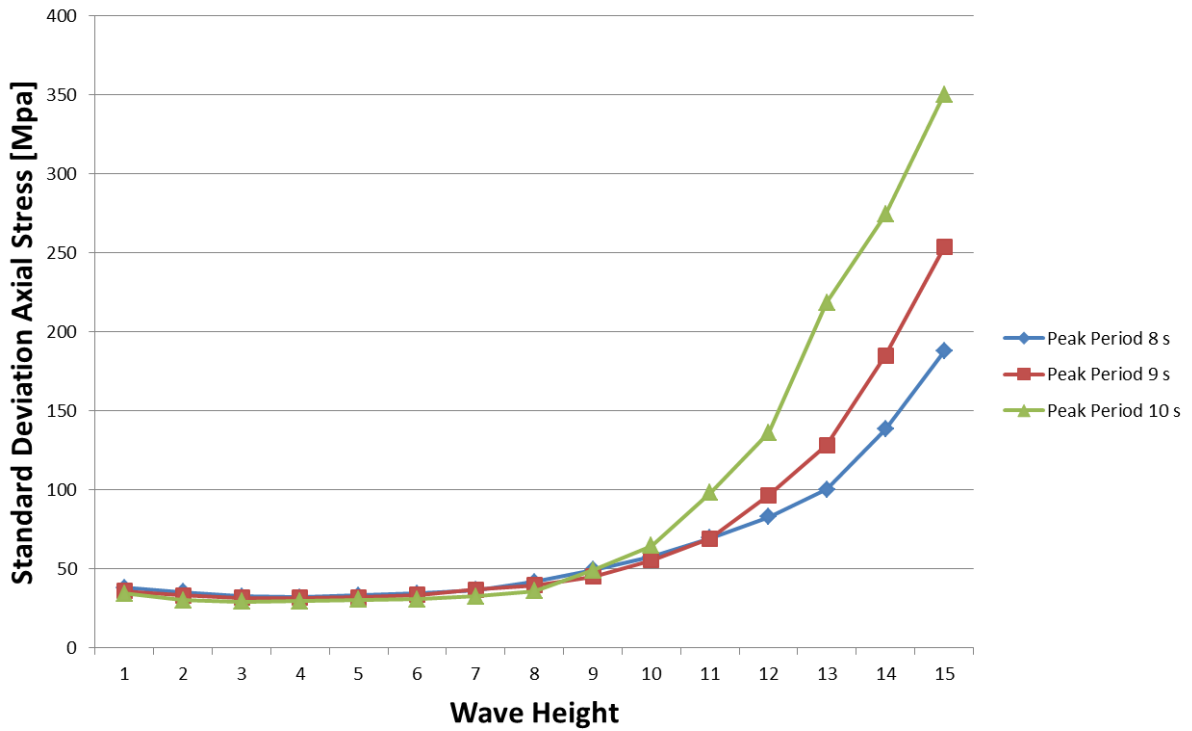


Figure 6-12 Standard Deviation of axial Stress for Peak Period Sensitivity Analysis

The accumulated rainflow fatigue damage based on axial stress for the load cases in this sensitivity analysis is shown in figure 6-15. From the figure we can see that the lowest peak period gives the highest damage for all wave heights. Up to a wave height of 8 m the damage follows the same pattern for the three peak periods. For wave heights within the range of 1 – 4 m the damage of periods of 8 and 9 seconds is close to each other with an average deviation of 11%. In the same range the damage of the 8 second period is in average 54 % higher than the damage of the 10 second period. For period of 8 seconds the damage almost linearly increases from a wave height of 4 m to 12 m. The damage of the 9 and 10 second periods seems to be more random for wave heights above 9 m.

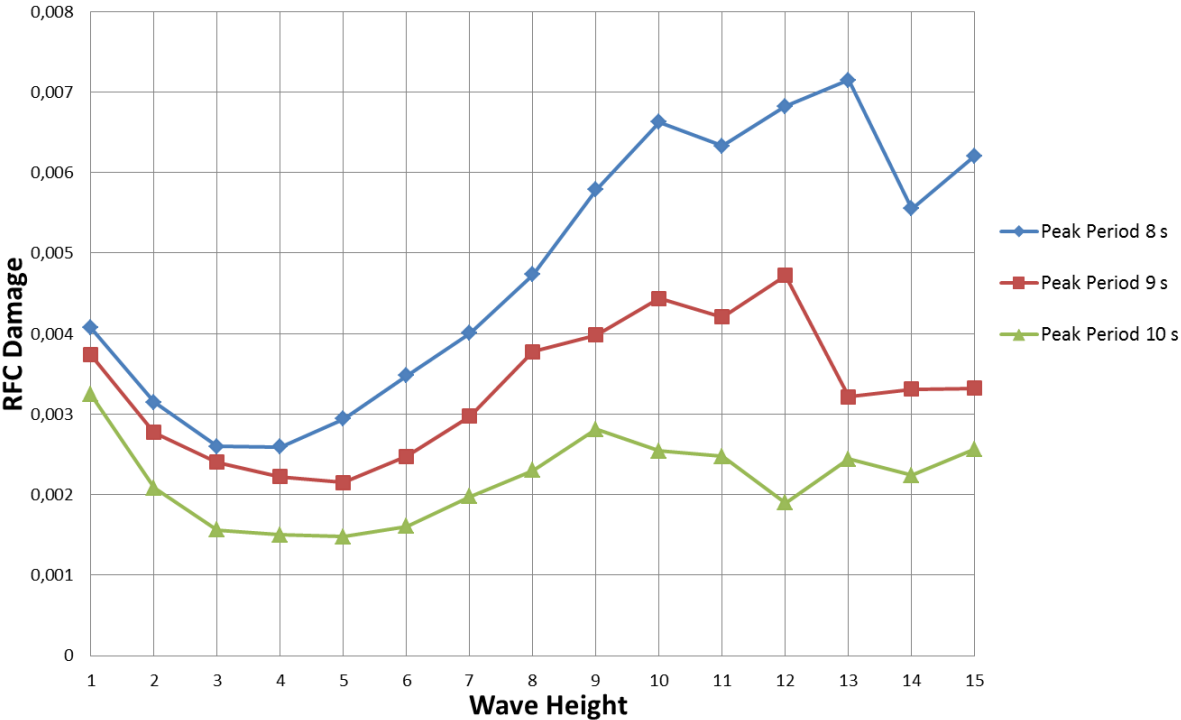


Figure 6-13 30 minute rainflow damage for different peak periods with varying wave heights averaged over 7 samples

Figure 7-16 shows the fatigue damage accumulated over one year. From the figure it seems that the damage will follow the marginal probability distribution for the load cases (see figure 5-2). Since the probability for wave heights above 5 m and mean wind speed of 4 m/s is close to zero, the contribution to damage will be minimal for these load cases. For wave heights smaller than 5 m, the 9 second peak periods will give the largest damage.

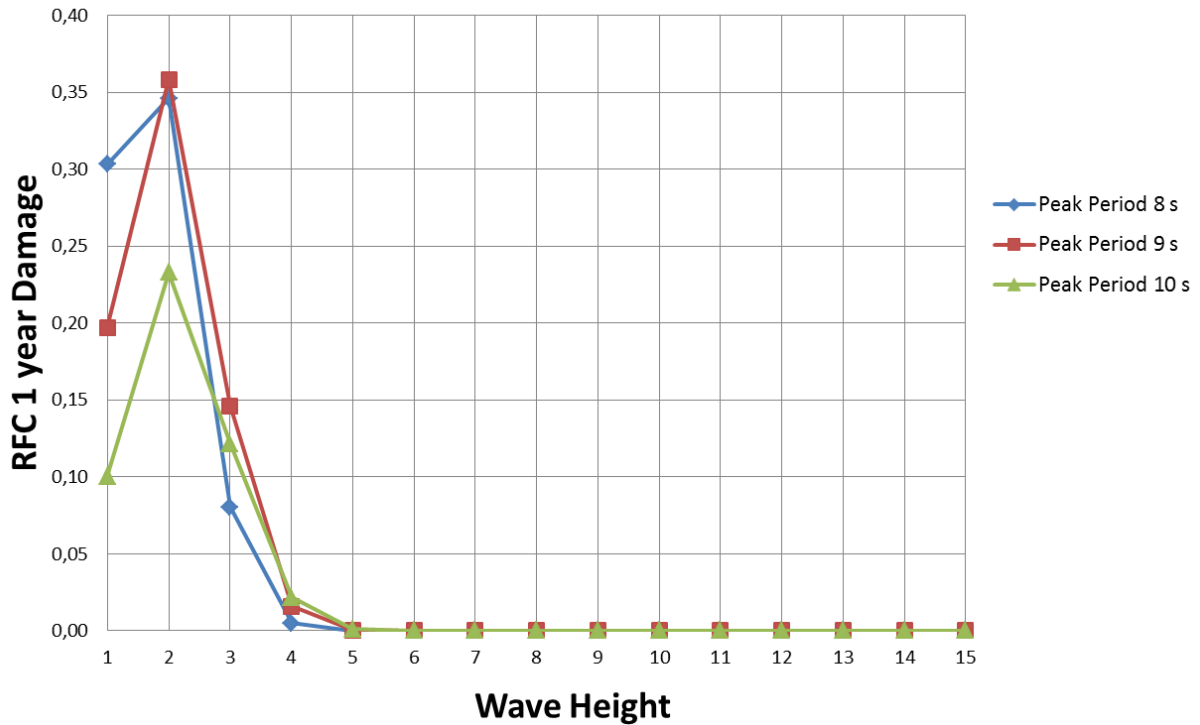


Figure 6-14 Fatigue damage accumulated over 1 year of peak period sensitivity

6.4 Sensitivity of Fatigue to Wave Height

In this chapter the sensitivity of varying peak period for constant wave height and wind speed is studied. The peak period varies from 5 seconds to 16 seconds for 7 different wave heights ranging from 1 m to 8 m. The wind speed is held constant equal to 4 m/s to give a clearer view of the effect of varying the peak period.

The total number of load cases in this analysis is 84, where each load case is executed seven times with different random seed number. The simulation length is 30 minutes and total number of simulations is 588. The load cases are listed in chapter 5.3.

The statistical properties of axial stress in the tower base based on seven simulations for each load case are listed in table 6-3. The variation of the mean value and standard deviation of axial stress is shown in figure 6-17 and 6-18 respectively. From figure 6-18 we can see that the standard deviation is close to constant for wave heights 1 – 2 m from peak periods of 5 seconds to 9 seconds. For peak periods above 9 seconds the variations of the standard deviation follow the same pattern for wave heights in the range 1 – 6 m. For 8 m wave height the variation of the standard deviation does not follow the same pattern as rest of the wave heights and the standard deviation is significantly higher for peak periods above 12 seconds.

Hs\Tp	5	6	7	8	9	10	11	12	13	14	15	16
Mean [MPa]												
1 m	-101,5	-101,5	-101,5	-101,5	-101,5	-101,4	-101,4	-101,4	-101,4	-101,4	-101,4	-101,4
2 m	-102,5	-102,4	-102,4	-102,4	-102,4	-102,3	-102,3	-102,3	-102,3	-102,4	-102,4	-102,4
3 m	-101,5	-101,5	-101,5	-101,5	-101,5	-101,5	-101,5	-101,4	-101,4	-101,4	-101,3	-101,3
4 m	-102,4	-102,4	-102,4	-102,4	-102,3	-102,2	-102,3	-102,2	-102,4	-102,4	-102,3	-102,3
5 m	-101,5	-101,5	-101,5	-101,5	-101,5	-101,4	-101,4	-101,3	-101,4	-101,3	-101,2	-101,1
6 m	-101,5	-101,5	-101,5	-101,5	-101,4	-101,3	-101,4	-101,4	-101,4	-101,3	-101,2	-100,8
8 m	-102,4	-102,4	-102,4	-102,2	-102,2	-102,4	-102,0	-102,1	-100,0	-99,8	-99,2	-102,0
Standard Deviation [MPa]												
1 m	34,1	33,8	33,7	34,7	35,9	34,3	28,6	25,5	23,9	24,8	27,3	24,3
2 m	27,2	26,4	26,5	27,1	28,3	22,7	15,9	11,0	10,1	11,5	14,0	12,5
3 m	27,6	27,1	28,0	28,9	31,8	29,2	25,9	22,2	19,9	19,6	20,9	20,8
4 m	21,0	20,6	23,4	22,2	23,0	16,3	10,0	6,4	5,3	5,6	10,8	12,2
5 m	24,6	25,2	29,8	30,3	31,9	30,4	26,5	25,1	23,5	24,1	26,1	25,3
6 m	24,2	26,1	33,1	33,4	33,7	30,9	27,0	27,1	26,4	27,8	30,0	28,8
8 m	20,6	26,4	40,5	35,3	29,9	23,2	27,6	26,4	40,3	49,5	60,3	44,2
Kurtosis												
1 m	2,64	2,71	2,71	2,70	3,04	4,18	8,78	11,46	10,50	6,82	4,36	5,96
2 m	2,12	2,21	2,24	2,40	2,79	4,54	8,50	12,16	7,92	7,20	4,96	4,63
3 m	5,00	5,54	5,30	8,47	7,34	12,41	24,59	30,74	45,88	45,80	30,83	21,29
4 m	3,07	3,30	3,26	4,31	4,96	7,96	10,19	22,89	7,77	10,36	10,57	9,94
5 m	7,95	7,86	6,39	11,85	11,75	15,38	24,19	32,52	45,42	35,86	25,18	21,91
6 m	8,42	7,77	5,85	8,50	11,04	16,12	25,84	30,54	37,81	30,62	21,54	20,09
8 m	4,70	4,03	4,32	4,90	4,52	5,04	7,60	8,38	7,55	11,23	12,84	7,62
Skewness												
1 m	0,20	0,22	0,22	0,21	0,25	0,41	0,87	1,18	1,09	0,70	0,42	0,64
2 m	0,00	0,00	0,00	-0,01	0,00	0,02	0,11	0,17	0,02	-0,09	0,00	-0,01
3 m	0,51	0,60	0,58	0,82	0,68	1,14	1,99	2,25	2,94	3,00	2,31	1,79
4 m	0,00	-0,01	0,00	0,01	0,04	0,18	0,19	1,52	0,10	-0,50	0,18	0,11
5 m	0,85	0,86	0,63	1,09	1,07	1,33	1,85	2,13	2,75	2,21	1,69	1,71
6 m	0,89	0,79	0,48	0,74	1,00	1,48	1,96	1,91	2,15	1,72	1,45	1,51
8 m	0,01	-0,03	-0,01	0,05	0,05	0,09	0,26	0,38	0,43	0,67	0,55	0,31

Table 6-4 Statistical properties of axial stress averaged over 7 samples with different random seed number

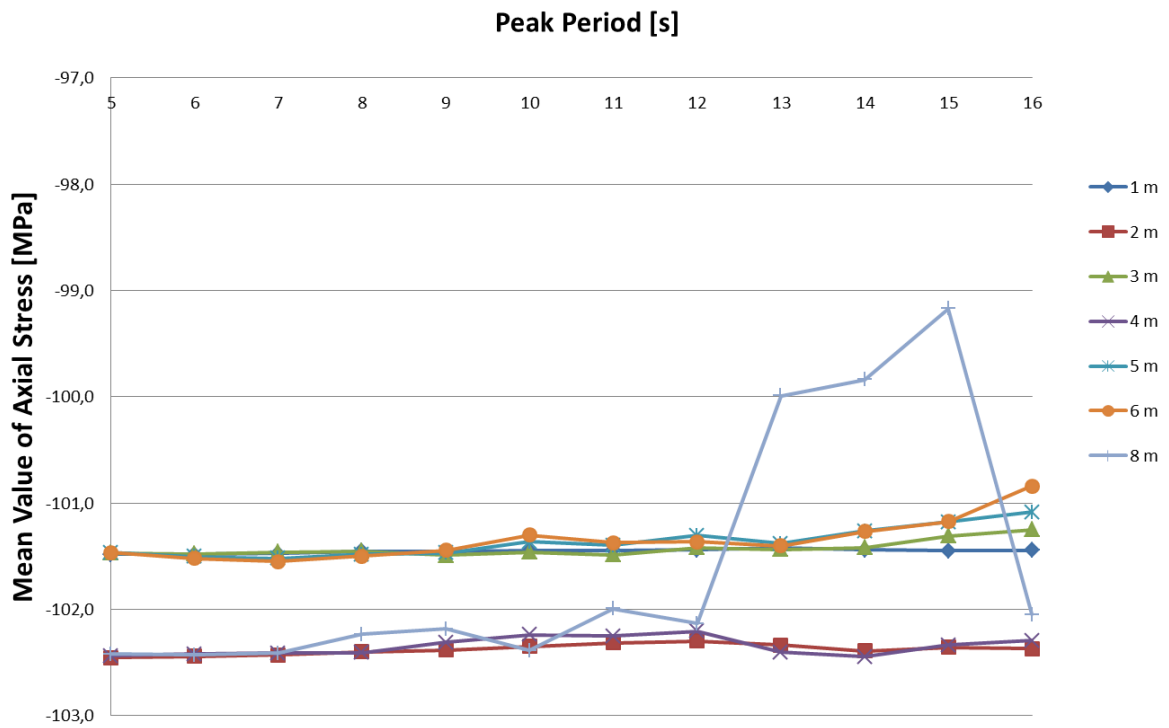


Figure 6-15 Mean Value of Axial stress for load cases in wave height sensitivity

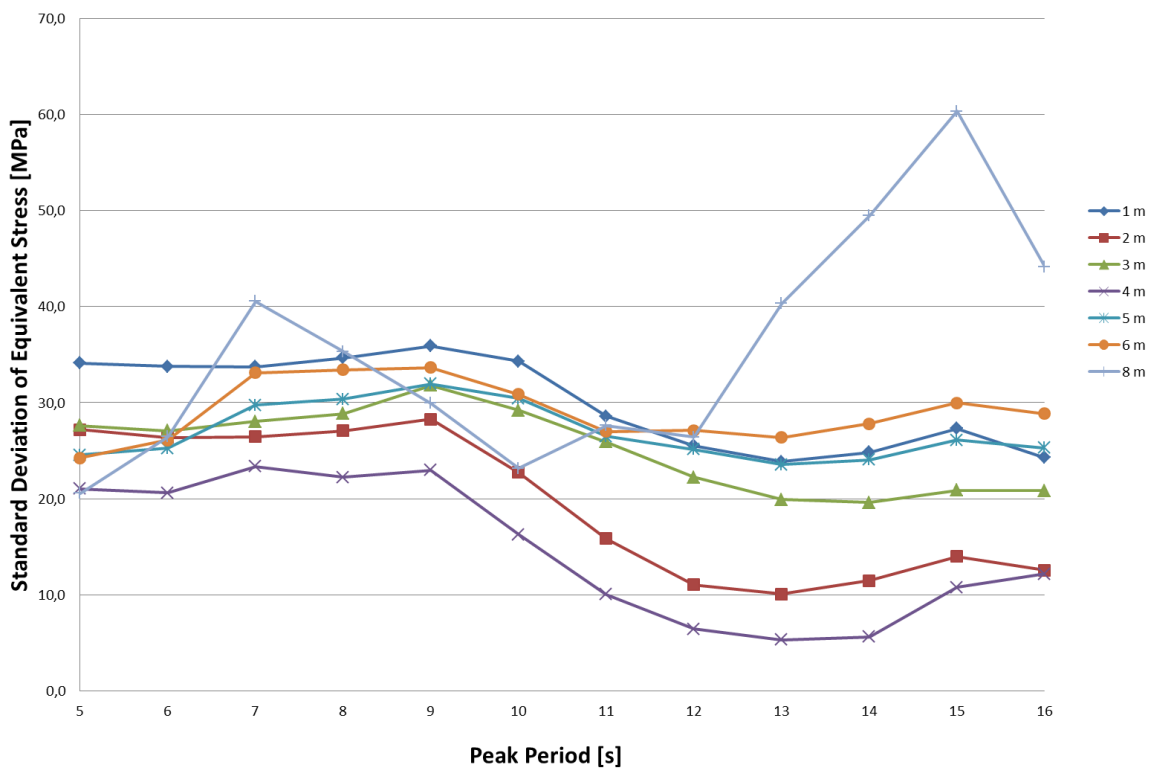


Figure 6-16 Standard Deviation of Axial Stress for load cases in wave height sensitivity

Figure 6-19 shows the 30 minute rainflow damage for the load cases in the wave height sensitivity analysis averaged over seven samples with different random seed number. From the figure we can see how the fatigue damage for the lowest wave heights (i.e. 1 – 3 m) follows the same pattern as the standard deviation. In the peak period range 5 – 9 s the fatigue damage follows a clear pattern for the different wave heights: for wave height of 1 and 2 m the fatigue damage is very close to constant. For wave height of 4 m a small peak arises for peak period of 7 seconds. This trend continues for increasing wave height. For each increasing wave height the peak is getting higher and the fatigue damage increases for peak periods adjacent to the 7 second peak period. This suggests that the highest waves dominate the fatigue damage for the smallest peak periods. If we consider the fatigue damage for peak periods above 9 seconds it seems that the deviation of the damage between the different wave heights decreases. For wave heights 3 – 6 m the fatigue damage is close to the same value for peak periods above 11 seconds with an average deviation of 1.11 %. For periods above 10 seconds, wave height of 1 m gives the largest rainflow damage.

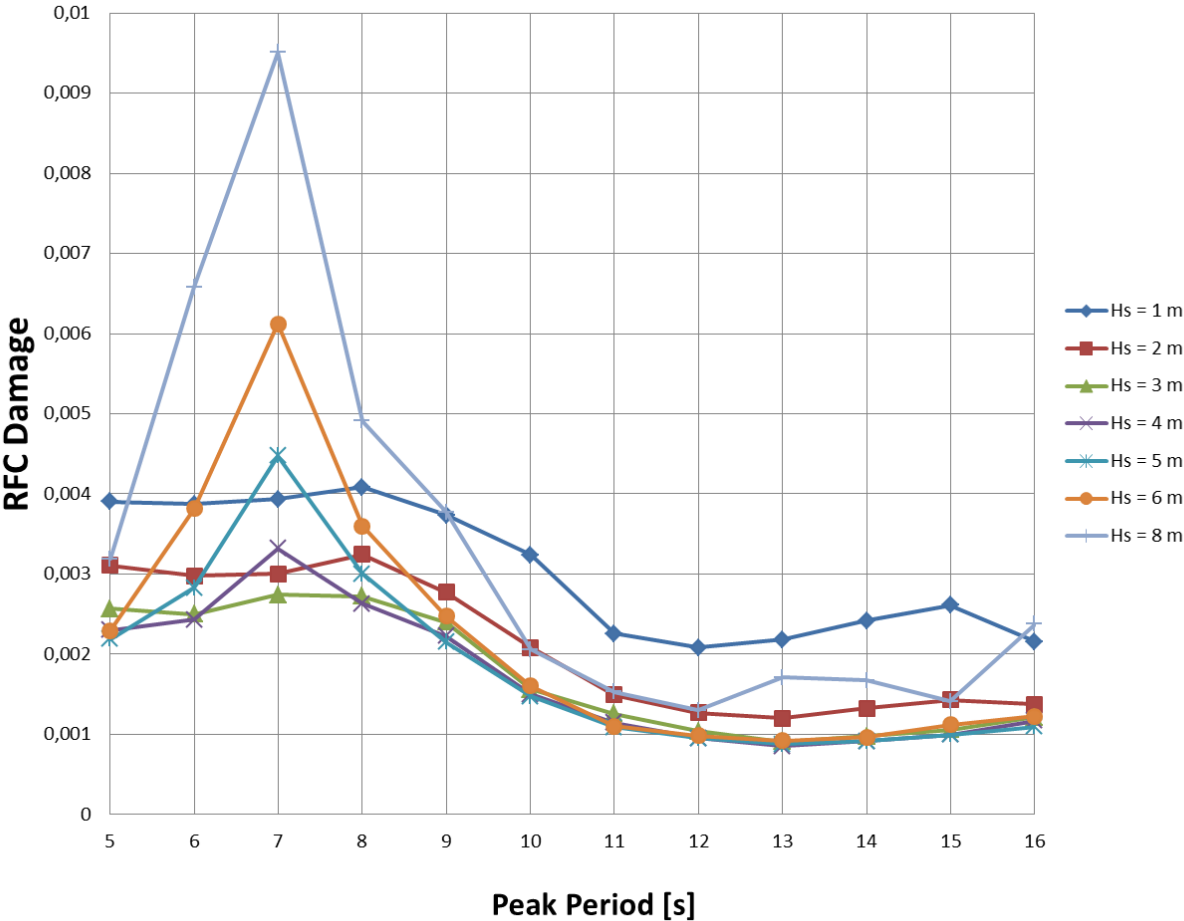


Figure 6-17 30 minute rainflow damage for different wave heights with varying peak periods averaged over 7 samples

Figure 6-20 shows damage accumulated over one year. From the figure we can see that the accumulated damage will depend more on the marginal probability distribution (see figure 5-3) than the rainfall damage. The one year accumulated fatigue damage will be largest for the load case where mean wind speed is 4 m/s, wave height is 2 m and peak period is 9 seconds. This load case is the environmental condition with the highest marginal probability in the joint distribution of simultaneous wind and waves. When the difference between the calculated rainfall damage is small, the accumulated damage over a certain long time period will be dominated by the marginal probability of the environmental condition.

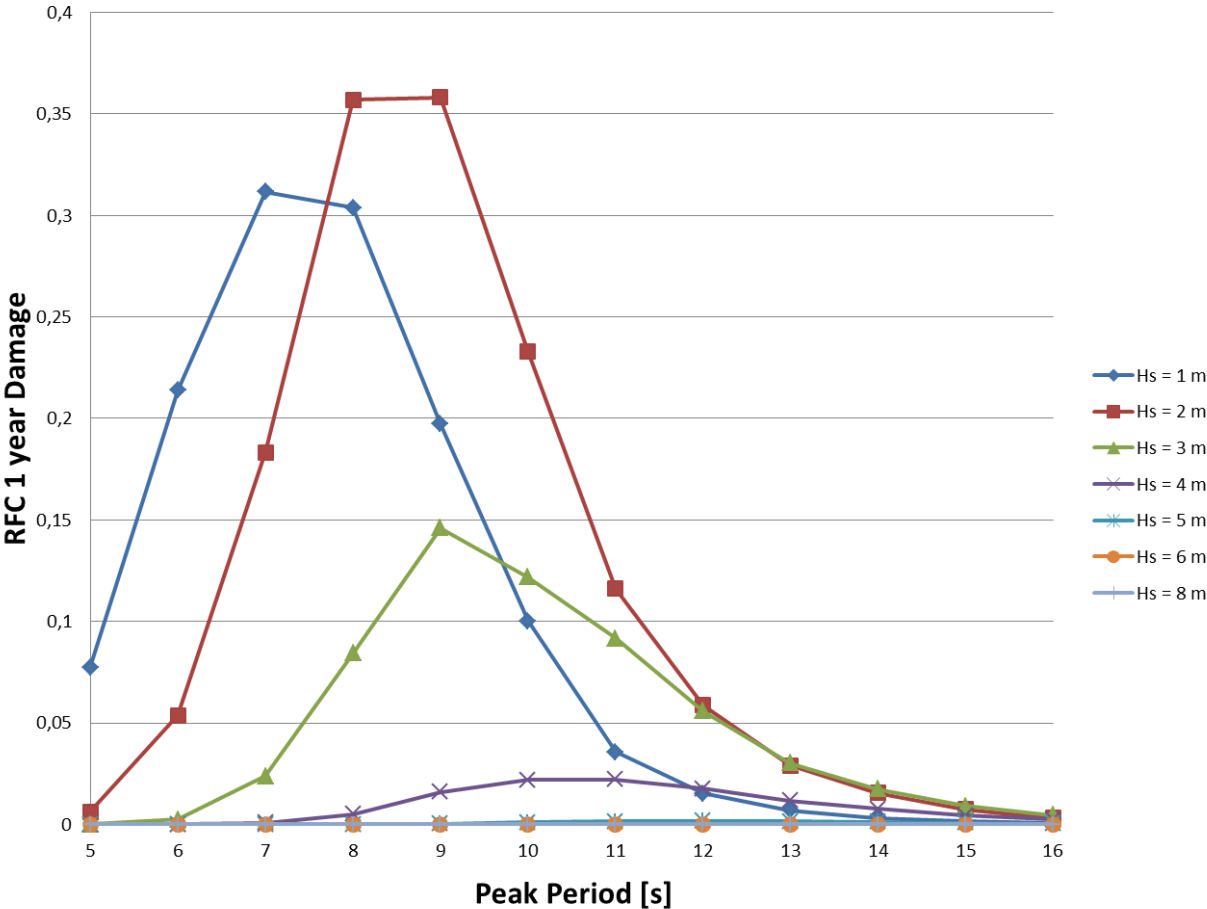


Figure 6-18 Fatigue damage accumulated over 1 year of wave height sensitivity

7 Conclusions and Further Work

The main objectives in this thesis have been to study which effect simulation length and variation of different parameter has on fatigue damage. The main conclusions from the thesis can be summarized in the following:

- In fatigue damage it is very important to choose the correct design stresses and the corresponding stress SN-curves. Von Mises stress can only be used in fatigue calculations of notches in base materials where initiation of fatigue crack is a significant part of the fatigue life.
- When SIMO/Riflex is used for simulation, the simulation length has to be increased with 30 minutes due to start-up transients. Start-up transients are not physical and give unnatural effects to the results.
- Accumulated standard deviation stabilizes for 5 samples or more. This holds for equivalent stress, axial stress, bending moment and shear force.
- Based on the statistical properties of axial stress and fatigue damage of the tower base of the analysis of different simulation length, 30 minutes should be sufficient simulation length. The deviation between 30 minute and 2.5 hour simulation length is negligible.
- For the sensitivity analysis of fatigue damage for wave height and peak period all the load cases have been simulated for wind speed of 4 m/s. This results in that the conclusions of these analyses only holds for this wind speed. This sensitivity study should be continued to check the sensitivity for other wind speeds, e.g. 8 m/s, 12 m/s, 16 m/s and 20 m/s.
- The standard deviation of equivalent stress in the sensitivity analysis of peak period is close to identical for peak periods 8 – 10 seconds and wave heights in the range 1 – 10 m. For a narrow banded process this suggests that the damage will be close to equal for all these load cases. Calculated rainflow damage shows that for wave heights below 10 m, the damage will follow the same pattern, but not be equal to each other for the studied peak periods.
- The calculated rainflow damage of the load cases in the wave height sensitivity analysis is close to constant for 1 and 2 m wave heights for peak periods of 5 – 9 seconds. From this we can conclude that the fatigue damage do not depend on the peak period within this range for 1 and 2 m wave height. For peak periods above 10 seconds the fatigue damage varies, but the values for each wave height and peak period is very close to each other, with an exception of 1 m and 8 m wave height. This makes it possible to only run simulation for one of the wave heights which are equal and include the other wave heights through the marginal probability.

- From all the analyses we see that if the deviations in the rainflow fatigue damage are small, than the dominating load cases in the accumulated fatigue damage will be given by the marginal probability distribution of the load cases. So it becomes very important to have a good probability model for the environmental conditions to achieve the correct long term fatigue damage.

The sensitivity study performed in this thesis should be continued for different wind speeds. The final objective should be to make a three-dimensional fatigue damage scatter-diagram for a spar-type floating wind turbine in moderate water depth.

8 References

1. WorldWindEnergyAssociation. *World Market recovers and sets a new record: 42 GW of new capacity in 2011, total at 239 GW 2012*; Available from: http://www.wwindea.org/home/index.php?option=com_content&task=view&id=345&Itemid=43.
2. EuropeanWindEnergyAssociation. *The European offshore wind industry key 2011 trends and statistics*. 2012; Available from: <http://www.gamesacorp.com/recursos/noticias/ewea-report-offshore-industry.pdf>.
3. Jonkman, J.M., *Dynamic Modeling and Loads Analysis of an Offshore Floating Wind Turbine*, in *National Renewable Energy Laboratory*, N.T.-. 500-41958, Editor 2007, National Renewable Energy Laboratory: U.S. Department of Commerce National Technical Information Service 5285 Port Royal Road Springfield, VA 22161.
4. Karimirad, M. and T. Moan, *Wave and Wind Induced Dynamic Response of a Spar-Type Offshore Wind Turbine* *Journal of Waterway, Port, Coastal, and Ocean Engineering*, 2011. **10**(061/(ASCE)WW.1943-5460.0000087).
5. DNV, *DeepC Theory Manual*, 2005, Det Norske Veritas: Høvik, Oslo.
6. Petersen, B., et al., *EVALUATE THE EFFECT OF TURBINE PERIOD OF VIBRATION REQUIREMENTS ON STRUCTURAL DESIGN PARAMETERS: TECHNICAL REPORT OF FINDINGS*, 2010: Applied Physical Sciences

Corp. 475 Bridge Street, Suite 100, Groton, CT 06340 (860) 448-3253
' www.aphysci.com.

7. Karimirad, M., *Stochastic Dynamic Response Analysis of Spar-Type Wind Turbines with Catenary or Taut Mooring System*, in *Department of Marine Technology* 2011, Norwegian University of Science and Technology: PhD Thesis, Trondheim, Norway.
8. Faltinsen, O.M., *Sea Loads on Ships and Offshore Structures*. Cambridge Ocean Technology 1995, Cambridge United Kingdom: Cambridge University Press.
9. Pettersen, B., *Hydrodynamics* 2007, Trondheim: Department of Marine Technology.
10. Myrhaug, D., *Uregelmessig sjø*. TMR 4180 Marin Dynamikk 2007, Trondheim: Department of Marine Technology.
11. MARINTEK, *SIMO Theory Manual*, 2009, MARINTEK: Trondheim.
12. Benasciutti, D. and R. Tovo, *On fatigue damage assessment in bimodal random processes*. International Journal of Fatigue, 2007. **29**(2).
13. Brodtkorb, P.A., et al., *WAFO - a Matlab Toolbox for Analysis of Random Waves and Loads*, 2011, Lund University Faculty of Engineering Centre for Mathematical Sciences Mathematical Statistics: Lund University. p. 185.
14. DNV, *DNV-RP-C203 Fatigue Design of Offshore Steel Structure*, 2011, Det Norske Veritas: Høvik, Oslo.

15. Moy, I., *Dynamic Response Analysis of a Spar-type Wind Turbine in Moderate Water Depth*, 2011, Norwegian University of Science and Technology: MTS, Trondheim, Project-thesis.
16. DNV, *HydroD User Manual*, 2010: Veritasveien 1 1322 Høvik Norway.
17. MARINTEK, *Riflex User Manual*, V3.6, Editor 2009, Marintek: MTS, Trondheim.
18. Jonkman, J., et al., *Definition of a 5-MW Reference Wind Turbine for Offshore System Development*, T.R. NREL/TP-500-38060, Editor 2009, National Renewable Energy Laboratory: NREL is a national laboratory of the U.S. Department of Energy Office of Energy Efficiency and Renewable Energy Operated by the Alliance for Sustainable Energy, LLC 1617 Cole Boulevard, Golden, Colorado 80401-3393.
19. AmericanPetroleumInstitute, *Design and Analysis of Stationkeeping Systems for Floating Structures*, 2005, API Publishing Services: Washington, D.C.
20. DNV, *Offshore Standard DNV-OS-E302 Offshore Mooring Chain*, 2008, Det Norske Veritas: Høvik, Oslo.
21. DNV, *Offshore Standard DNV-OS-E303 Offshore Mooring Fibre Ropes*, 2010, Det Norske Veritas: Høvik, Oslo.
22. Yttervik, R., *TDHMILL3D User Documentation*, 2009.

23. Johannesen, K., T.S. Meling, and S. Haver, *Joint Distribution for Wind and Waves in the Northern North Sea*. In Proceedings of the Eleventh International Offshore and Polar Engineering Conference., 2001. **3**(1-880653-54-0).

APPENDIX A Input files SIMO/RIFLEX

Templates

These input files are used as template input files. The variables are marked as yellow. Due to the length of sys-Analysis2.dat.mal, sys-Analysis.dat.mal and Analysis_inpmod.inp files they are only included electronically.

A.1 DYN.MAC

/	' Use default file names ? (Y)
Read initial con	' DYNMOD main menu
Set simulation p	' DYNMOD main menu
/	' Default main analysis parameters ? (N)
FFT only	' Select method for calculation of waves
>>iseed	' Random generator seed for waves
16	' Integer power of 2 - NFFT
0.05	' Time step - DT
4	' Number of subdivision each step
y	' Default method parameters ? (N)
n	' Write visualization file ? (Inactive) (N)
y	' Default storage parameters ? (N)
Initialize simul	' DYNMOD main menu
/	' Should wave time series be read from file ? (N)
Terminate	' DYNMOD main menu

A.2 Analysis_dynmod.inp.mal

```
'=====
' DATA SECTION A
'=====
'-----
' DYNMOD CONTROL INFORMATION 3.6
'-----
```

File generated by :DeepC V4.5-05

Export from: Analysis, DATE : March 20, 2012 - 14:48:32

dynamic analysis

```
'-----  
'  irunco ianal idris idenv idstat idirr idres  
  ANAL IRRE SLEND1 LC2 STA1 IRR1 DYN1
```

```
'=====
```

DATA SECTION D

```
'=====
```

IRREGULAR TIMESERIES PARAMETERS

```
'-----  
'  irand timewf dtwf  dtlf  
>>iseed  3276.8 5.e-002 0.4
```

```
'-----
```

IRREGULAR RESPONSE ANALYSIS

```
'-----  
'  ircno time dt  irwav irmot irlfm tbeg iscale  
  1  >>time >>dt NONE NONE NONE 0  0
```

```
'=====
```

DATA SECTION E

```
'-----
```

TIME DOMAIN PROCEDURE

```
'-----  
'  itdmet inewil idisst iforst icurst istrst  
  2  1  1  1  0  0  
'  betin gamma theta a1 a2  a1t a1to a1b a2t a2to a2b  
  4  0.5 1.5 0 1.e-003 0 0 0 0 0 0  
'  indint indhyd maxhit epshyd  tramp indrel iconre istepr ldamp  
  1  1  5  1.e-002 10 0 0 0 0
```

```
'-----
```

NONLINEAR INTEGRATION PROCEDURE

```
'-----  
'  itfreq isolit maxit daccu  icocod ivarst istat  
  1  1  10 1.e-006 1  2  1
```

```

'-----
DISPLACEMENT RESPONSE STORAGE
'-----
' idisp nodisp idisfm cfndis
2 1
' ilin iseg inod
18 1 6
'-----
FORCE RESPONSE STORAGE
'-----
' ifor noforc iforfm cfnfor
2 1
' ilin iseg ielm
18 1 5
'-----
ENVELOPE CURVE SPECIFICATION
'-----
' ienvd ienvf ienvc tenvs tenve nprend nprenv nprenc ifilmp ifilas
1 1 0 10 43200 1 1 1 4 0
'=====
END
'=====
START DEEPC RESULT PROCESSING
END DEEPC RESULT PROCESSING

```

A.3 **tdh3d_nrel5mwwt.inp**

Dette er input-fil eksempel.

Modellert av Rune Yttervik. Case : 1

Rotorspesifikasjon:

```

RADIUS NRX1 NRX2 NRX3 RPM RIXR WINDIR
63.0 1.0 0.0 0.0 >>rpm 35460. 0.0

```

Reguleringsmetode:

```

IMETH TMEAN

```

0 6.

Notch filter:

INOTCH OMEGA0 ZETAD ZETAN DT

>>notch 0.22 1 0.01 >>dt

Thrustkoeffisienter:

NCT

37

u ct

3	0.868270818
4	0.815504234
5	0.815487867
6	0.815822488
7	0.816097134
8	0.815913418
9	0.815539596
10	0.793882938
11	0.751113511
11.3	0.734628191
11.4	0.660034743
11.5	0.649199838
11.8	0.581815117
12	0.535667664
13	0.405290958
14	0.313184624
15	0.250122518
16	0.204489835
17	0.170220653
18	0.143790381
19	0.122959304
20	0.106322439
21	0.092785547
22	0.081647478
23	0.072400089
24	0.064628381
25	0.004106246
30	0.004106246

35 0.004106246
40 0.004106246
45 0.004106246
50 0.004106246
55 0.004106246
60 0.004106246
65 0.004106246
70 0.004106246
75 0.004106246

Effektkoeffisienter:

NCP

37

u cp

3 0.464002528
4 0.47301052
5 0.473887799
6 0.47495033
7 0.476031046
8 0.477460338
9 0.478666053
10 0.478968161
11 0.47131478
11.3 0.466979048
11.4 0.446313237
11.5 0.443552751
11.8 0.417269422
12 0.395084719
13 0.319505762
14 0.25576648
15 0.207908825
16 0.171247659
17 0.142716983
18 0.120205349
19 0.102168789
20 0.087564231
21 0.075612998

22 0.065739115
23 0.057521095
24 0.050607443
25 0.043526
30 0.000000
35 0.000000
40 0.000000
45 0.000000
50 0.000000
55 0.000000
60 0.000000
65 0.000000
70 0.000000
75 0.000000

A.4 S2X.MAC

```
/          ' Use default file names ? (Y)
EXPORT to separate ASCII file ' S2XMOD main menu
Analysis
/
Terminate          ' S2XMOD main menu
```

A.5 vind_nrel5mwwt.dat

```
' IWTYP IPRINT
-1  1
' UMEAN TURB LAMBDA TSLEN FMIN FMAX ISEED
>>umean >>turb >>lambda >>tslen >>fmin >>fmax >>iseed
' ICOH NRINT
1  20
```

A.6 Analysis_stamod.inp

```
=====
' DATA SECTION A
=====
'-----
    STAMOD CONTROL INFORMATION 3.6
'-----
File generated by :DeepC V4.5-05
  Export from: Analysis, DATE : March 20, 2012 - 14:48:31
Analysis static analysis
'-----
' irunco idris ianal iprdat iprcat iprfem ipform iprnr ifilm
  1  SLEND1 1  5  1  1  2  1  2
'-----
    RUN IDENTIFICATION
'-----
    STA1
'-----
    ENVIRONMENT REFERENCE IDENTIFIER
'-----
' idenv
  LC2
=====
' DATA SECTION B
=====
'-----
    STATIC CONDITION INPUT
'-----
' nlcomp icurin curfac lcons isolvr
  0  0  1  1  2
'-----
    COMPUTATIONAL PROCEDURE
'-----
' ameth
  FEM
```

'-----
FEM ANALYSIS PARAMETERS

'-----
LOAD GROUP DATA

'-----
' nstep maxit racu
20 500 1.e-006
' lotype
VOLUME
SFOR

'-----
LOAD GROUP DATA

'-----
' nstep maxit racu
20 500 1.e-006
' lotype
DISP

'-----
LOAD GROUP DATA

'-----
' nstep maxit racu
20 500 1.e-006
' lotype
FLOA

'=====

END

'=====

A.7 STA.MAC

/ ' Use default file names ? (Y)
/ ' Use default values ? (Y)
Read system desc ' STAMOD main menu
Write initial co ' STAMOD main menu
/ ' Initial condition identificator
/
/
/
Terminate ' STAMOD main menu

APPENDIX B Python Scripts

These scripts were used to generate the input files and run SIMO/Riflex. They were made in Python with help from Marit Kvittem.

B.1 generate_simoriflex_input.py

This script generated the input files and is an example files for given load condition.

```
import sys
import os,string,shutil
##import pylab as p
import numpy as n
sys.path.append('F:\\Analyser')
from mik_funcs import mik_replace_strings
##
## June 2012 I. Moy
##
##### INPUT #####
## Wind, wave height and wave period vectors
w_hub = n.array([4.,4.,4.,4.,4.,4.,4.,4.,4.,4.,4.,4.,4.,4.]) # Wsp [m/s]
at hub
h = n.array([1.,2.,3.,4.,5.,6.,7.,8.,9.,10.,11.,12.,13.,14.,15.]) # Hs [m]
t = n.array([9.,9.,9.,9.,9.,9.,9.,9.,9.,9.,9.,9.,9.,9.]) # Tp [s]
theta = n.array([0.,0.,0.,0.,0.,0.,0.,0.,0.,0.,0.,0.,0.,0.]) # wave dir
(deg)
p =
n.array([0.0056,0.0082,0.0071,0.0061,0.005,0.0031,0.0019,0.001,0.00064147,0.00033391,0.000154240,0.000079099,0.,0.,0.])# Probability density limit #
Probability density limit
t_max = 3600.0 # Simulation time, include transient
dt = 0.0125 # time step
## Wind simulation parameters
#~ Nf = 6000 # number of harmonic components
z_hub = 100.0
#~ dz = 0.5
#~ R = 63.0 # Radius rotor
#~ I_ref=0.15 # Turbulence intensity given by table 1 in IEC61400-1
(turbulence characteristics)
Lambdai=42.0 #if z>60 m
fmin = 0.0 # minimum freq included in wind sim [Hz]
fmax = 3.0 # max freq
iseed = 1.0 # Seed for wind and wave, wind and waves are independent
#~ sigmalh = 0.2 # 0.0 if 10 min stationarity
maindir = 'F:\\Analyser\\WaveHeight_%d' %t_max+'s_seed%d' %iseed +'\\' #
Main directory
winddir = 'F:\\Analyser\\Wind\\' # Directory for wind time series
tempdir = 'F:\\Analyser\\Templates\\' # Templates directory
##
prefix = 'Analysis'
infile1 = prefix+'_inpmod.inp.mal'
outfile1 = prefix+'_inpmod.inp'
infile2 = prefix+'_dynmod.inp.mal'
outfile2 = prefix+'_dynmod.inp'
infile3 = 'sys-'+prefix+'.dat.mal'
outfile3 = 'sys-'+prefix+'.dat'
infile4 = prefix+'_stamod.inp'
```

```

infile5 = 'tdh3d_nrel5mwwt.inp.mal'
outfile5 = 'tdh3d_nrel5mwwt.inp'
infile6 = 'vind_nrel5mwwt.dat.mal'
outfile6 = 'vind_nrel5mwwt.dat'
infile7 = 'DYN.MAC.mal'
outfile7 = 'DYN.MAC'
##### END INPUT #####
if not os.path.isdir(maindir):
    os.mkdir(maindir)

#
#~ os.mkdir(maindir)
os.chdir(maindir)
## Find wind at 10 m
#~ w_hub = w10*(z_hub/10.0)**0.14
w10= w_hub*(10.0/z_hub)**0.14
## Finds list of [W(10) Hs Tp p] with probability above plim
Nlc = len(w_hub)
LC_list = []
for i in range(Nlc):
    LC_list.append([w10[i],h[i],t[i],p[i],theta[i]])

f=open('load_cases.txt','w')
f.write('Load Case      Wsp10      Hs      Tp      Prob      Wavedir \n')

## Make directories and generate input files for each load combination
for i in range(Nlc):
    dirname = 'LC%d' %(i+0)
    if not os.path.isdir(maindir+dirname):
        os.mkdir(maindir+dirname)
    os.chdir(maindir+dirname)
    thisdir = os.path.abspath('.')
    lc = LC_list[i]
    f.write('%10s' %dirname + '%7.1f%7.1f%7.1f%12.6f%7.1f' %tuple(lc)
+' \n')
    w10 = lc[0]
    hi = lc[1]
    ti = lc[2]
    pi = lc[3]
    thetai = lc[4]
    ## Find pairs of w10 and whub
    for j in range(len(w10)):
        if w10[j] == w10:
            wihub = w_hub[j]

    if wihub <= 3.0:
        infile3 = 'sys-'+prefix+'2.dat.mal'

## if i == (Nlc-1) or i == (Nlc-2):
shutil.copy(tempdir + infile1, thisdir)
shutil.copy(tempdir + infile2, thisdir)
shutil.copy(tempdir + infile3, thisdir)
shutil.copy(tempdir + infile4, thisdir)
shutil.copy(tempdir + infile5, thisdir)
shutil.copy(tempdir + infile6, thisdir)
shutil.copy(tempdir + infile7, thisdir)
shutil.copy(tempdir + 'STA.MAC', thisdir)
shutil.copy(tempdir + 'TDHMILL3D_main.DLL', thisdir)
shutil.copy(tempdir + 'S2X.MAC', thisdir)

if wihub<11.4:

```

```

        rpm = (12.1-6.9)/(11.4-3.0)*(wihub-3.0)+6.9
        notch = 0.0
    else:
        rpm = 12.1
        notch = 1.0

    I_v = 0.103+0.8/wihub #Turbulence intensity as function of wsp
IEC61400-1

## if i == (Nlc-1) or i == (Nlc-2):
    # Replace strings in mal-files and make new input files
    ## Inpmod
    oldstrings1 = ['>>sigwahe', '>>tp', '>>wadir']
    newstrings1 = [hi, ti, thetai]
    format1 = ['%9.1f', '%9.1f', '%9.0f']
    mik_replace_strings(infile1, outfile1, oldstrings1, newstrings1, format1)

    ## Dynmod
    oldstrings2 = ['>>iseed', '>>time', '>>dt']
    newstrings2 = [iseed, t_max, dt]
    format2 = ['%4d', '%8d', '%5.5f', '%5.2f']
    mik_replace_strings(infile2, outfile2, oldstrings2, newstrings2, format2)

    ## Sys
    oldstrings3 = ['>>siwahe', '>>tpeak', '>>wadir', '>>wsp']
    newstrings3 = [hi, ti, thetai, wil0]
    format3 = ['%9.1f', '%9.1f', '%7.0f', '%7.1f'] #
    mik_replace_strings(infile3, outfile3, oldstrings3, newstrings3, format3)

    ## Turbin
    oldstrings5 = ['>>rpm', '>>notch', '>>dt']
    newstrings5 = [rpm, notch, dt]
    format5 = ['%5.1f', '%3i', '%5.5f'] #
    mik_replace_strings(infile5, outfile5, oldstrings5, newstrings5, format5)

    ## Vind
    oldstrings6 =
['>>umean', '>>turb', '>>lambda', '>>tslen', '>>fmin', '>>fmax', '>>iseed']
    newstrings6 = [wihub, I_v, Lambdai, t_max, fmin, fmax, iseed]
    format6 = ['%7.1f', '%7.2f', '%7.1f', '%7.1f', '%6.1f', '%6.1f', '%6d'] #
    mik_replace_strings(infile6, outfile6, oldstrings6, newstrings6, format6)

    ## dyn.mac
    oldstrings7 = ['>>iseed']
    newstrings7 = [iseed]
    format7 = ['%d'] #
    mik_replace_strings(infile7, outfile7, oldstrings7, newstrings7, format7)

    os.remove(infile1)
    os.remove(infile2)
    os.remove(infile3)
    os.remove(infile5)
    os.remove(infile6)
    os.remove(infile7)

    os.chdir(maindir)

f.close()

```

B.2 run_simoriflex.py

This file runs SIMO/Riflex for multiple analyses.

```
import os,time,string,sys,datetime

prefix = 'Analysis'
ddr = 'F:\\Analyser\\'
directories = [ddr+'Period_Hm1_2000s_seed1',ddr+'Period_Hm1_2000s_seed122']
dirlist =
['LC0', 'LC1', 'LC2', 'LC3', 'LC4', 'LC5', 'LC6', 'LC7', 'LC8', 'LC9', 'LC10', 'LC11']

for dir in directories:
    os.chdir(dir)

    Ndir = len(dirlist)
    for c in dirlist:

        os.chdir(c)
        os.system('riflexbatch inpmod '+prefix)
        os.system('rsimobatch '+ prefix +' dummy stamod batch sta')
        os.system('riflexbatch stamod ' +prefix)
        os.system('rsimobatch ' +prefix +' dummy dynmod batch dyn')
        os.system('riflexbatch dynmod ' + prefix )
        os.system('rsimobatch ' +prefix +' dummy s2xmod batch s2x')

        os.chdir('..')

    os.chdir('..')
```

APPENDIX C Extract result files from outmod/s2xmod

These files extract the wanted results from SIMO/Riflex by utilizing outmod of Riflex and s2xmod of SIMO.

C.1 Description of how to extract results from Riflex

1. Make the Analysis_outmod.inp file. This contains the information about what you want to extract. It can look like this: (Riflex Manual, green is description)

```
'outmod This says which program is ran
'-----
OUTMOD IDENTIFICATION TEXT 3.8
'----- A1 -
*** ***
*** ***
*** ***
'-----
NEW PLOT FILE Create a new plot, Riflex Man page 4
'Line0x Seg02 Element 10
STARTIMES FILES Appendix B Riflex Man
TOTFORCE TIME SERIES Specify which type of time series you want to extract, Riflex Man C2.14 page 39
1 3 1 10000000 1 This line specifies type of output, degree of freedom etc, see page C2.14 page 39
18 1 5 This is which line, segment and element you want the results for. C2.17.4. The number from Analysis_dynmod.inp.
PLOT
'-----
END
'-----
```

2. Check the stdin.inp file. This creates the outmod-files. It should look like this:

```
Analysis_outmod.inp
Analysis_outmod.res
Analysis_ifnsta.ffi
Analysis_ifnirr.ffi
Analysis_ifndyn.ffi
Analysis_ifnfre.ffi
Analysis_ifnplo.ffi
Analysis_outmod.mpf
Analysis_outmod.ts
```

3. Start outmod.exe with the command **outmod < stdin.inp**

4. Run prtsc.exe with the command **prtsc Analysis_outmod.ts printfile.dat**

The .ts-file is the time series file that should read. The information about the time series number and version number will be printed to the .dat file and can look like this:

```
TS-File: C:\Users\Inge Moy\Documents\NTNU\Master\DeepC\Master\LC2S1800S1\Analysis_outmod.
no.ver points dt date time identification
```

```
.....
58.01 72000 0.0250 *. *. Totforc Z-mom-1 IELM 281*.
```

5. The time series and version number will be used in tsprn.exe to call up the right forces.

6. Last step is to create the .dat-file with the results. This is done by following command:

```
tsprn Analysis_outmod.ts 58.01 Totforc_Z_mom_1.dat
```

58.01 is the time series and version number to the Z – moment on the specified line and element.

7. All these command can be programmed into one single script, a .bat-file. A very simple script is shown below:

```

set Riflex=C:\Program_Files_(x86)\DNVS\DeepC_V4.5-05\Riflex\Bin
set Model=Master
set Ana=LC2S1800S1
set Dir=.\%Ana%
set ReturnDir=..\
outmod.exe < %Dir%\stdin_outmod.inp
prtsc.exe %Dir%\Analysis_outmod.ts test5.dat
tsprn.exe %Dir%\Analysis_outmod.ts 56.01 %Ana%_Moment_Y_Bottom_Tower.dat

```

C.2 Extract.bat

```

set Riflex=W:\DeepC_postprocess\Riflex
set Simo=W:\DeepC_postprocess\Simo
set Sed=W:\GnuWin32\bin\sed

set LC=LC1
set D=D000
set LoadCase=%LC%_%D%
set Model=Spar
set Dir=.\%Model%_%LC%\Analysis_Period_%LoadCase%
set ReturnDir=..\

set Sim=S1800
set Ana=1800s_seed1
set LC=LC0
set Model=spar
set Dir=.\%Sim%\%Ana%\%LC%
set Results=.\Result
set ReturnDir=..\
copy Analysis_outmod.inp %Dir%
copy stdin.inp %Dir%
cd %Dir%
%Riflex%\outmod.exe < stdin.inp
%Riflex%\prtsc.exe Analysis_outmod.ts %ReturnDir%\outinfo.dat
%Riflex%\tsprn.exe Analysis_outmod.ts 56.01 %Ana%_%LC%_Moment_Y_Bottom_Tower.dat
%Sed% -e 1,9d %Ana%_%LC%_Moment_Y_Bottom_Tower.dat > temp.dat
copy temp.dat %Ana%_%LC%_Moment_Y_Bottom_Tower.dat
copy %Ana%_%LC%_Moment_Y_Bottom_Tower.dat
%ReturnDir%\%Results%\%Ana%_%LC%_Moment_Y_Bottom_Tower.dat

```

```

%Riflex%\tsprn.exe Analysis_outmod.ts 58.01 %Ana%_%LC%_Moment_Z_Bottom_Tower.dat
%Sed% -e 1,9d %Ana%_%LC%_Moment_Z_Bottom_Tower.dat > temp.dat
copy temp.dat %Ana%_%LC%_Moment_Z_Bottom_Tower.dat
copy %Ana%_%LC%_Moment_Z_Bottom_Tower.dat
%ReturnDir%\%Results%\%Ana%_%LC%_Moment_Z_Bottom_Tower.dat
%Riflex%\tsprn.exe Analysis_outmod.ts 60.01 %Ana%_%LC%_Shear_Y_Bottom_Tower.dat
%Sed% -e 1,9d %Ana%_%LC%_Shear_Y_Bottom_Tower.dat > temp.dat
copy temp.dat %Ana%_%LC%_Shear_Y_Bottom_Tower.dat
copy %Ana%_%LC%_Shear_Y_Bottom_Tower.dat
%ReturnDir%\%Results%\%Ana%_%LC%_Shear_Y_Bottom_Tower.dat
%Riflex%\tsprn.exe Analysis_outmod.ts 62.01 %Ana%_%LC%_Shear_Z_Bottom_Tower.dat
%Sed% -e 1,9d %Ana%_%LC%_Shear_Z_Bottom_Tower.dat > temp.dat
copy temp.dat %Ana%_%LC%_Shear_Z_Bottom_Tower.dat
copy %Ana%_%LC%_Shear_Z_Bottom_Tower.dat
%ReturnDir%\%Results%\%Ana%_%LC%_Shear_Z_Bottom_Tower.dat
%Riflex%\tsprn.exe Analysis_outmod.ts 76.01
%Ana%_%LC%_Torsional_Stress_Bottom_Tower.dat
%Sed% -e 1,9d %Ana%_%LC%_Torsional_Stress_Bottom_Tower.dat > temp.dat
copy temp.dat %Ana%_%LC%_Torsional_Stress_Bottom_Tower.dat
copy %Ana%_%LC%_Torsional_Stress_Bottom_Tower.dat
%ReturnDir%\%Results%\%Ana%_%LC%_Torsional_Stress_Bottom_Tower.dat
%Riflex%\tsprn.exe Analysis_outmod.ts 78.01
%Ana%_%LC%_Axial_and_Bending_Stress_Bottom_Tower.dat
%Sed% -e 1,9d %Ana%_%LC%_Axial_and_Bending_Stress_Bottom_Tower.dat > temp.dat
copy temp.dat %Ana%_%LC%_Axial_and_Bending_Stress_Bottom_Tower.dat
copy %Ana%_%LC%_Axial_and_Bending_Stress_Bottom_Tower.dat
%ReturnDir%\%Results%\%Ana%_%LC%_Axial_and_Bending_Stress_Bottom_Tower.dat
%Riflex%\tsprn.exe Analysis_outmod.ts 81.01
%Ana%_%LC%_Equivalent_Stress_Bottom_Tower.dat
%Sed% -e 1,9d %Ana%_%LC%_Equivalent_Stress_Bottom_Tower.dat > temp.dat
copy temp.dat %Ana%_%LC%_Equivalent_Stress_Bottom_Tower.dat
copy %Ana%_%LC%_Equivalent_Stress_Bottom_Tower.dat
%ReturnDir%\%Results%\%Ana%_%LC%_Equivalent_Stress_Bottom_Tower.dat
cd %ReturnDir%

copy Analysis.mac %Dir%

```



```

copy rsimo_run.bat %Dir%
cd %Dir%
%Simo%\rsimo Analysis dummy s2xmod batch Analysis
copy B01r29c001 %ReturnDir%\%Model%_%LoadCase%_Spar_GlobalPosition_X.dat
copy B01r29c002 %ReturnDir%\%Model%_%LoadCase%_Spar_GlobalPosition_Y.dat
copy B01r29c003 %ReturnDir%\%Model%_%LoadCase%_Spar_GlobalPosition_Z.dat
copy B01r29c004 %ReturnDir%\%Model%_%LoadCase%_Spar_GlobalPosition_X_rot.dat
copy B01r29c005 %ReturnDir%\%Model%_%LoadCase%_Spar_GlobalPosition_Y_rot.dat
copy B01r29c006 %ReturnDir%\%Model%_%LoadCase%_Spar_GlobalPosition_Z_rot.dat
copy B02r02c001 %ReturnDir%\%Model%_%LoadCase%_TotalWaveElevationAtOrigo.dat
copy m001.m %ReturnDir%\%Model%_%LoadCase%_m001.m
cd %ReturnDir%

```

C.3 outinfo.inp

TS-File: F:\Analyser\Period_Hm5\Period_Hm5_2000s_seed1\LC2\Analysis_outmod.ts

```

no.ver points dt date time identification
.....
56.01 80000 0.0250 *. *. Totforc Y-mom-1 IELM 281*.
      *.
58.01 80000 0.0250 *. *. Totforc Z-mom-1 IELM 281*.
      *.
60.01 80000 0.0250 *. *. Totforc Y-shear-1 IELM 281*.
      *.
62.01 80000 0.0250 *. *. Totforc Z-shear-1 IELM 281*.
      *.
76.01 80000 0.0250 *. *. Tors. stress, e1 IELM 281*.
      *.
78.01 80000 0.0250 *. *. Ax.+bend. str, e1 IELM 281*.
      *.
81.01 80000 0.0250 *. *. Eq. stress, e1 IELM 281*.
      *.

```

C.4 Analysis_outmod.inp

```

'outmod
'-----
      OUTMOD IDENTIFICATION TEXT 3.8
'----- A1 -
***   ***
***   ***
***   ***
'-----

```

```

NEW PLOT FILE
'Line0x Seg02 Element 10
STARTTIMES FILES
TOTFORCE TIME SERIES
1 3 1 10000000 1
18 1 5
PLOT
STARTTIMES FILES
TOTFORCE TIME SERIES
1 5 1 10000000 1
18 1 5
PLOT
STARTTIMES FILES
TOTFORCE TIME SERIES
1 7 1 10000000 1
18 1 5
PLOT
STARTTIMES FILES
TOTFORCE TIME SERIES
1 9 1 10000000 1
18 1 5
PLOT
STARTTIMES FILES
STRESS TIME SERIES
1 2 1 10000000 0 1
0 2 1
18 1 5
PLOT
STARTTIMES FILES
STRESS TIME SERIES
1 4 1 10000000 0 1
0 2 1
18 1 5
PLOT
STARTTIMES FILES
STRESS TIME SERIES
1 7 1 10000000 0 1
0 2 1
18 1 5
PLOT
'-----
END
'-----

```

C.5 Stdin.inp

```

Analysis_outmod.inp
Analysis_outmod.res
Analysis_ifnsta.ffi
Analysis_ifnirr.ffi
Analysis_ifndyn.ffi

```

Analysis_ifnfre.ffi
Analysis_ifnplo.ffi
Analysis_outmod.mpf
Analysis_outmod.ts

APPENDIX D Plot of joint probability distribution

D.1 Matlab Script of the joint distribution of wind and waves

```
clc;
clear;
%Joint Distribution for Wind and Waves

%Parameter for Mean Peak Period
c1=4.883;
c2=2.68;
c3=0.529;

%Parameter for Mean Wind Speed
d1=1.764;
d2=3.426;
d3=0.78;

%Paramter for Peak Period
theta=-0.19;
gamma=1;

%Paramter for Wind Density
alfaw=1.708;
betaw=8.426;

for w = 1:1:24
for h = 1:1:20;
    for t = 1:1:20

%Paramter for Hm0 given wind
alfah=2+0.135*w;
betah=1.8 + 0.1*w^1.322;

ET(h)=c1+c2*h^c3;
EW(h)=d1+d2*h^d3;

T(h)=ET(h)*(1+theta*((w-EW(h))/EW(h))));

sigmaTp(h)=(-0.0017+0.259*exp(-0.113*h))*T(h);

vyTp(h)=sigmaTp(h)/T(h);

mylnTp(h)=log(T(h)/(sqrt(1+vyTp(h)^2)));

sigmalnTp(h)=sqrt(log(vyTp(h)^2+1));

fTp(t,h)=(1/(t*sigmalnTp(h)*sqrt(2*pi)))*exp(-0.5*((log(t)-
mylnTp(h))/(sigmalnTp(h)))^2);

fw=(alfaw/betaw)*(w/betaw)^(alfaw-1)*exp(-(w/betaw)^alfaw);

fh(h)=(alfah/betah)*(h/betah)^(alfah-1)*exp(-(h/betah)^alfah);

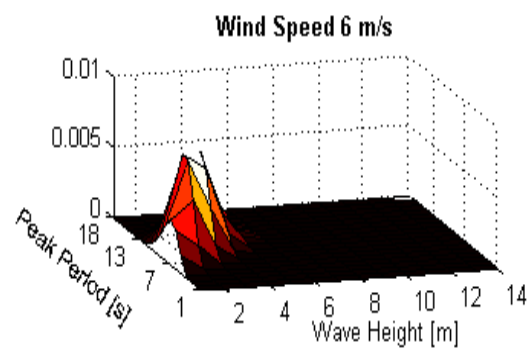
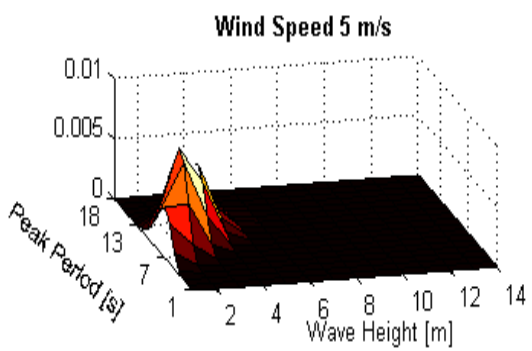
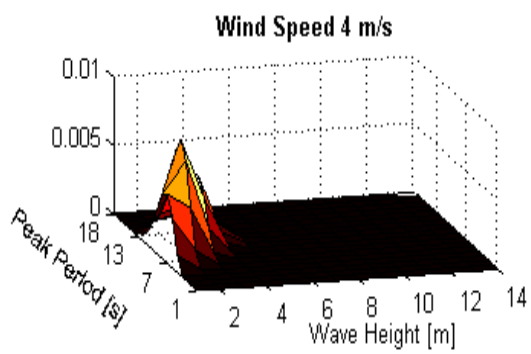
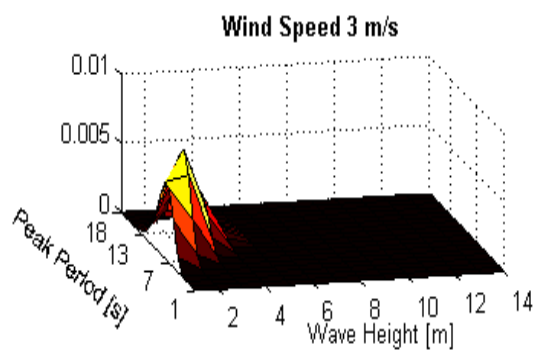
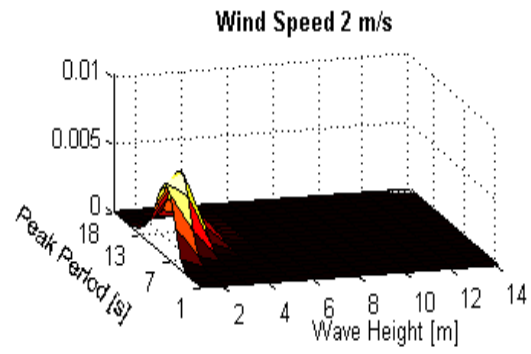
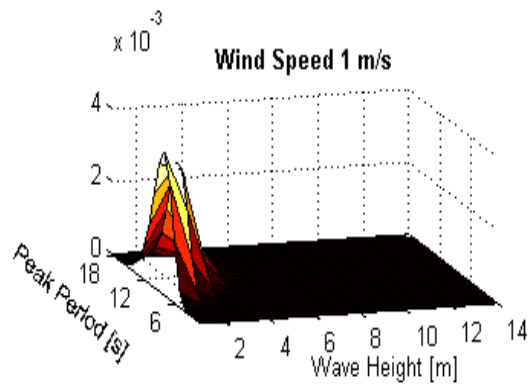
JDensFunc(t,h)=fw*fh(h)*fTp(t,h); %Joint Distribution with constant wind
```

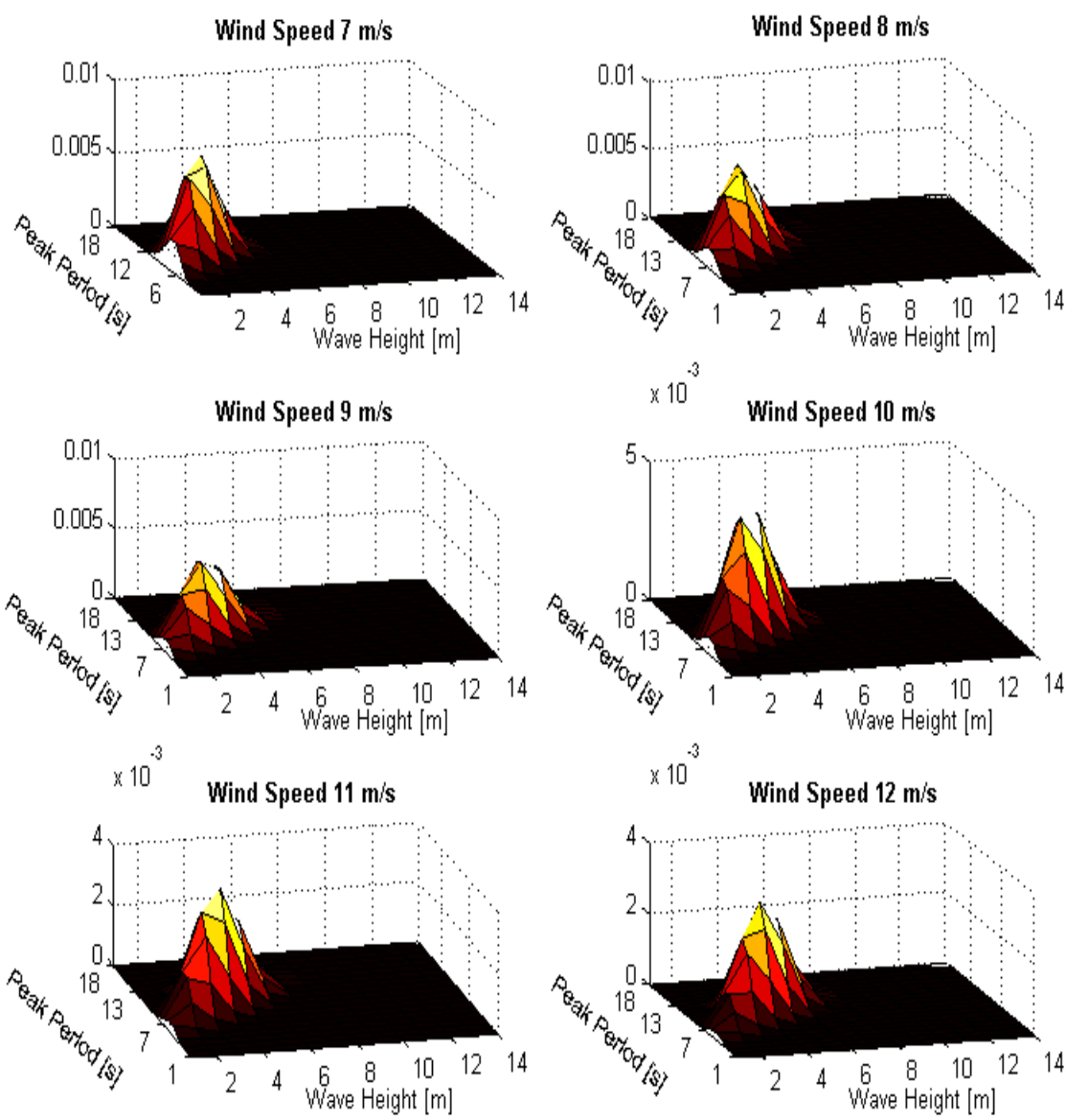
```
fff(w,t,h)=JDensFunc(t,h); % Total Joint distribution

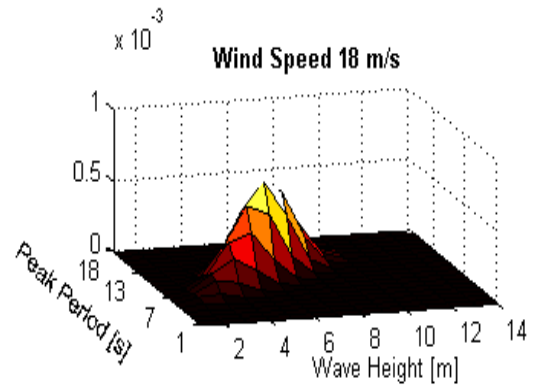
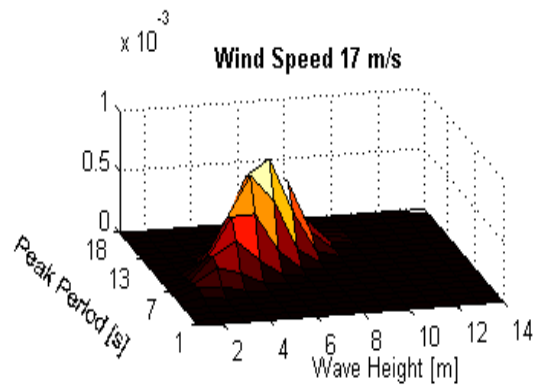
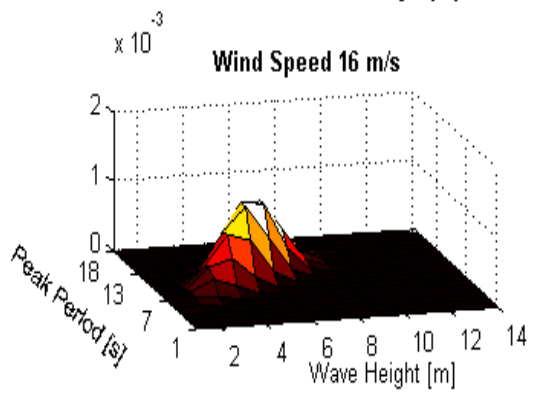
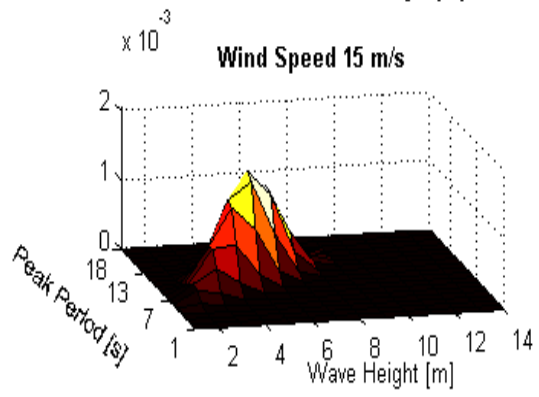
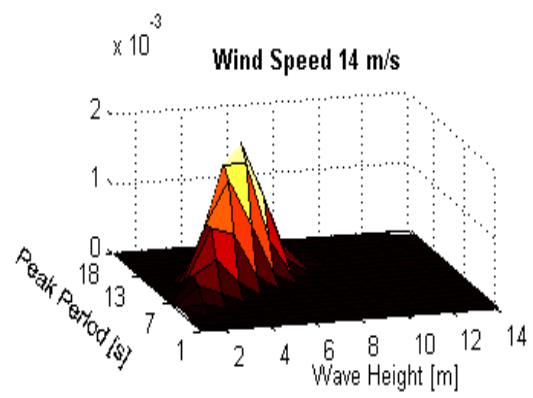
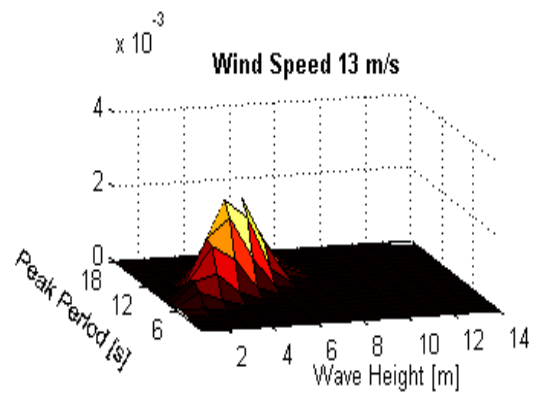
    end
end
end

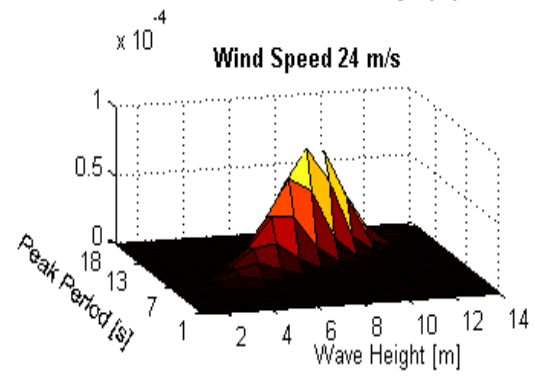
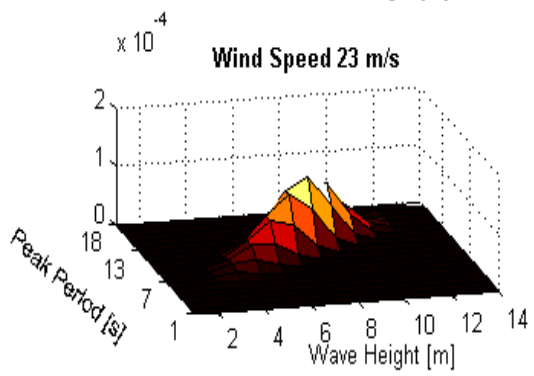
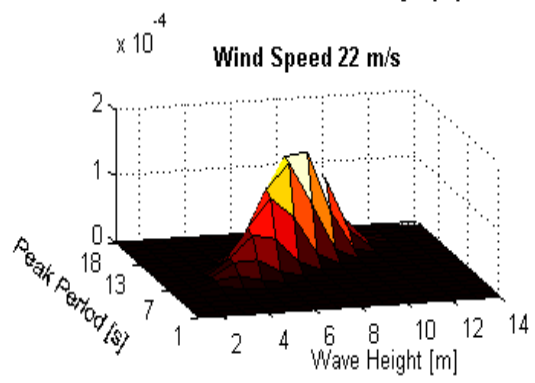
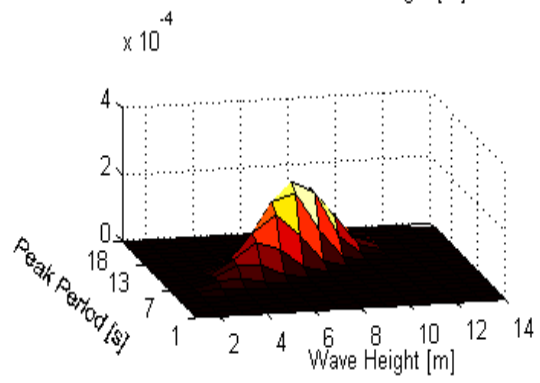
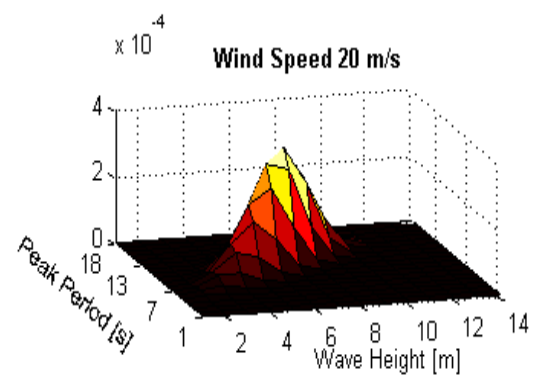
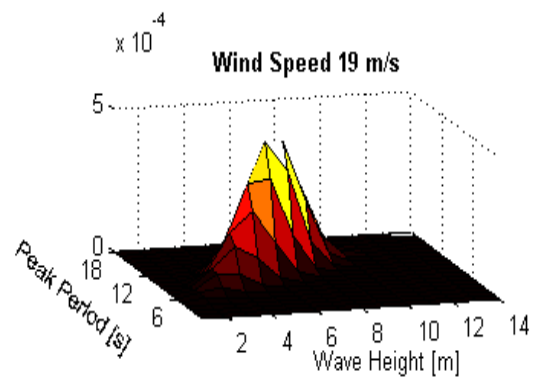
%Marginal Probability of Each Load Case
for i = 1:1:16
    for k = 1:1:15
        ProbTp(i,k)=fff(4,i,k);
    end
end
for j= 1:1:15
    for l = 8:1:10
        ProbHm0(j,l)=fff(4,l,j);
    end
end
end
```

D.2 Surfaceplots

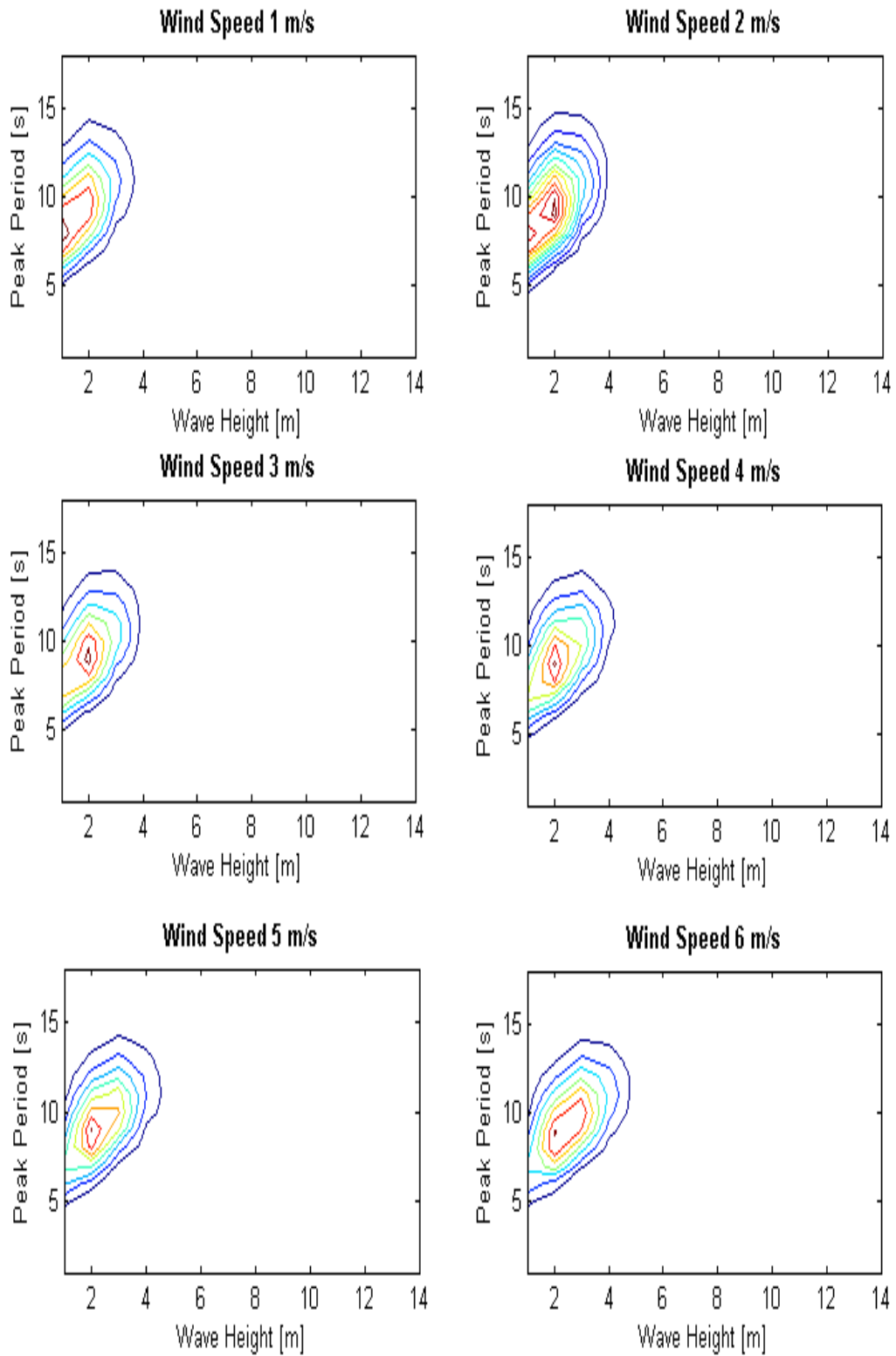


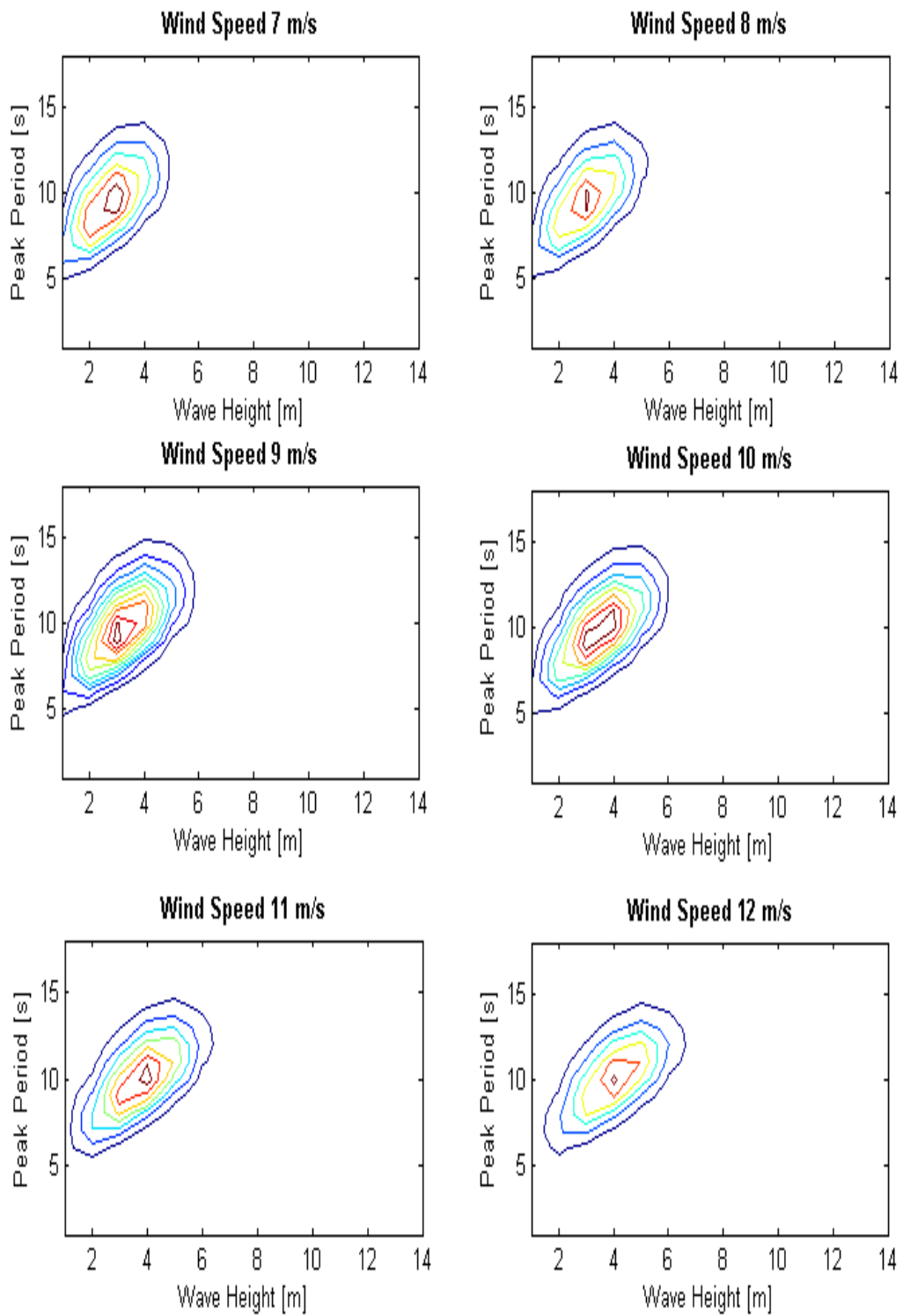


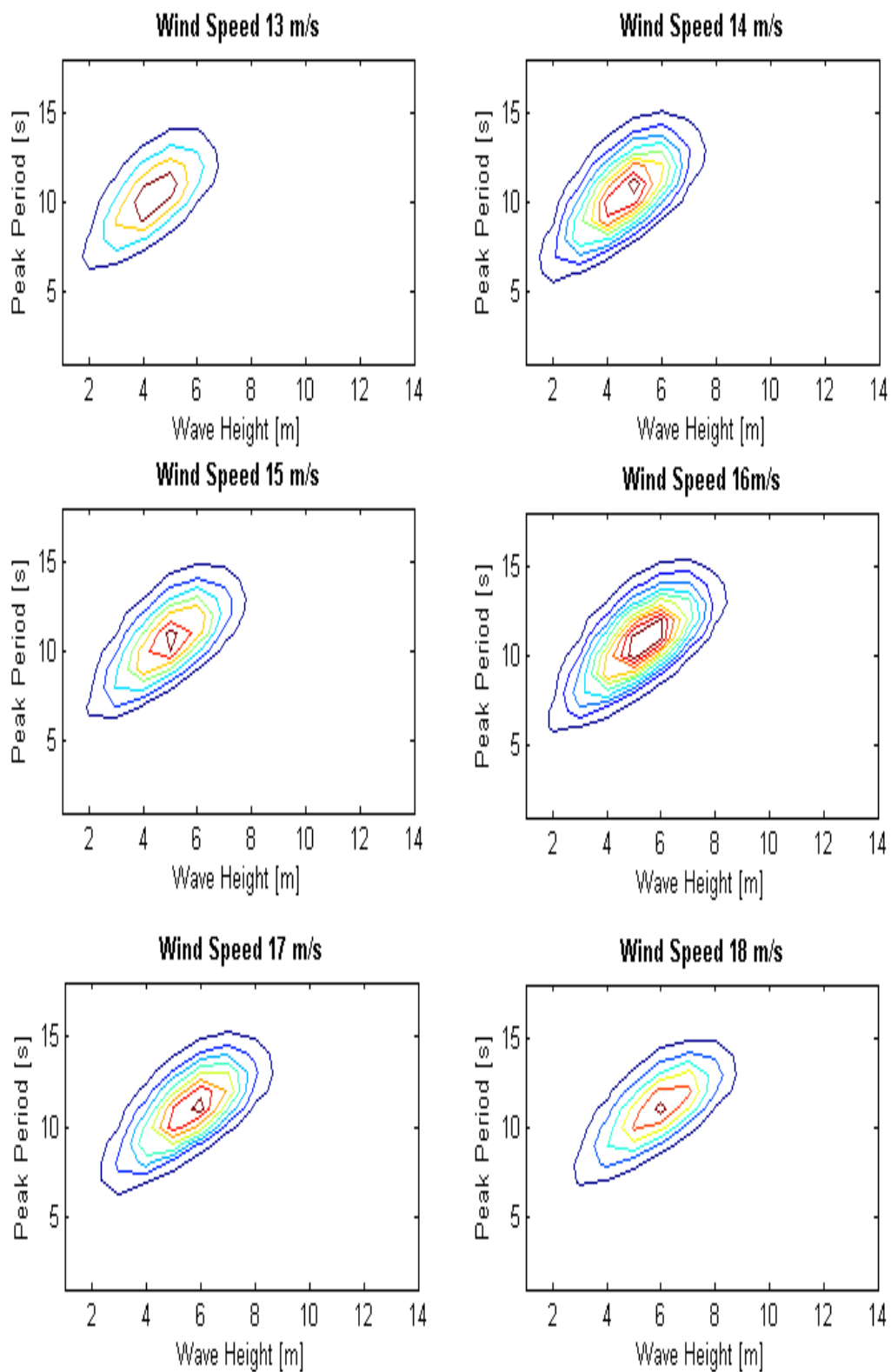


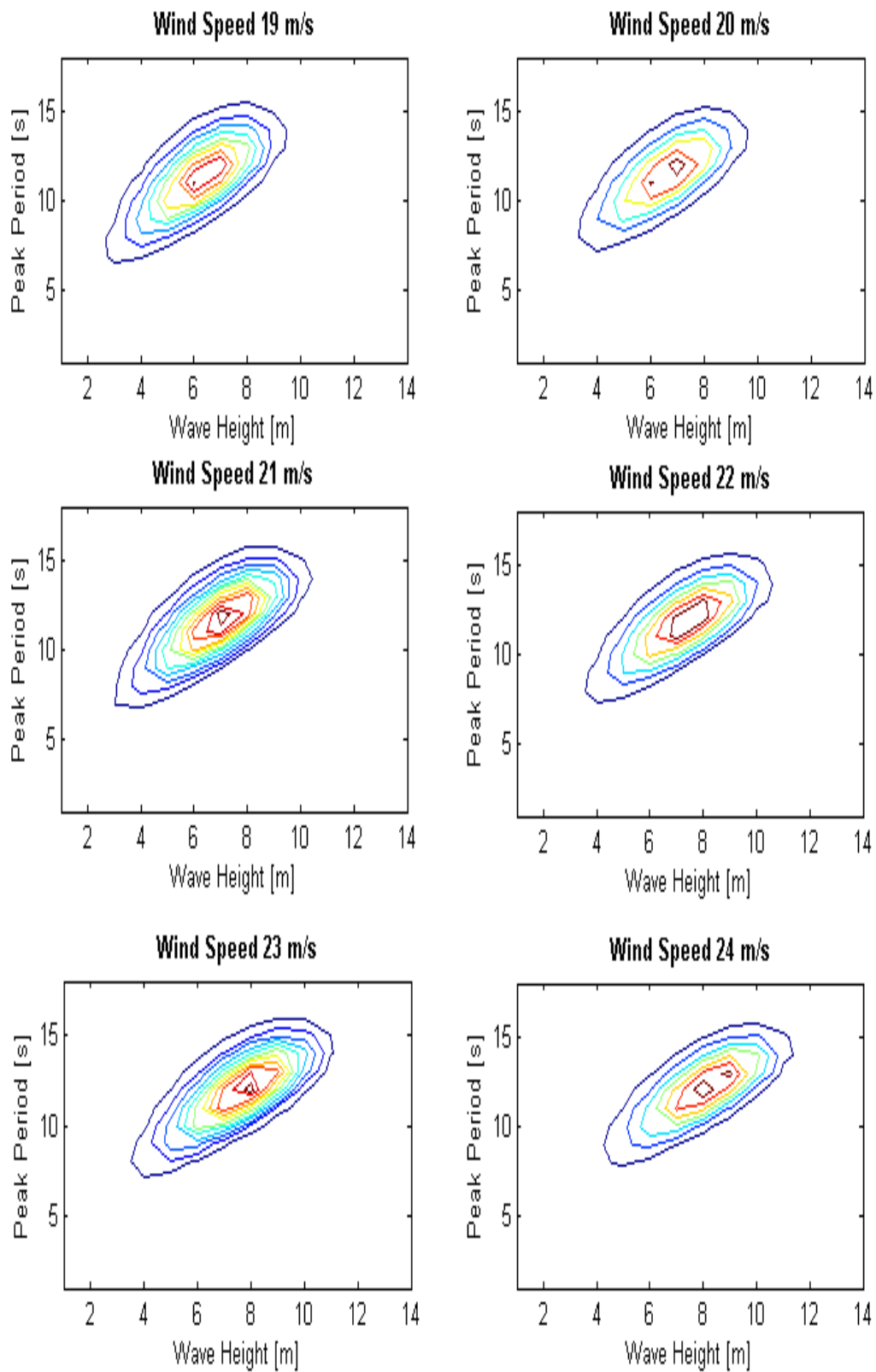


D.3 Contour plots









APPENDIX E Matlab Scripts Used for post-processing

E.1 Load and Damage Calculations

%This script loads the force, moment and stress time series generated from %outmod. This file is can only be run together with the .dat files, or the %saved structure-variable.

```
clc;
initwafo;
beta=3;
K=1.99e-11;
par = [-1 1 64];

for i = 1:6 %[1 122 868 901 985 1313 6546]
    for j = 0:11
        Seed = ['seed' num2str(i)];
        LC = ['LC' num2str(j)];

        %Loading and Structures

        Res10800.(Seed).(LC).MY = load(['10800s_' Seed '_' LC
'_Moment_Y_Bottom_Tower.dat']);
        Res10800.(Seed).(LC).MZ = load(['10800s_' Seed '_' LC
'_Moment_Z_Bottom_Tower.dat']);
        Res10800.(Seed).(LC).SY = load(['10800s_' Seed '_' LC
'_Shear_Y_Bottom_Tower.dat']);
        Res10800.(Seed).(LC).SZ = load(['10800s_' Seed '_' LC
'_Shear_Z_Bottom_Tower.dat']);
        Res10800.(Seed).(LC).S = load(['10800s_' Seed '_' LC
'_Axial_and_Bending_Stress_Bottom_Tower.dat']);
        Res10800.(Seed).(LC).T = load(['10800s_' Seed '_' LC
'_Torsional_Stress_Bottom_Tower.dat']);
        Res10800.(Seed).(LC).E = load(['10800s_' Seed '_' LC
'_Equivalent_Stress_Bottom_Tower.dat']);

        Res10800.(Seed).(LC).MeanMY = mean(Res10800.(Seed).(LC).MY(:,2));
        Res10800.(Seed).(LC).MeanMZ = mean(Res10800.(Seed).(LC).MZ(:,2));
        Res10800.(Seed).(LC).MeanSY = mean(Res10800.(Seed).(LC).SY(:,2));
        Res10800.(Seed).(LC).MeanSZ = mean(Res10800.(Seed).(LC).SZ(:,2));
        Res10800.(Seed).(LC).MeanS = mean(Res10800.(Seed).(LC).S(:,2));
        Res10800.(Seed).(LC).MeanT = mean(Res10800.(Seed).(LC).T(:,2));
        Res10800.(Seed).(LC).MeanE = mean(Res10800.(Seed).(LC).E(:,2));

        %Rainflow Matrix
        Res10800.(Seed).(LC).RFM.MY = dat2rfm(Res10800.(Seed).(LC).MY);
        Res10800.(Seed).(LC).RFM.MZ = dat2rfm(Res10800.(Seed).(LC).MZ);
        Res10800.(Seed).(LC).RFM.SY = dat2rfm(Res10800.(Seed).(LC).SY);
        Res10800.(Seed).(LC).RFM.SZ = dat2rfm(Res10800.(Seed).(LC).SZ);
        Res10800.(Seed).(LC).RFM.S = dat2rfm(Res10800.(Seed).(LC).S);
        Res10800.(Seed).(LC).RFM.T = dat2rfm(Res10800.(Seed).(LC).T);
        Res10800.(Seed).(LC).RFM.E = dat2rfm(Res10800.(Seed).(LC).E);

        % Damage Matrix
```

```

Res10800.(Seed).(LC).Dam.MY =
cmat2dmat(par,Res10800.(Seed).(LC).RFM.MY,beta,K);
Res10800.(Seed).(LC).Dam.MZ =
cmat2dmat(par,Res10800.(Seed).(LC).RFM.MZ,beta,K);
Res10800.(Seed).(LC).Dam.SY =
cmat2dmat(par,Res10800.(Seed).(LC).RFM.SY,beta,K);
Res10800.(Seed).(LC).Dam.SZ =
cmat2dmat(par,Res10800.(Seed).(LC).RFM.SZ,beta,K);
Res10800.(Seed).(LC).Dam.S =
cmat2dmat(par,Res10800.(Seed).(LC).RFM.S,beta,K);
Res10800.(Seed).(LC).Dam.T =
cmat2dmat(par,Res10800.(Seed).(LC).RFM.T,beta,K);
Res10800.(Seed).(LC).Dam.E =
cmat2dmat(par,Res10800.(Seed).(LC).RFM.E,beta,K);

%Tot Damage
Res10800.(Seed).(LC).TotDam.MY = sum(sum(Res10800.(Seed).(LC).Dam.MY));
Res10800.(Seed).(LC).TotDam.MZ = sum(sum(Res10800.(Seed).(LC).Dam.MZ));
Res10800.(Seed).(LC).TotDam.SY = sum(sum(Res10800.(Seed).(LC).Dam.SY));
Res10800.(Seed).(LC).TotDam.SZ = sum(sum(Res10800.(Seed).(LC).Dam.SZ));
Res10800.(Seed).(LC).TotDam.S = sum(sum(Res10800.(Seed).(LC).Dam.S));
Res10800.(Seed).(LC).TotDam.T = sum(sum(Res10800.(Seed).(LC).Dam.T));
Res10800.(Seed).(LC).TotDam.E = sum(sum(Res10800.(Seed).(LC).Dam.E));

end
end

save Res10800

```

E.2 Calcualte Statistical Properties

```

clc;
load Res1800
for i = 1:7 % [1 122 868 901 985 1313 6546]
    for j = 0:11
        Seed = ['seed' num2str(i)];
        LC = ['LC' num2str(j)];

        % Mean of each time serie
        MeanMY_1800(i,(j+1))=mean(Res1800.(Seed).(LC).MY(8000:end,2));
        MeanMZ_1800(i,(j+1))=mean(Res1800.(Seed).(LC).MZ(8000:end,2));
        MeanSY_1800(i,(j+1))=mean(Res1800.(Seed).(LC).SY(8000:end,2));
        MeanSZ_1800(i,(j+1))=mean(Res1800.(Seed).(LC).SZ(8000:end,2));
        MeanS_1800(i,(j+1))=mean(Res1800.(Seed).(LC).S(8000:end,2));
        MeanT_1800(i,(j+1))=mean(Res1800.(Seed).(LC).T(8000:end,2));
        MeanE_1800(i,(j+1))=mean(Res1800.(Seed).(LC).E(8000:end,2));

        % Standard Deviation of each time serie
        StdMY_1800(i,(j+1))=std(Res1800.(Seed).(LC).MY(8000:end,2));
        StdMZ_1800(i,(j+1))=std(Res1800.(Seed).(LC).MZ(8000:end,2));
        StdSY_1800(i,(j+1))=std(Res1800.(Seed).(LC).SY(8000:end,2));
        StdSZ_1800(i,(j+1))=std(Res1800.(Seed).(LC).SZ(8000:end,2));
        StdS_1800(i,(j+1))=std(Res1800.(Seed).(LC).S(8000:end,2));
        StdT_1800(i,(j+1))=std(Res1800.(Seed).(LC).T(8000:end,2));
        StdE_1800(i,(j+1))=std(Res1800.(Seed).(LC).E(8000:end,2));
    end
end

```

```

%Skewness of each time serie
Skewness_MY_1800(i, (j+1))=skewness(Res1800.(Seed).(LC).MY(8000:end,2));
Skewness_MZ_1800(i, (j+1))=skewness(Res1800.(Seed).(LC).MZ(8000:end,2));
Skewness_SY_1800(i, (j+1))=skewness(Res1800.(Seed).(LC).SY(8000:end,2));
Skewness_SZ_1800(i, (j+1))=skewness(Res1800.(Seed).(LC).SZ(8000:end,2));
Skewness_S_1800(i, (j+1))=skewness(Res1800.(Seed).(LC).S(8000:end,2));
Skewness_T_1800(i, (j+1))=skewness(Res1800.(Seed).(LC).T(8000:end,2));
Skewness_E_1800(i, (j+1))=skewness(Res1800.(Seed).(LC).E(8000:end,2));

%Kurtosis of each time serie
Kurtosis_MY_1800(i, (j+1))=kurtosis(Res1800.(Seed).(LC).MY(8000:end,2));
Kurtosis_MZ_1800(i, (j+1))=kurtosis(Res1800.(Seed).(LC).MZ(8000:end,2));
Kurtosis_SY_1800(i, (j+1))=kurtosis(Res1800.(Seed).(LC).SY(8000:end,2));
Kurtosis_SZ_1800(i, (j+1))=kurtosis(Res1800.(Seed).(LC).SZ(8000:end,2));
Kurtosis_S_1800(i, (j+1))=kurtosis(Res1800.(Seed).(LC).S(8000:end,2));
Kurtosis_T_1800(i, (j+1))=kurtosis(Res1800.(Seed).(LC).T(8000:end,2));
Kurtosis_E_1800(i, (j+1))=kurtosis(Res1800.(Seed).(LC).E(8000:end,2));

end
end

for i = 1:12
    Mean_Std_MY_1800(:,i)=mean(StdMY_1800(:,i));
    Mean_Std_MZ_1800(:,i)=mean(StdMZ_1800(:,i));
    Mean_Std_SY_1800(:,i)=mean(StdSY_1800(:,i));
    Mean_Std_SZ_1800(:,i)=mean(StdSZ_1800(:,i));
    Mean_Std_S_1800(:,i)=mean(StdS_1800(:,i));
    Mean_Std_T_1800(:,i)=mean(StdT_1800(:,i));
    Mean_Std_E_1800(:,i)=mean(StdE_1800(:,i));

    Mean_Mean_MY_1800(:,i)=mean(MeanMY_1800(:,i));
    Mean_Mean_MZ_1800(:,i)=mean(MeanMZ_1800(:,i));
    Mean_Mean_SY_1800(:,i)=mean(MeanSY_1800(:,i));
    Mean_Mean_SZ_1800(:,i)=mean(MeanSZ_1800(:,i));
    Mean_Mean_S_1800(:,i)=mean(MeanS_1800(:,i));
    Mean_Mean_T_1800(:,i)=mean(MeanT_1800(:,i));
    Mean_Mean_E_1800(:,i)=mean(MeanE_1800(:,i));

    Mean_Skewness_MY_1800(:,i)=mean(Skewness_MY_1800(:,i));
    Mean_Skewness_MZ_1800(:,i)=mean(Skewness_MZ_1800(:,i));
    Mean_Skewness_SY_1800(:,i)=mean(Skewness_SY_1800(:,i));
    Mean_Skewness_SZ_1800(:,i)=mean(Skewness_SZ_1800(:,i));
    Mean_Skewness_S_1800(:,i)=mean(Skewness_S_1800(:,i));
    Mean_Skewness_T_1800(:,i)=mean(Skewness_T_1800(:,i));
    Mean_Skewness_E_1800(:,i)=mean(Skewness_E_1800(:,i));

    Mean_Kurtosis_MY_1800(:,i)=mean(Kurtosis_MY_1800(:,i));
    Mean_Kurtosis_MZ_1800(:,i)=mean(Kurtosis_MZ_1800(:,i));
    Mean_Kurtosis_SY_1800(:,i)=mean(Kurtosis_SY_1800(:,i));
    Mean_Kurtosis_SZ_1800(:,i)=mean(Kurtosis_SZ_1800(:,i));
    Mean_Kurtosis_S_1800(:,i)=mean(Kurtosis_S_1800(:,i));
    Mean_Kurtosis_T_1800(:,i)=mean(Kurtosis_T_1800(:,i));
    Mean_Kurtosis_E_1800(:,i)=mean(Kurtosis_E_1800(:,i));

end

```



```

accumStd_MY_1800=cummean(StdMY_1800);
accumStd_MZ_1800=cummean(StdMZ_1800);
accumStd_SY_1800=cummean(StdSY_1800);
accumStd_SZ_1800=cummean(StdSZ_1800);
accumStd_S_1800=cummean(StdS_1800);
accumStd_T_1800=cummean(StdT_1800);
accumStd_E_1800=cummean(StdE_1800);

```

E.3 Calculate Accumulated Damage

```

clc;
for i = 1:7  %[1 122 868 901 985 1313 6546]
    for j = 0:11
        Seed = ['seed' num2str(i)];
        LC = ['LC' num2str(j)];

        TotDamage1800_MY(i,j+1) = Res1800.(Seed).(LC).TotDam.MY;
        TotDamage1800_MZ(i,j+1) = Res1800.(Seed).(LC).TotDam.MZ;
        TotDamage1800_S(i,j+1) = Res1800.(Seed).(LC).TotDam.S;
        TotDamage1800_E(i,j+1) = Res1800.(Seed).(LC).TotDam.E;

    end
end

for i = 1:12

    Mean_TotDamage1800_MY(1,i) = mean(TotDamage1800_MY(:,i));
    Mean_TotDamage1800_MZ(1,i) = mean(TotDamage1800_MZ(:,i));
    Mean_TotDamage1800_S(1,i) = mean(TotDamage1800_S(:,i));
    Mean_TotDamage1800_E(1,i) = mean(TotDamage1800_E(:,i));
end

P = load('ProbWind.dat');
for j = 1:12
    Damlyear_MY_1800(1,j)=P(j)*48*365*Mean_TotDamage1800_MY(1,j);
    Damlyear_MZ_1800(1,j)=P(j)*48*365*Mean_TotDamage1800_MZ(1,j);
    Damlyear_S_1800(1,j)=P(j)*48*365*Mean_TotDamage1800_S(1,j);
    Damlyear_E_1800(1,j)=P(j)*48*365*Mean_TotDamage1800_E(1,j);
end

```